

GIANT SPARKS AT COSMOLOGICAL DISTANCES?

S. R. KULKARNI,¹ E. O. OFEK,² J. D. NEILL,³ Z. ZHENG⁴ & M. JURIC^{5,6}

Draft of March 3, 2014

ABSTRACT

Millisecond duration bright radio pulses in the 1.4-GHz band and with inferred dispersion measures (DM) well in excess of Galactic values have been reported by Lorimer *et al.* and Thornton *et al.*. The all-sky rate of these events is large, $\approx 10^4$ per day above ~ 1 Jy. To add to the mystery there now exists “Perytons” – also pulsed and dispersed sources but most certainly of local (artificial or atmospheric) origin. The suggested models now range from sources originating in the Earth’s atmosphere, in stellar coronae, in other galaxies and at even cosmological distances. Using a series of physically motivated assumptions combined with the observed properties of these bursts, we explore possible constraints on sites or processes that can account for such high DMs. In our analysis, we focus on the first such reported event by Lorimer *et al.*: a 30 Jy, 5-ms duration burst with a dispersion measure of $375 \text{ cm}^{-3} \text{ pc}$ and exhibiting a steep frequency-dependent pulse width (hereafter dubbed as the *Sparker*). Assuming that the DM of the *Sparker* is produced by propagation through a cold plasma and using all available observations we constrain its distance to be greater than 300 kpc. A similar analysis on the four other reported events (all with larger DMs) would lead to a stronger conclusion, namely these “Fast Radio Bursts (FRBs)” (the moniker given to this group by the discoverers) are of extragalactic origin, *provided that the inferred DM arises due to propagation through cold plasma*. We then explore proposed extra-galactic as well as stellar coronal models for FRBs and find most of them either unable to account for the high daily rate or have difficulty in having an ultra-clean explosion site (essential to the production of high brightness temperature pulse) or suffer from free-free absorption on length scales beyond the immediate production of the radio pulses. A model in which FRBs are a by-product of giant flares from soft gamma-ray repeaters appears to be attractive on most counts including naturally explaining why some FRBs exhibit pulses whose width increases rapidly with wavelength. The model does require significant efficiency (10^{-5}) of converting the giant flare energy into radio emission. In our attempt to be complete in our exploration, we drop the assumption that the high DMs are produced by propagation through a plasma and adopt the view that the source itself produces pulses with frequency-dependent arrival time (“chirped signals”). Within this framework we explore a scenario in which Perytons, the *Sparker* and the FRBs are all atmospheric phenomenon but occurring at different distances (heights). However, this model is *ad hoc* in that we are unable to explain why Perytons occurring at higher altitudes should show greater inferred DMs or exhibit narrower pulses. Nonetheless, we argue on empirical grounds that the *Sparker* may be a Peryton. We end with two remarks. First, the detection of a single FRB by an interferometer with a kilometer (or longer) baselines will, in one stroke, prove that FRBs are not of terrestrial origin. Second, we urge astronomers to energetically pursue observations and understanding of Perytons since (at the very least) they form a formidable foreground for the FRBs.

Subject headings: ISM: general – radio continuum: general – pulsars: general— galaxies: individual (SMC)

1. INTRODUCTION

The subject of radio transients seems to have finally come of age. The Galactic list starts with GCRT J1745–3009, an erratic source in the meter-wave band (Hyman *et al.* 2005) and is followed by neutron stars which produce strong pulses occasionally, the so-called Rotating Radio Transients (RRATs; McLaughlin *et al.* 2006). Radio afterglows appear to routinely follow giant flares from soft-gamma repeaters (Frail, Kulkarni & Bloom 1999). Recently, an entirely new type of radio source (Zauderer *et al.* 2011)

was unexpectedly discovered first in the hard X-ray band, Swift J164449.3+573451 (Burrows *et al.* 2011). To within the exquisite astrometric precision afforded by radio VLBI the radio counterpart coincides with the nucleus of a small star-forming galaxy at $z = 0.35$ (Levan *et al.* 2011). The Lorentz factor of this relativistic explosion, ~ 10 , is smaller by an order of magnitude to those inferred in gamma-ray bursts. A plausible model for the source is blazar activity initiated by feeding a tidally disrupted star to a nuclear black hole (Bloom *et al.* 2011). A recent summary of the rates of extra-galactic radio transients can be found in Frail *et al.* (2012).

Lorimer *et al.* (2007) reported the discovery of an intense (30 Jy) and short duration (5-ms) burst in the decimeter band (1.4 GHz). This transient was found as a result of the archival analysis of the Parkes Multi-Beam pulsar data obtained towards the Magellanic Clouds. At first blush, this transient appears to be a Galactic RRAT, albeit a bright one. However, the dispersion measure (DM) of this burst, $375 \text{ cm}^{-3} \text{ pc}$, considerably exceeded the sum of the estimated dispersion measure contributed by the interstellar medium of our own Galaxy and that contributed by the Magellanic Clouds. Follow-up obser-

¹ Caltech Optical Observatories 249-17, California Institute of Technology, Pasadena, CA 91125

² Department of Particle Physics & Astrophysics, Weizmann Institute of Science, Rehovot 76100, Israel

³ Space Radiation Laboratory 290-17, California Institute of Technology, Pasadena, CA 91125

⁴ Department of Physics & Astronomy, University of Utah, 115 South 1400 East #201, Salt Lake City, UT 84112

⁵ Steward Observatory, 933 N. Cherry Avenue, Tucson, AZ 85721

⁶ Large Survey Synoptic Survey Telescope, 933 N. Cherry Avenue, Tucson, AZ 85721

vations did not show any repeating burst.

Lorimer and colleagues proposed that most of the dispersion measure arose from electrons in the inter-galactic medium (IGM). Using currently accepted values for the density of the IGM they estimated the redshift to this event – which, here after, we call the *Sparker* – to be about 0.12 (~ 500 Mpc).

The *Sparker* would be the first impulsive radio transient event seen from outside the Local Group. If so, this discovery assumes a seminal stature. Specifically, the sharp pulse will enable astronomers to probe the column density, magnetic field and turbulence of the IGM (Macquart & Koay 2013; Cordes 2013). The discovery appeared timely given that several countries have undertaken massive investments in radio astronomy in the meter and decimetric bands – the Low Frequency Array (LOFAR; Falcke *et al.* 2007), the Murchison Wide Field Array (MWA; Bhat *et al.* 2007) and the Australian Square-Kilometre-Array Pathfinder (ASKAP; Johnston *et al.* 2008). In short, in the parlance so popular with funding agencies, the discovery reported by Lorimer *et al.* (2007) could be a transformational finding.

The discovery of the *Sparker* motivated further archival searches. Additional transients were found with some features similar to that of the *Sparker* (Burke-Spolaor *et al.* 2011). Some of these bursts exhibited a trajectory in a plane of arrival-time (t) and frequency (ν) as follows: $t(\nu) \propto \nu^{-n}$ but with $n \approx 2$. We remind the reader that for a pulse traveling through cold plasma, n is exactly 2. Furthermore, some of the bursts showed “lumpy” emission (that is, the broad band spectrum could not be described by a simple power law). Most troubling was that these events were detected in many beams. These sources were dubbed *Perytons* by the discoverers. Burke-Spolaor and colleagues argue that Perytons are atmospheric phenomenon and explain the detection in all (most) beams to pickup by distant side lobes. Kocz *et al.* (2012) found additional Perytons in a second re-analysis and noted that a cluster of Perytons were separated by about 22 s and suggested that Perytons are artificial signals. Regardless, it is now accepted that Perytons are terrestrial in origin. The DM of the *Sparker* was noted to be similar to that inferred for Perytons, and as a result some doubt was cast on the extra-galactic nature of the *Sparker*.

Another archival search of the Parkes Galactic Plane Survey data found a transient event in a single beam and with a dispersion measure of $746 \text{ cm}^{-3} \text{ pc}$ (Keane *et al.* 2012). Earlier this year, Thornton *et al.* (2013) reported the finding of four short duration bursts. One of these events showed a frequency dependent arrival time with $n = 2$ to within the precision offered by the measurements. These bursts with peak fluxes of about 1 Jy also showed dispersion measures (ranging from $553 \text{ cm}^{-3} \text{ pc}$ to $1104 \text{ cm}^{-3} \text{ pc}$) in considerable excess of that expected from the Galactic interstellar medium. Unlike the Perytons these four events were found in only one beam. This archival analysis drew data from the “High Time Resolution Universe” (HTRU) survey which in turn used a digital filter bank (Keith *et al.* 2010), whereas the older Parkes data were obtained with an analog filter bank. Thornton and colleagues, like Lorimer *et al.* (2007) before, argue that the excess dispersion arose primarily in the IGM and infer redshifts ranging from $z = 0.45$ to 0.96 . These authors quote an all-sky rate of $\dot{\mathcal{N}} \approx 10^4 \text{ events day}^{-1}$. This is a remarkably high rate for an extra-galactic population (assuming no repetitions).

Curiously, the brightest burst in Thornton *et al.* (2013) ex-

hibits an asymmetric pulse shape, with a rise time smaller than the decay time. Furthermore, for this event and the *Sparker*, the pulse width is frequency dependent with the pulse width $\propto \nu^{-m}$ and $m \approx 4$. Such a characteristic pulse frequency-dependent broadening is also seen in pulsars with large DMs and attributed to multi-path scattering as the radio pulse traverses through inhomogeneous structures in the interstellar medium. In contrast, the Perytons show symmetrical pulse profiles.

To summarize, analysis of the Parkes Multi-Beam data with two different pulsar backends (one analog and the other digital) taken during the course of pulsar searches in the 1.4 GHz band at the Parkes Observatory have shown three types of impulsive radio bursts: Perytons (Burke-Spolaor *et al.* 2011), the *Sparker* (Lorimer *et al.* 2007) and “Fast Radio Bursts” (Thornton *et al.* 2013). There is agreement that Perytons are of terrestrial origin. In contrast, the *Sparker* and FRBs have been argued to arise from extra-galactic sources.

2. THE RATIONALE AND LAYOUT OF THE PAPER

The inference that the *Sparker* and FRBs are of extra-galactic origin is not unreasonable. However, great claims need great proofs. It is important to explore if there are plausible explanations of the excess electron column density arising either in our own Galaxy or in its extended environs. It is this exploration of alternative frameworks that is the primary purpose of this paper.

There are only three observational clues for FRBs:

- I. The arrival time of the pulses vary as ν^{-2} where ν is the sky frequency of the pulse.
- II. For two events the width of the pulse scales as ν^{-4} .
- III. The all-sky rate of the FRBs is $\dot{\mathcal{N}} \approx 10^4$ events per day.

Beyond this we have little information about their angular distribution (isotropic versus Galactic) or homogeneity (how rapidly does the source count increase with decreasing flux or fluence?).

The first version of this paper was completed and submitted (to the Astrophysical Journal) a few months after the Lorimer *et al.* (2007) paper was published. The primary result of that manuscript was that, if the frequency dependent arrival time was due to propagation, then the *Sparker* had to be located beyond the Local Group. However, after inspection of the raw data of the *Sparker* (kindly provided by D. Lorimer) we developed some doubts about the celestial nature of the event and so we withdrew the manuscript. Subsequently, the emergence of Perytons further questioned the celestial origin of the *Sparker*. The publication by Thornton *et al.* (2013) showed that the *Sparker* was not unique. Furthermore, the rash of papers attempting to explain the origin of FRBs shows the general acceptance of the extra-galactic nature of FRBs. Our interest was revived – whence this paper.

The paper is quite long and so a summary of the goals is likely to help prepare the reader as she/he gets ready to read the rest of the paper. The goals of this paper are three fold:

- A. Accepting that the ν^{-2} arrival time pulse sweep arises from propagation in cold plasma, we attempt to constrain the size (L) and distance (d) to the nebula which contains this cold plasma. Clearly d is smaller than the distance to the source, D .

- B. The events, by virtue of being impulsive, must arise in compact regions. We investigate whether the proposed models would allow for decimetric radio pulses to propagate freely from the explosion site.
- C. Given the difficulty of an extra-galactic origin for the *Sparker* and FRBs, we consider the possibility that the trajectory of the pulse in the arrival-time-frequency plane is a property of the source itself⁷ and that Perytons, the *Sparker* and FRBs are all local sources. We confront this “unified” model with the observations.

The outline is as follows. The *Sparker* by its sheer brilliance, by having the lowest DM of the proposed Fast Radio Burst family, and by having a DM similar to Perytons still claims an important position in this discussion. As such we review this event in considerable detail. In §3 we summarize the basic observations of the *Sparker*. In §4 we posit an intervening nebula that can account for the excess DM inferred for the *Sparker*. Using H α surveys, *Galaxy Evolution Explorer* (GALEX) ultraviolet (UV) data, and the fact that the decimetric signal from the *Sparker* cannot be heavily absorbed by the ionized nebula, we exclude portions of the *L-d* phase space. We conclude that the *Sparker* cannot be located in our Galaxy, in the SMC, nor even in the Local Group. We investigate potential caveats to this important conclusion: a porous nebula (§5), a nebula ionized by shocks instead of UV photons (§6) and the possibility that the hot corona of a star can provide the excess DM (§7).

In §8 we conclude that the simplest explanation is that the *Sparker*, and by implication the FRBs, is located well outside the Local Group. In §9–10 we review the proposed models for FRBs. We check whether the models allow for successful propagation of decimetric radiation from the site of the explosion, and separately we check if the large daily rate of FRBs can be accommodated by the proposed models. We find several proposed models fail on the first test and all but one physically motivated models are severely challenged by the large daily rate of FRBs. We find that a model in which the radio pulses arise from giant flares from young extra-galactic magnetars is attractive on both counts (§10). In §11 we investigate the frequency dependent broadening seen in one FRB and the *Sparker* and conclude that this broadening (if due to propagation) is best explained as due to multi-path propagation in dense interstellar medium in the vicinity of the progenitor star.

In §12 we abandon the assumption that the v^{-2} arrival time pulse sweep is due to propagation, but instead attribute the frequency sweep as a property of the source itself. We investigate plausible man-made, solar and stellar sources. The Perytons are undeniably local phenomena and yet share many features with the *Sparker* and the FRBs. In §13 we present a plausible model unifying these three phenomena with the Perytons taking place close to the Parkes telescope and the FRBs the furthest away with the *Sparker* in between. We readily admit that our model for “unifying” the Perytons, the *Sparker*, and the FRBs is not based on a physically motivated model.

We summarize in §14. In short, there is little doubt that Perytons are terrestrial signals. We are struck by and troubled by the DM of the *Sparker* being the same as the mode of the DMs of the Perytons. It is not unreasonable to conclude that the *Sparker* is a Peryton that occurred in the first

(or so) Fresnel zone for the Parkes telescope. It is not a great leap to conclude that FRBs are simply distant versions of the *Sparker*. Of the extra-galactic models, we favor the model in which FRBs result from giant flares from young magnetars. The model can explain the high daily rate of FRBs.

We end this section by noting that unlike in 2007 we now have the *Sparker* and at least four FRBs. Given this situation, a reader, at first blush, may wonder why is it important to discuss one specific case (the *Sparker*) in some detail. In our opinion, when one is confronted by a new and astonishing phenomenon, it is almost always useful to approach the observations with elementary but robust analyses. In some cases it may well be that a simpler explanation would suffice (e.g., the event of Keane *et al.* 2012, and other claimed FRBs at low Galactic latitudes are arguably RRATs hiding behind H II regions).⁸ Second, while we are not able to make concrete progress (establish or reject an extra-galactic hypothesis) we are open to the idea that astronomers at Parkes have indeed uncovered a most fantastic phenomenon – brilliant sparks at extra-galactic distances. Consistent with our (presently) agnostic view, we detail in §E the potential use of FRBs to probe intergalactic matter.

3. THE SPARK

The event reported by Lorimer *et al.* (2007) was found in a re-analysis of data obtained with the 13-beam system mounted at the Cassegrain focus of the Parkes 64-m radio telescope. The data from which this pulse was discovered was originally obtained to look for pulsars in the Small Magellanic Cloud (SMC). For each of the two linear polarizations, the signal from each of the thirteen beams (sky frequency 1.28–1.52 GHz; Staveley-Smith *et al.* 1996) was fed into a filter bank with 96 channels, each 3 MHz wide, and followed by square-law detection. The detected signal from the two polarization signals was summed, filtered, and digitally sampled at the rate of 4 kHz (Manchester *et al.* 2001). The authors searched the data stream for single pulses in the range 1 ms to 1 s and DMs between 0 and 500 cm⁻³ pc.

A single intense burst of short duration (< 5 ms; epoch, UTC 2001 Aug 24, 19:50:01) with best fit DM of 375 ± 1 cm⁻³ pc was identified. The burst was so intense that it saturated one of the beams [signal-to-noise ratio (SNR) > 100] and was readily detected in two adjacent beams (see §A for further analysis). The peak flux was estimated to be $S \approx 30 \pm 10$ Jy. The high precision with which the DM was inferred means that the data are consistent with a cold plasma dispersion model to equally good precision.

Our attempts to better localize the position of the *Sparker* by accounting for the measured signal levels in different beams with the (far field) Parkes Multi-Beam response function (updated by L. Staveley-Smith following Staveley-Smith *et al.* 1996) did not converge to a well defined region. In order to make progress we adopt a localization that makes use of approximate circular symmetry of the beams. This localization region is a polygon (aka “kite”) and is displayed graphically in Figure 1 and numerically in Table 5 (§A). When a single position is needed (e.g., to compute foreground extinction) we use the position of the beam in which the signal was

⁷ a “chirped signal” in the parlance of electrical engineering

⁸ Indeed, as we go to press, a plausible intervening H II region which can account for the large inferred DM has been identified (Bannister & Madsen 2014) for the FRB reported by Keane *et al.* (2012). In a similar vein, we note that the same caution would apply to Arecibo events found close to the Galactic equator.

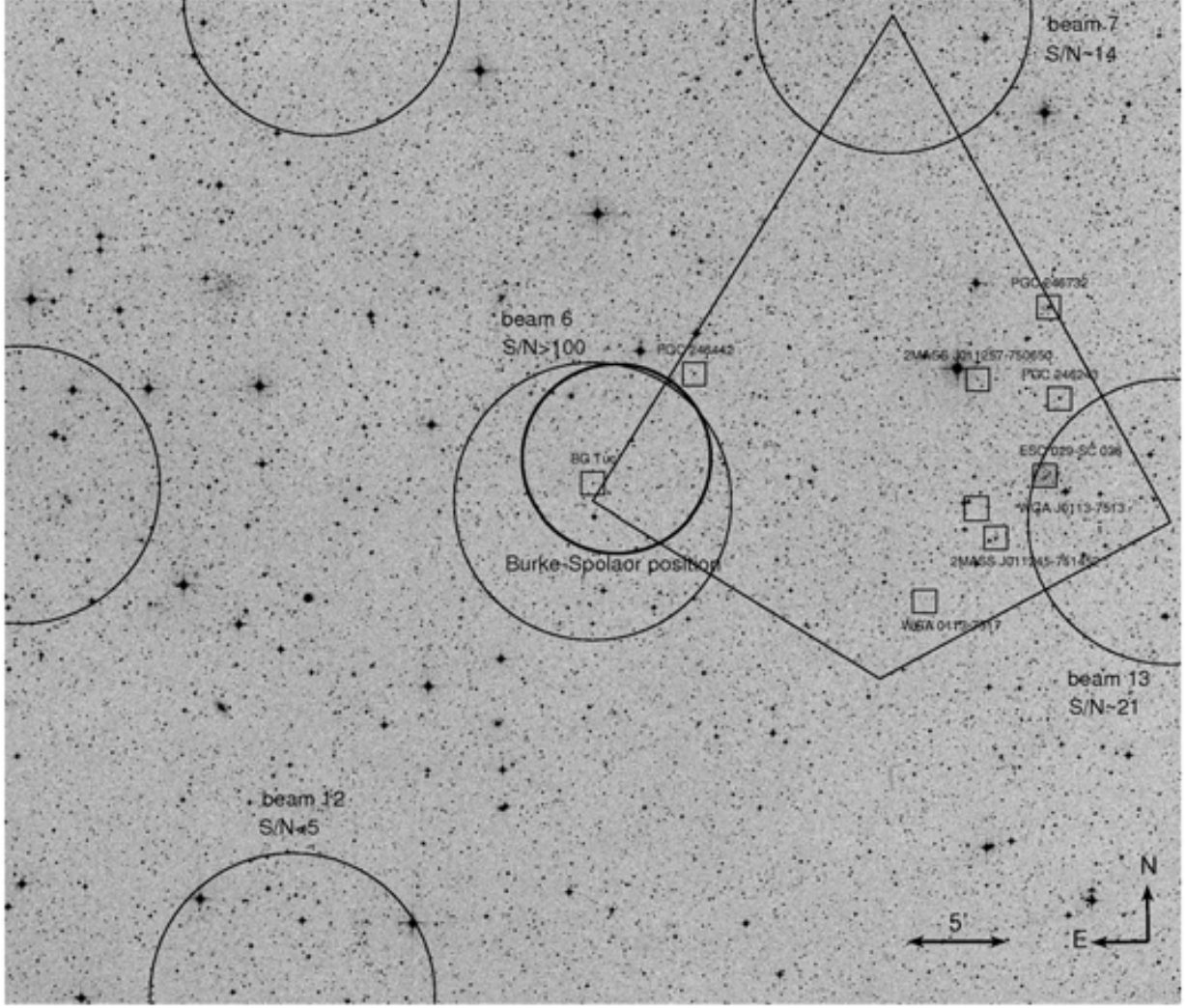


FIG. 1.— A localization of the *Sparker*. The black circles of radius 7.05 or 7.25 arc-minute represent the Parkes beams (see Table 3 for further details). The polygon is a conservative localization region for the *Sparker* (see §A for details). The black smaller circle marked “Burke-Spolaor position” is the best fit position for the *Sparker* obtained by Burke-Spolaor *et al.* (2011). The background is from the Digitized Sky Survey with the original data coming from the UK Schmidt Second Epoch Survey (IIIaF+RG610). Objects noted in SIMBAD or NED are noted. The object marked as ESO 029-SC 036 is a cluster of galaxies.

saturated: RA=01h18m06.0 $\delta = -75:12:19$. (J2000).

3.1. Energetics

We adopt the following values for the *Sparker* at the fiducial frequency, $\nu_0 = 1.4$ GHz: peak flux density, $S_0 = 30$ Jy, measured pulse width of $\Delta\tau_0 = 5$ ms and intrinsic pulse width, $\Delta t = 1$ ms. The broad band spectrum of the *Sparker* appears not to be well determined (D. Lorimer, pers. comm. and our own analysis). The usable data for the *Sparker* are from the unsaturated beams and so one can expect the data to suffer from chromatic effects.

In contrast to the *Sparker* the four events reported by Thornton *et al.* (2013) are found only in one beam. Thus the broad band spectrum of these events can be expected to be less prone to chromatic problems discussed above. The four events show reasonably good SNR across the entire 1.28–1.52 GHz range. This rough uniformity suggests that a power law spectrum is adequate to describe the broad-band spectrum and the power law index, α is not too far from zero. We assume a power law

model for the fluence spectrum, $\mathcal{F}(\nu) \propto \nu^\alpha$. When a specific value is called for, we use $\alpha = -1$.

The broadband fluence of the *Sparker* is

$$\mathcal{F} \approx -\frac{S_0 \tau_0 \nu_0}{\alpha + 1} \left(\frac{\nu_0}{\nu_l} \right)^{\alpha+1}, \text{ for } \alpha < -1, \quad (1)$$

$$= S_0 \nu_0 \tau_0 \ln \left(\frac{\nu_u}{\nu_l} \right) \text{ for } \alpha = -1; \quad (2)$$

for here ν_u and ν_l are the upper and lower cutoff frequencies of the broad band spectrum and we assume that $\nu_0 \ll \nu_u$. A conservative estimate of the bolometric fluence is obtained with $\alpha = -1$ and setting the log factor to 10. With these two assumptions we find $\mathcal{F} \approx 2.1 \times 10^{-14}$ erg cm $^{-2}$. Thus the isotropic radiated energy in the radio band alone is

$$\mathcal{E}_R \approx 2.5 \times 10^{30} D_{\text{kpc}}^2 \text{ erg} \quad (3)$$

where D_{kpc} is the distance to the source.⁹

3.2. Constraints from Brightness Temperature

The brightness temperature can be computed from the Rayleigh-Jeans formula, $S_0 = 2kT_B(v_0^2/c^2)\pi(R/D)^2$, where R is the radius of the source. Provided that there are no relativistic flows $R < c\Delta t$, and the minimum brightness temperature is

$$T_B(v_0) \lesssim 1.6 \times 10^{24} \left(\frac{D}{1 \text{ kpc}} \right)^2 \left(\frac{\Delta t}{1 \text{ ms}} \right)^{-2} \text{ K}. \quad (4)$$

The emission mechanism is either incoherent or coherent. We will consider the first option. It is well known that brightness temperatures in excess of 10^{12} K lead to severe Compton losses (Kellermann & Pauliny-Toth 1969). If, however, there is a relativistic outflow (with a bulk Lorentz factor, Γ), then the observed duration is compressed by the forward motion (towards us) and also the flux enhanced (for the same reason). As a result the inferred brightness temperature (Equation 4) is $\approx \Gamma^3$ larger than that in the rest frame of emission (Padmanabhan 2002, pp. 490). Limiting the brightness temperature in the source frame to 10^{12} K then leads us to

$$D_{\text{kpc}}^2 \lesssim \frac{\Gamma^3}{10^{12}}. \quad (5)$$

Gamma-ray bursts (GRBs), cosmic explosions with the most relativistic bulk outflows, have inferred values of Γ as high as 10^3 . In this scenario, $D \leq 100$ pc. Thus, the observed excess dispersion measure must clearly arise from the source (or its circumstellar medium). We investigate this possibility in §7. Conversely, should we find incontrovertible evidence that the *Sparker* is located at great distances (say, even 1 kpc), then the emission process must be coherent. In principle, coherent processes can produce (almost) arbitrarily high brightness temperature radiation – provided that the emitting region consists of highly relativistic matter.

4. THE DISTANCE TO AND THE SIZE OF THE DM NEBULA

The excess DM inferred towards the *Sparker* requires that there be an intervening ionized nebula. Our goal in this section is to derive some constraints on the size (or diameter), L , and the distance, d , to the nebula. We will assume the following values for Galactic ionized gas: DM and emission measure (EM; see below) towards the Galactic pole of $25 \text{ cm}^{-3} \text{ pc}$ and $2 \text{ cm}^{-6} \text{ pc}$ (Cox 2000; §21.1).

For simplicity, we assume the nebula is a sphere of hydrogen with uniform electron density, n_e . Such a nebula will manifest itself via $\text{H}\alpha$ recombination radiation and free-free absorption. Separately, provided the nebula is photo-ionized, the UV continuum from the ionizing source may be detectable. Our approach is to compute the expected signatures (recombination radiation, UV continuum, free-free absorption) and use existing observations to constrain the phase space of d and L . We will accept the IGM solution only if our exploration rules out Galactic or near-Galactic possibilities.

The primary parameter which determines the strength of the $\text{H}\alpha$ emission and free-free absorption is the emission measure. The dispersion measure of the intervening nebula is

$\text{DM} = L_{\text{pc}} n_e \text{ cm}^{-3} \text{ pc}$ and the corresponding EM (in the usual units) is

$$\text{EM} = \text{DM}^2 L_{\text{pc}}^{-1} \text{ cm}^{-6} \text{ pc}, \quad (6)$$

where $L_{\text{pc}} = L/(1 \text{ pc})$.

4.1. Free-free absorption

The free-free optical depth is given by

$$\tau_{\text{ff}}(\nu) = 4.4 \times 10^{-7} \text{EM} \left(\frac{T_e}{8,000 \text{ K}} \right)^{-1.35} \left(\frac{\nu}{1 \text{ GHz}} \right)^{-2.1}, \quad (7)$$

where T_e is the electron temperature and ν is the frequency in GHz (Lang 1974; p. 47). The temperature normalization is appropriate for a photo-ionized nebula. Combining Equations 6 and 7 we find

$$\tau_{\text{ff}}(\nu) = 2.7 \left(\frac{\nu}{\nu_0} \right)^{-2.1} \left(\frac{T_e}{8,000 \text{ K}} \right)^{-1.35} \left(\frac{L}{0.01 \text{ pc}} \right)^{-1} \quad (8)$$

where we have set $\text{DM} = 350 \text{ cm}^{-3} \text{ pc}$ (accounting for a Galactic contribution of $25 \text{ cm}^{-3} \text{ pc}$). From this equation we immediately see that invoking very compact nebulae, $L < 0.01 \text{ pc}$, is problematic. The observed fluence spectrum, $\mathcal{F}(\nu)$, is related to the true fluence spectrum, $F(\nu)$, as follows:

$$\mathcal{F}(\nu) \propto F(\nu) \exp \left[-\tau_0 \left(\frac{\nu}{\nu_0} \right)^{-2.1} \right]. \quad (9)$$

As discussed earlier (§3.1) the fluence spectrum is not well measured. In the vicinity of frequency ν , we can make an expansion

$$\begin{aligned} \alpha' &\equiv \frac{d \ln \mathcal{F}(\nu)}{d \ln \nu} \Big|_{\nu} \\ &= \beta + 2.1 \tau_0 \left(\frac{\nu}{\nu_0} \right)^{-2.1}, \end{aligned} \quad (10)$$

where the intrinsic spectrum in the vicinity of ν_0 is assumed to be a power law, $F(\nu) \propto \nu^\beta$. Thus even a modest amount of optical depth can result in extra-ordinarily steep spectrum for the underlying spectrum. There are two consequences.

First, an intrinsic spectrum as steep as the values discussed above would be remarkable. Millisecond pulsars possess the reputation for having the “steepest” spectra. Examples include PSR 1937+21 ($\alpha = -2.7$; Backer *et al.* 1982; Erickson 1983) and PSR 1957+20 ($\alpha = -3$; Fruchter *et al.* 1990). A perusal of the literature shows two sources which are even steeper: the Sun (Giménez de Castro *et al.* 2006) and GCRT J1745–3009 (Hyman *et al.* 2007). For the latter source, a weak burst was found to have a spectral index of $\alpha = -13.5 \pm 3$. This was measured over a limited frequency range from 310 to 338 MHz. The Sun is much better studied. For some spiky bursts from the Sun the spectrum is exponential, consistent with the spectrum emitted by a mono-energetic electron gyrating in a uniform field (see §B). An exponential spectrum can give an arbitrarily high power law index for frequency (see §B).

A steep intrinsic spectral index would thus favor (on empirical grounds) an exponential distribution for $F(\nu) \propto \exp(-\nu/\nu_c)$, where ν_c is the characteristic frequency. In this case, Equation 10 becomes

$$\alpha' = -\frac{\nu}{\nu_c} + 2.1 \tau_0 \left(\frac{\nu}{\nu_0} \right)^{-2.1}. \quad (11)$$

¹⁰ We use the convention that a particular quantity is normalized with the appropriate physical unit displayed as a subscript in Roman font. Thus D_{kpc} is the distance to the source in units of kpc.

It is clear from this equation that a large value of τ_0 ($\gg 1$) would result in α' varying rapidly even over the 1.2–1.5 GHz band of the Parkes pulsar spectrometer. We see no evidence for such strong spectral curvature for either the *Sparker* or the FRBs.¹¹

Next, the bolometric fluence in the exponential model is

$$\mathcal{F} = S_0 \tau_0 v_c \exp(v_0/v_c + \tau_0). \quad (12)$$

Let us consider the implication of invoking significant free-free absorption. For instance, setting $\tau_0 = 5$ in Equation 11, we find $v_c \approx v_0/12$. Propagating this choice of v_c to Equation 12 results in an isotropic emission of nearly $5 \times 10^{35} D_{\text{kpc}}^2$ erg. Even at 100 pc the inferred energy loss in the radio band would severely challenge what is observed from the most active stars.

Continuing with this theme and setting $\tau_0 < 5$ we find, from Equation 8,

$$L > L_{\text{ff}} = 5.6 \times 10^{-3} \text{ pc}. \quad (13)$$

Note that this severe constraint on L has no dependence on d . It also has no dependence on the angular size of the nebula since by assumption the angular size of the *Sparker* is assumed to be smaller than that of the putative nebula. The nebula size, L_{ff} (Equation 13), corresponds to $2 \times 10^5 R_\odot$.

From Equation 13 we conclude that *Sparker* cannot arise from a terrestrial phenomenon. The reader may find it instructive to read §C to appreciate typical DM and EM in any reasonable stellar context (including compact binaries with a main sequence companion and so on). Luan (2014) arrived at the same conclusion independently. The only way to avoid a stellar model for FRBs is to invoke high temperatures – a possibility that we treat in depth in §7.

4.2. Dispersion Measure: Galactic Contribution

In Figure 2 we present a wide-field overview of the region of the *Sparker*. The *Sparker* is about three degrees South of the center of the SMC (see Figure 2). The projected transverse distance is 3.1 kpc, assuming a distance of 60 kpc to the SMC (Storm *et al.* 2004). In Figure 3 we present a zoom-in of the field centered around the SMC. As noted by Lorimer *et al.* (2007) the *Sparker* lies outside the bright H I and the bright H α boundaries of the SMC.

In the region of the sky containing the *Sparker* and the SMC there are six pulsars¹² (Manchester *et al.* 2005) and one magnetar (McGarry *et al.* 2005). One pulsar (PSR J0057–7201) has a DM of $27 \text{ cm}^{-3} \text{ pc}$ (Crawford *et al.* 2001) – consistent with being a Galactic pulsar located above the Warm Ionized Medium (WIM) layer. The DMs of the remaining five pulsars range from 70 to $205 \text{ cm}^{-3} \text{ pc}$ (McConnell *et al.* 1991; Crawford *et al.* 2001; Manchester *et al.* 2006). These five pulsars are generally thought to be associated with the SMC. As a matter of reference, the pulsars in the Large Magellanic Cloud (LMC) have an excess (over the Galactic value) of about $100 \text{ cm}^{-3} \text{ pc}$. Five degrees away and located at a distance of 4 kpc (in the inner halo of our Galaxy), the globular cluster 47 Tucanae hosts a hive of pulsars with typical DMs of about $24 \text{ cm}^{-3} \text{ pc}$.

¹¹ Parenthetically we note that should a pulse be found with positive and large observed spectral index (that is $\alpha \gg 1$; but not so high that the pulse is entirely absorbed) then a plausible explanation is that $\tau_0 \gtrsim 1$.

¹² <http://www.atnf.csiro.au/research/pulsar/psrcat>

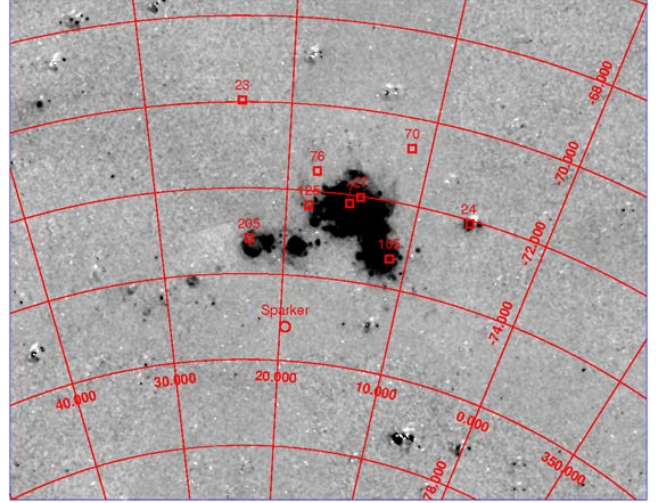


FIG. 2.— Tangential projection of the known pulsars (marked by squares; the number next to each square is the dispersion measure of the pulsar) in the vicinity of the SMC with North up and East to the left. The *Sparker* is marked by a circle. The background is the diffuse H α emission obtained from the Southern H α Sky Survey (Gaustad *et al.* 2001). The grid marks the right ascension (RA) and the declination (Dec), both in units of degrees. The South Celestial Pole is towards the bottom of the Figure. The pulsar-rich globular cluster, 47 Tucanae, is located at RA $\approx 6^\circ$ and Dec $\approx -72^\circ$ (square box; the mean dispersion measure of the pulsars in this cluster is $24 \text{ cm}^{-3} \text{ pc}$). The Large Magellanic Cloud (not marked) is located to the North and East of the SMC and lies outside this map.

Thus, the first conclusion is that the Galactic contribution to the observed DM of the *Sparker* (assuming, say, a halo location) is no more than $25 \text{ cm}^{-3} \text{ pc}$. As can be gathered from discussion at the beginning of this section, the Galactic contribution to the EM is negligible.

Next, the angular size of the DM-inducing nebula for the *Sparker* cannot be larger than, say, $\theta_{\text{DM}} \sim 5^\circ$. Otherwise, we would expect a larger DM for the pulsars in the neighborhood. This conclusion is true whether the *Sparker* is located in the halo or the SMC. Thus we obtain our first constraint:

$$L < d\theta_{\text{DM}}, \quad (14)$$

provided that $D < 60 \text{ kpc}$ (the distance to the SMC).

4.3. Dispersion Measure: SMC Contribution

With respect to Figure 3 and noting the DMs of PSR J0045–7042 ($70 \text{ cm}^{-3} \text{ pc}$) and PSR J0111–7131 ($76 \text{ cm}^{-3} \text{ pc}$), we suggest that the SMC has an extended (diameter of 4 degrees) ionized halo which contributes about $50 \text{ cm}^{-3} \text{ pc}$ (which when added to the Galactic DM yields a total of $75 \text{ cm}^{-3} \text{ pc}$). Assuming a spherical geometry and a diameter of 4 kpc, this extended diffuse halo of the SMC has a mean electron density of 0.0125 cm^{-3} and the corresponding EM contribution is $0.63 \text{ cm}^{-6} \text{ pc}$. Incidentally, we note that the H I column density towards PSR J0045–7042 (DM = $70 \text{ cm}^{-3} \text{ pc}$) is $2.1 \times 10^{20} \text{ cm}^{-2}$ (Figure 4) and is comparable to the column density arising from the ionized SMC halo.

We conclude that the Galactic+SMC DM contribution is about $75 \text{ cm}^{-3} \text{ pc}$. Thus, were the *Sparker* to be located in or behind the SMC, the excess DM is $300 \text{ cm}^{-3} \text{ pc}$ and corre-

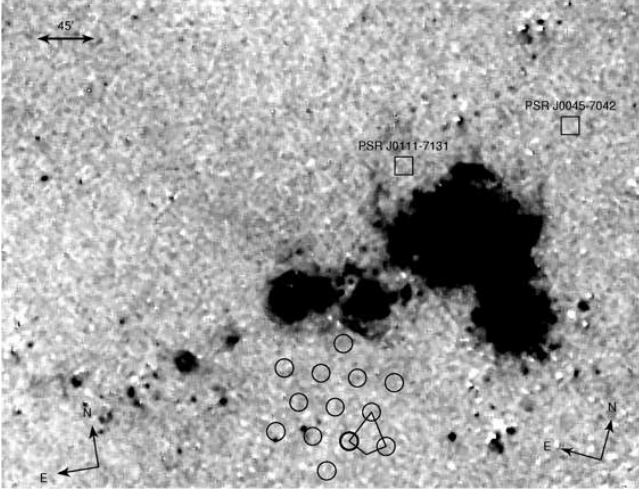


FIG. 3.— A zoom-in of the Southern Sky $H\alpha$ Survey containing the localization of the *Sparker*. The beams listed in Table 3 are shown as circles with radius of about 7 arcminutes (the main beam size for each of the beams). The beam in which the *Sparker* saturated is shown with a thicker line. The polygon described in Table 5 is also displayed. Also marked are two SMC pulsars (open squares and marked by their names). Notice the absence of detectable $H\alpha$ emission towards the *Sparker* and the two SMC pulsars. The faint emission towards the North-East is the Magellanic Stream.

spondingly the emission measure is¹⁴,

$$EM^S = 9 \times 10^4 L_{pc}^{-1} \text{ cm}^{-6} \text{ pc}. \quad (15)$$

The superscript “S” (“G”) is used to indicate the expected EM assuming an origin for the *Sparker* at the distance of the SMC or beyond (or in the Galaxy). For the Galactic case, the excess DM corresponds to 350–375 $\text{cm}^{-3} \text{ pc}$.

4.4. Recombination Radiation: $H\alpha$

An ionized nebula emits recombination radiation (e.g., the Balmer series). The $H\alpha$ brightness is determined by the recombination rate and the fraction of recombinations that result in $H\alpha$ emission (see Reynolds 1984). For $T \sim 8,000 \text{ K}$ and assuming case B¹⁵ we find $I = 1.09 \times 10^{-7} \times EM \text{ erg cm}^{-2} \text{ s}^{-1} \text{ sr}^{-1}$, whence the usual statement that 1 Rayleigh¹⁶ of photon intensity corresponds to an EM of $2.2 \text{ cm}^{-6} \text{ pc}$.

The Southern $H\alpha$ Sky Survey (SHASS; see Figure 3) imaged the entire Southern Sky in a narrow band ($\Delta\lambda_{\text{SHASS}} = 16 \text{ \AA}$; this corresponds to a velocity width of $\pm 365 \text{ km s}^{-1}$) centered on the rest wavelength of $H\alpha$ (6563 \AA) and at an angular resolution of $0.8'$ (Gaustad *et al.* 2001). The rms per pixel is about 2 Rayleigh. When dealing with surface brightness it helps to divide the discussion into two parts: objects with a size bigger (“resolved”) or smaller (“compact”) than the angular size of the beam(s) of the survey(s).

¹⁴ We ignore the contributions to the EM from our own Galaxy and the SMC.

¹⁵ See Equation 9 of Valls-Gabaud 1998. We adopt the following recombination coefficient: $\alpha_B = 8.7 \times 10^{-14} T_4^{-0.89} \text{ cm}^3 \text{ s}^{-1}$, where T_4 is the temperature in units of 10^4 K (Osterbrock & Ferland 2006).

¹⁶ A unit of surface brightness commonly used in aeronomy. One Rayleigh is $10^6/(4\pi)$ photons per square centimeter per steradian per second. For the $H\alpha$ line, the intensity in cgs units is $2.41 \times 10^{-7} \text{ erg cm}^{-2} \text{ s}^{-1} \text{ sr}^{-1}$.

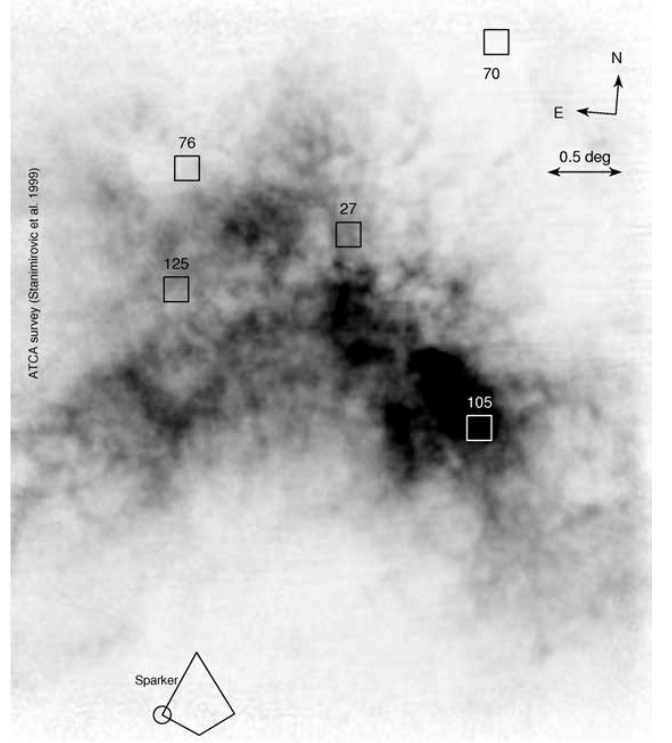


FIG. 4.— The neutral hydrogen ($H\text{ I}$) column density integrated over the heliocentric velocity range $88.5\text{--}215.5 \text{ km s}^{-1}$ in the direction towards the *Sparker*. The data were obtained with the ATCA (beam FWHM of 98 arcsec) supplemented by the Parkes 64-m single dish images. The polygon at the bottom of the image represents the *Sparker* localization (§A), while the circle shows the position and FWHM size of the beam in which the *Sparker* saturated the detector (Table 3). The gray-scale intensity range is -3×10^{19} to $8.4 \times 10^{21} \text{ atom cm}^{-2}$. Boxes (white and black) show the positions of known SMC and Galactic pulsars while the number accompanying each box shows the pulsar measured DM. At the position of the *Sparker*, the $H\text{ I}$ column density is $3.5 \times 10^{20} \text{ cm}^{-2}$. From Stanimirovic *et al.* (1999).

We first consider the resolved case. We determined that the SHASS 5- σ detection limit for a 1-degree diameter nebula is about 0.5 Rayleigh. The upper limit at a scale of one arc minute is naturally larger and was found to be 6 Rayleigh. We thus find

$$\frac{EM}{2.2 \text{ cm}^{-6} \text{ pc}} = 0.45 DM^2 L_{pc}^{-1} \lesssim R_{\text{SHASS}}, \quad (16)$$

where R_{SHASS} is the surface brightness (on the relevant angular scale). Using Equation 15 we obtain our second constraint:

$$\begin{aligned} L &\gtrsim 82 \text{ kpc for } \theta \sim 1^\circ, \\ L &\gtrsim 6.8 \text{ kpc for } \theta \sim 1'. \end{aligned} \quad (17)$$

Here $\theta = L/d$ is the angular diameter of the nebula. Note that the size constraint is independent of d , provided that the nebula has an angular size $\gtrsim 1^\circ$ or $\gtrsim 1'$, respectively.

Next consider the case of a nebula whose angular size is smaller than that of the resolution of the SHASS. The expected $H\alpha$ flux is

$$F_{H\alpha} = h\nu_\alpha R_{\text{SHASS}} \frac{\pi\theta^2}{4}, \quad (18)$$

where $h\nu_\alpha$ is the energy of an $H\alpha$ photon. Combining this equation with Equation 15 (and likewise for a Galactic location), we find

$$F_{H\alpha}^G = 10.5 \times 10^{-9} L_{\text{pc}} d_{\text{kpc}}^{-2} \text{ erg cm}^{-2} \text{ s}^{-1}, \quad (19)$$

$$F_{H\alpha}^S = 7.8 \times 10^{-9} L_{\text{pc}} d_{\text{kpc}}^{-2} \text{ erg cm}^{-2} \text{ s}^{-1}. \quad (20)$$

The point source limit for a single pixel of SHASS is $R_{\text{SHASS}} \Delta\Omega$ where $\Delta\Omega \sim 5.4 \times 10^{-8}$ steradian (corresponding to one SHASS pixel). Given that $R_{\text{SHASS}} = 6$ Rayleigh (see above) we find

$$F_{H\alpha} \lesssim 7.8 \times 10^{-14} \text{ erg cm}^{-2} \text{ s}^{-1}. \quad (21)$$

Combining the inequality (Equation 21) with Equations 19 and 20 we derive the following constraints:

$$L_{\text{pc}} d_{\text{kpc}}^{-2} \lesssim 0.75 \times 10^{-5} \quad (\text{Galactic}) \quad (22)$$

$$L_{\text{pc}} d_{\text{kpc}}^{-2} \lesssim 1 \times 10^{-5} \quad (\text{SMC and Beyond}) \quad (23)$$

Combining Equation 22 with Equation 13 we find the nebula cannot be located any closer than

$$d_{\text{min}}(H\alpha) \sim 27 \text{ kpc}. \quad (24)$$

Parenthetically, we note that, *in principle*, a similar exercise can be carried out for the two-photon emission, traced by UV observations.

TABLE 1
THE PHYSICAL PARAMETERS OF THE ALLOWED IONIZED
NEBULA

d (kpc)	L (pc)	θ (arcsec)	$\langle n_e \rangle$ cm^{-3}	\dot{N}_R s^{-1}
27	5.6×10^{-3}	0.04	5.4×10^4	2.0×10^{45}
60	2.7×10^{-2}	0.09	1.1×10^4	9.8×10^{45}
303	0.69	0.47	4.35×10^2	2.5×10^{47}
1000	7.5	1.55	40	2.7×10^{48}

Notes: d is the distance to the ionized spherical nebula, L is the maximum permitted diameter at that distance, $\theta = L/d$ is the corresponding angular diameter, $\langle n_e \rangle = DM/L$ is the corresponding mean electron density in the nebula, and \dot{N}_R is corresponding inferred rate of recombinations (see §4.4). For the first entry we used the DM appropriate for a Galactic location, $DM = 350 \text{ cm}^{-3} \text{ pc}$. For the remaining we used $DM = 300 \text{ cm}^{-3} \text{ pc}$. For all distances, $d > 27 \text{ kpc}$, the size of nebula is constrained to lie between L_{ff} (Equation 13) and the values indicated in the second column.

4.5. UV Continuum

A nebula ionized by one or more hot stars would be accompanied by a strong underlying stellar continuum. Here we explore archival data to see if suitable ionizing stars exist within the *Sparker* region. We then match the rate of recombination for the nebula (which is a function of L and thence of d), \dot{N}_R , to the rate of ionization by possible ionizing sources, \dot{N}_I . The strongest plausible ionizing source or the most distant ionizing source then provides the largest d . It is important to understand that this exercise will only constrain ionizing sources within (at best) the Local Group. The exercise does not constrain very distant ionizing sources (e.g., the IGM)

The rate of recombinations is $\dot{N}_R = \pi/6 n_e^2 \alpha_B L^3$ where α_B is the recombination coefficient (see footnote 15). Consistent with the spirit of this section (namely, a photo-ionization

model), we assume $T = 8,000 \text{ K}$. For a given distance, d , we derive a maximum nebular diameter, L , using the constraints provided in the previous section and thence \dot{N}_R . The calculations are summarized in Table 1. We find that \dot{N}_R is as small as $2 \times 10^{45} \text{ s}^{-1}$ and as large as $2.7 \times 10^{48} \text{ s}^{-1}$ (at 1 Mpc). The corresponding minimum luminosity in ionizing photons (assuming photons with energy just above the Lyman continuum) is $\dot{N}_R h\nu_1$ where $h\nu_1$ is the energy of a photon at the Lyman edge. This luminosity ranges between $4.4 \times 10^{34} \text{ erg s}^{-1}$ and $5.9 \times 10^{37} \text{ erg s}^{-1}$. The inferred ionizing rates should be compared with that expected from O and B stars (Schaerer & de Koter 1997): $\log(\dot{N}_I) = 49.85$ for an O3V star [$T_{\text{eff}} = 51230 \text{ K}$ and $\log(L_{\text{bol}}/L_\odot) = 6.0$] and $\log(\dot{N}_I) = 47.77$ for a B0.5V star [$T_{\text{eff}} = 32060 \text{ K}$ and $\log(L_{\text{bol}}/L_\odot) = 4.7$].

The *Galaxy Evolution Explorer* (GALEX) UV space telescope (Martin *et al.* 2005) is well suited to search for and characterize potential hot (and thus ionizing) sources. The GALEX images are shown in Fig. 5, and have exposure times of 135 s in both the far-UV (FUV) channel (center wavelength, 1538 Å; FWHM = 226 Å) and the near-UV (NUV) channel (2289 Å; FWHM = 794 Å).

Only hot stars with $T_{\text{eff}} \gtrsim 2 \times 10^4 \text{ K}$ are capable of ionizing hydrogen atoms. The extinction-corrected GALEX Color-Magnitude diagram (CMD; assuming all sources are outside the Galaxy) for detected sources in the *Sparker* region is shown in Figure 6. The extinction was corrected using the Galactic color excess in the direction of the *Sparker* (Schlegel, Finkbeiner & Davis 1998), a total-to-selective extinction ratio derived from the Cardelli, Clayton & Mathis (1989) extinction law (see §2.3 of Wyder *et al.* 2007), and assuming $R_V = 3.08$. As can be seen from Bianchi *et al.* (2007, Figure 7), the GALEX color, $\Delta_{UV} \equiv FUV - NUV$, of stars with $T_{\text{eff}} \gtrsim 2 \times 10^4 \text{ K}$ is $\Delta_{UV} < 0$.

Although some objects in the polygon region (Figure 6) have $\Delta_{UV} < 0$, we argue that these stars are too faint to be the ionizing sources responsible for the DM nebula. The brightest object (labeled star A in Figures 5 and 6) with $\Delta_{UV} < 0$ within the polygon region has FUV AB magnitude of 16. From Δ_{UV} we compute an effective black-body temperature of 44,000 K. There are two possibilities: star A is either a foreground white dwarf or a main sequence B star located at 530 kpc. We note that the number of ionizing photons emitted by a 44,000 K WD is smaller by a factor of about 10^6 , relative to a main sequence star with the same effective temperature. Thus if star A is a foreground white dwarf then its ionizing capacity is negligible. Should star A be a young star in the outskirts of our Local Group (530 kpc) then it has the ability to power a nebula with $L = 0.69 \text{ pc}$ (see Table 1) and this nebula could account for the excess DM. However, the *Sparker* will either have to arise in this nebula or, if behind, be closely aligned with this star (recall that the angular size of the nebula is $0.4''$; see Table 1).

Using the same arguments as above, we conclude that all the other blue objects with fainter FUV magnitudes are not consistent with being hot main sequence stars in the SMC or closer according to the models in Bianchi *et al.* (2007). These objects are more likely to be foreground white dwarfs or background unresolved star-forming galaxies.

To summarize: we did not find any suitable ionizing source capable of maintaining a $DM = 350 \text{ cm}^{-3} \text{ pc}$ (Galactic origin) or $DM = 300 \text{ cm}^{-3} \text{ pc}$ (SMC or beyond location) nebula. We translate this constraint as follows. We equate the Lyman continuum flux of the hottest and brightest star in the localization

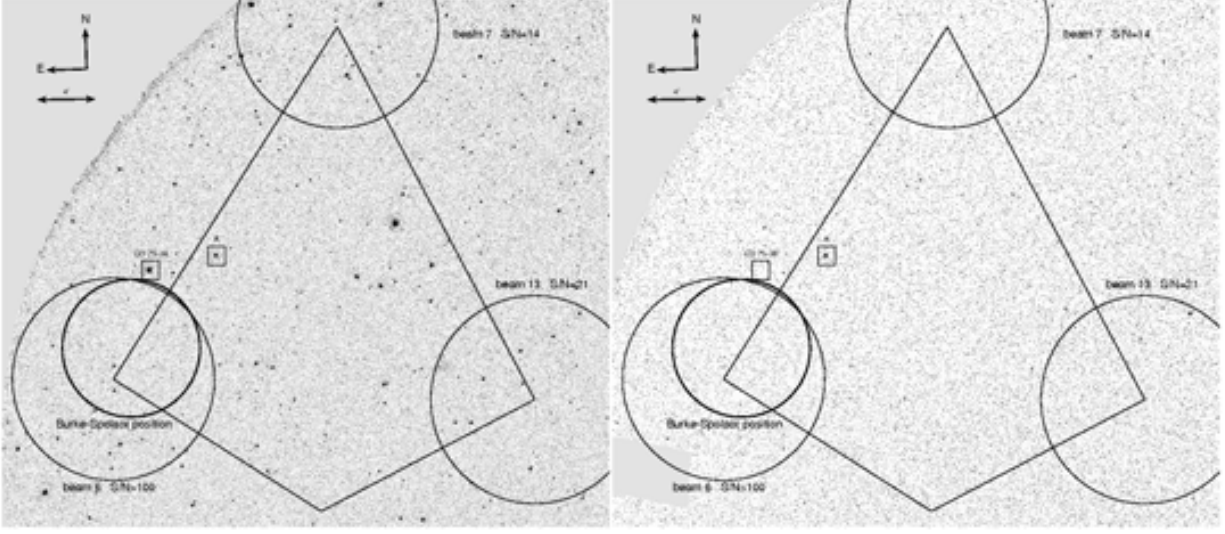


FIG. 5.— *GALEX* NUV (left) and FUV (right) images of the field of the *Sparker*. The signal-to-noise ratio = 3 limit corresponds to $FUV = 20.5$ mag and $NUV = 21.4$ mag. Here, following standard convention, the *GALEX* magnitudes are defined in the AB system (Oke 1974). CD-75 38 is a useful comparison star with $V = 10.35$, $B = 10.98$, $NUV = 15.310 \pm 0.001$ and $FUV = 22.23 \pm 0.08$. Star A is the hottest star within the polygon. See §4.5 for more discussion.

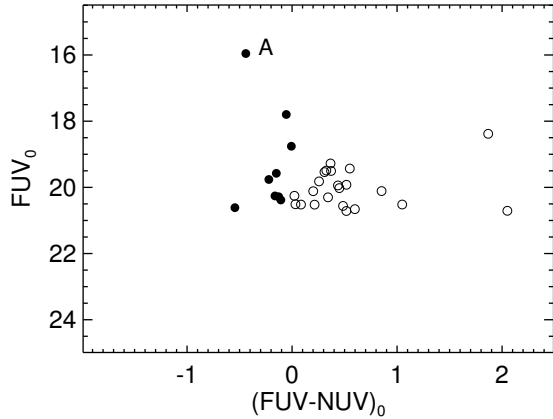


FIG. 6.— *GALEX* Color-Magnitude diagram (CMD) around the *Sparker* region. The colors and magnitudes were derived from the *GALEX* All-sky Imaging Survey image of this field. The magnitudes are extinction corrected [$E(B - V) = 0.054$ giving $A_{FUV} = 0.447$ mag and $A_{NUV} = 0.445$ mag]. The CMD is restricted to well-detected stars ($SNR > 3$, in both bands) within the polygon (see Figure 1). Stars with $\Delta UV < 0$ are marked by filled circles. The *GALEX* data were taken from the 7th data release.

region to the recombination rate of a photo-ionized nebula of diameter L . Since this is the maximum possible luminosity we derive our fifth constraint.

$$L_{\text{pc}} d_{\text{kpc}}^{-2} \lesssim 6 \times 10^{-8}. \quad (25)$$

When Equation 25 is combined with the free-free constraint (Equation 13) we find $d \gtrsim 303$ kpc. This demand is marked by an open square in Figure 7. The minimum distance estimate can be further improved by determining the luminosity class of star A (via spectroscopic observations). In any case, even if star A is indeed a young main sequence B star in the outskirts of the Local Group, then the *Sparker* is located at a distance of 530 kpc. This is shown by the inverted triangle

in Figure 7. In this framework star A cannot supply any more ionizing photons than that required for the minimum size nebula (at this distance; see Table 1) we can exclude any nebula with a size larger than that of the minimum nebula at 530 kpc or larger distance – whence the vertical line in Figure 7.

4.6. A Large Ionized Galactic Corona?

At this point one can imagine a location for the *Sparker* at the edge of our Local Group (though the progenitor population would have to be non-stellar and exotic). Is there any constraint on such a hypothesis?

To start with, we note that the DM contribution from the diffuse interstellar medium (ISM) in the Galactic halo and the Local Group is less than $5 \text{ cm}^{-3} \text{ pc}$ (Bregman 2007; Wang 2007). Nonetheless, let us be bold and postulate that our Local Group is adorned by a large ionized corona of radius $R_{\text{C,kpc}}$ and attribute all of DM^S to this corona.

With the DM^S fixed, assuming that the corona is composed of only Hydrogen, the mass of ionized gas in this corona is

$$M_C = 2.8 \times 10^7 R_{\text{C,kpc}}^2 M_{\odot}. \quad (26)$$

A corona with size of 100 kpc and 1 Mpc would have a mass of $2.8 \times 10^{11} M_{\odot}$ and $2.8 \times 10^{13} M_{\odot}$. To our knowledge there is no indication of such a massive interstellar halo in our Local Group (Bregman 2007; also, M. Shull, pers. comm.). As a result, we derive our last constraint, namely, we exclude any large structure on the scale of the Local Group, giving a constraint on the minimum distance of about 1 Mpc.

4.7. Allowed Phase Space

The following discussion is aided by inspecting Figure 7. There are two regions of phase space that are not excluded. First we discuss the small triangle in the lower right corner. Second we discuss the small rectangle in the upper-right corner. It is important to note that the phase space diagram is – consistent with the SHASS bandwidth – limited to distances less than 5 Mpc (assuming Hubble expansion).

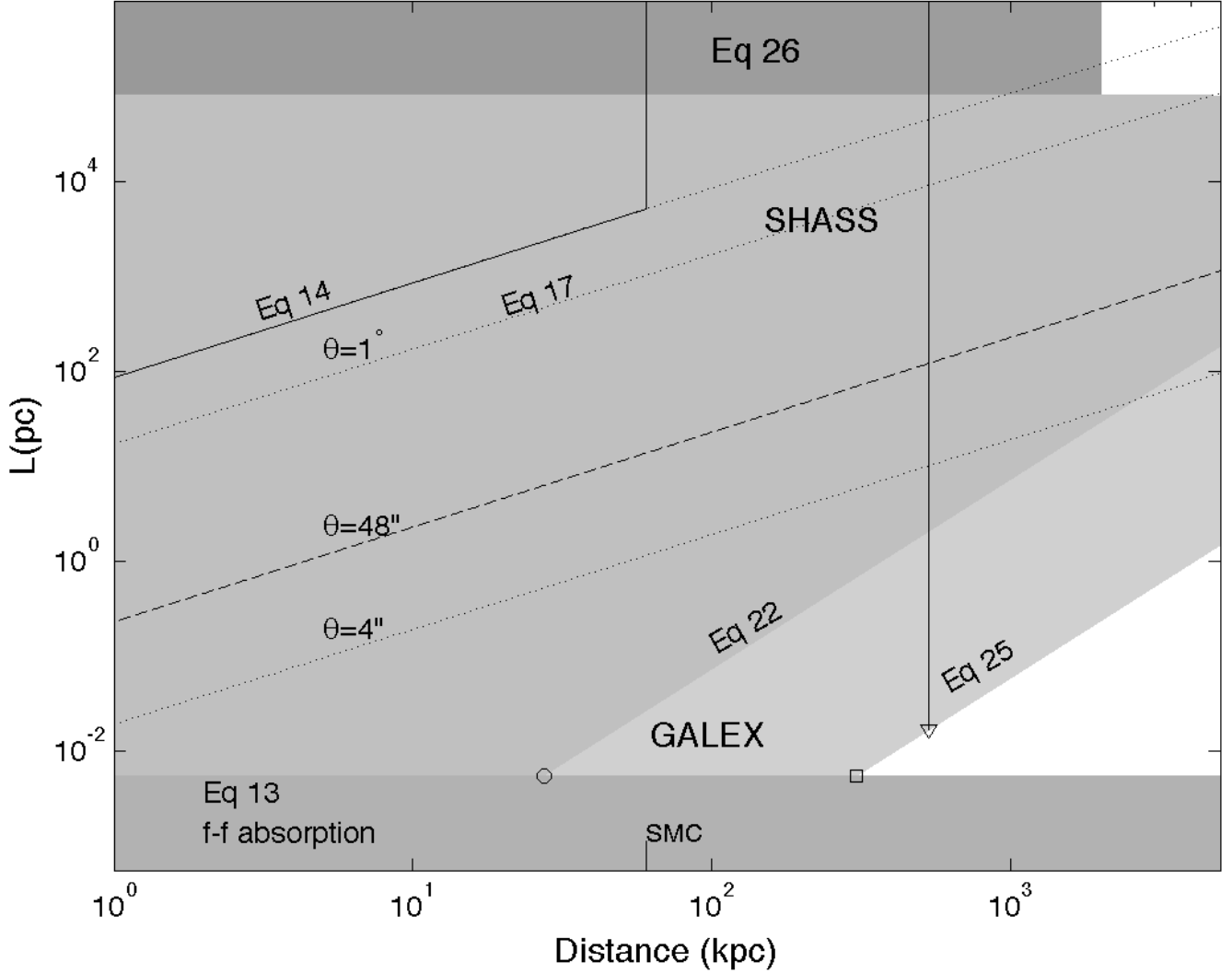


FIG. 7.— Parameter space of the size of the nebula (L in pc) and the distance to the nebula (d in kpc) based on the DMs of pulsars in the vicinity of the *Sparker* (Equation 14), the lack of radio free-free absorption of the burst itself (Equation 13), the surface brightness limit from SHASS (Equation 17), and the point source limit obtained from SHASS (Equation 22). The dashed line marks the lower edge of the phase space excluded by the lack of suitably powerful ionizing source (§25). The constraint on the mass of the interstellar halo leads to the top rectangle (marked as Equation 26). The circle [$d = d_{\min}(H\alpha) \sim 27$ kpc] and square [$d = 303$ kpc] mark the minimum allowed distance based on the absence of $H\alpha$ and Lyman continuum (GALEX) data. The SHASS constraint is limited to a distance of several Mpc due to the small width of the SHASS $H\alpha$ filter ($\pm 8 \text{ \AA}$). For this reason the plot cuts off at 5 Mpc.

Let us consider the lower triangle region. Any allowed nebula cannot be located any closer than $d_{\min}(H\alpha) = 27$ kpc (using only the $H\alpha$ data and Equation 13; marked by an open circle). If we assume photo-ionization, then the intervening nebula is beyond 303 kpc (marked by an open square). However, there is no reason to believe that the outer reaches of our Galaxy is peppered with any dense interstellar clouds ($n_e \sim 435 \text{ cm}^{-3}$; see Table 1), nor stars capable of ionizing such compact nebulae. Given the paucity of stars at such distances, postulating such a nebulae routinely (not only for the *Sparker* but for each FRB) is most artificial. On the other hand, a host galaxy located well outside the Local Group would be entirely allowed by the observations.

Next let us consider the upper right region in Figure 7. Here we are allowed to have large nebulae ($L \gtrsim 20$ kpc) but at great distances ($d > 2$ Mpc). This requirement is easily met by the IGM.

We conclude that the circumstantial evidence is not consistent with a Galactic or SMC origin nor even a Local Group origin. The following possibilities are allowed: the excess DM arises in the IGM or in a galaxy well outside the Local Group or both. In §5 and §6 we discuss possible loopholes in reaching this conclusion.

5. A POROUS NEBULA?

The discussion thus far in this section is based on the assumption of a homogeneous intervening nebula. We now consider the implications of a porous nebula. Specifically, we assume that the nebula is composed of N ionized clumps of size l . For mathematical simplicity, we assume that both the nebula and the clumps are cubes. We define the volume filling factor as $\phi_V = Nl^3/L^3$. Let $n_c = N/L^3$ be the number density of clumps. Since the cross-section of the clumps is l^2 , on average we encounter n_cl^2L clumps along a given line-of-sight.

The average dispersion measure is then

$$\text{DM} = n_e l^2 L \times n_{el} = \phi_V n_e L, \quad (27)$$

and the average emission measure is

$$\text{EM} = n_e l^2 L \times n_e^2 l = \phi_V n_e^2 L, \quad (28)$$

where n_e is the electron number density in the clumps. Therefore,

$$\frac{\text{DM}^2}{\text{EM}} = \phi_V L. \quad (29)$$

That is, the size of the nebula inferred from the DM and EM is the filling factor times the physical size of the region.

In the previous section, a unity volume filling factor is assumed (i.e., no clumps). All constraints related to the nebula size inferred from the DM and EM are affected if the filling factor is not unity, with some strengthened and some weakened. Mathematically, the effect is to replace L in the relevant constraint equations with $\phi_V L$.

Apparently, the constraint from the spatial range of the nebula limited by the DM of pulsars (Equation 14) is not affected. The constraint from free-free absorption (Equation 13) becomes $\phi_V L > L_{\text{ff}}$ and the corresponding line in Figure 7 moves up by a factor of $1/\phi_V$. Similarly, L in Equation 17 is also replaced by $\phi_V L$ and the corresponding line in Figure 7 moves up. Constraints from Equations 14 and 17 are thus strengthened by requiring a larger size of the nebula region and shrinking the allowed region (that above the line) in the parameter space. Replacing L by $\phi_V L$ in Equations 22 and the UV constraints (§4.5) also moves up the corresponding lines in Figure 7, but this change expands the allowed region (region below each line) and thus weakens the constraints. We note, however, that because the relevant lines move up by the same factor, the minimum distance set by combining equation 13 and equation 22 (or that by equation 13 and equation 23) remains unchanged.

In summary, a porous nebula does not change the minimum distance to the nebula. The free-free constraint *increases* the minimum size of the nebula. Thus, on both grounds Galactic models are excluded even more strongly.

6. CAVEAT: A NEBULA NOT POWERED BY PHOTO-IONIZATION

In the previous section the strongest constraint on the minimum distance to the *Sparker* came from examining the *GALEX* UV data. This constraint is meaningful only if the DM nebula is photo ionized. However, one could think of free electrons being produced by other mechanisms. Three mechanisms come to mind: cosmic ray ionization, radiative shocks and a flash ionized nebula. The *GALEX* limits would be rendered useless should we be able to develop a plausible case for any of these mechanisms. Separately, dust extinction would attenuate UV photons and also potentially dilute the *GALEX* constraints.

Historically, cosmic rays were the first to be suggested as ionizing sources for the diffuse ISM (see Spitzer 1978). The ionization cross-section is dominated by low energy (non-relativistic) protons and ions (see Webber 1998). The estimated cosmic ray ionization rate lies in the range $(3\text{--}300) \times 10^{-17} \text{ s}^{-1}$ per H atom (Wolfire *et al.* 2003; Le Petit, Roueff & Herbst 2004). We can easily show that matching the recombination time to any of the nebular parameters listed in Table 1 to the ionization timescale would require a cosmic ray flux 10^7 times larger than the above value.

6.1. Ionization by Shocks

Shocks, usually the product of supernova blast waves or stellar winds, provide an alternative ionization mechanism. The amount of DM generated depends on the properties of the medium (most notably, the ambient particle density n_0), the energy carried by the shock and the fraction transferred to the ISM. Here and below, unless stated otherwise, when computing the $\text{H}\alpha$ flux a nominal temperature of 10^4 K is assumed.

On one side of the energy spectrum are strong, high velocity, shocks such as those originating in supernova blast waves (e.g., Heng & McCray 2007). For example, an $E = 10^{51} \text{ erg}$ supernova that expends, say, $f = 10\%$ of the total energy on ionization of the surrounding ISM requires an ambient H I density of:

$$n_0 = 8.5 f^{-1/2} E_{51}^{-1/2} \text{DM}_{300}^{3/2} \text{cm}^{-3} \quad (30)$$

to produce the expected levels of DM. The size ($\sim 35 \text{ pc}$) and the emission measure ($\text{EM} \sim 2600 \text{ cm}^{-6} \text{ pc}$) of the resulting nebula would make it easily detectable by SHASS, even if located within the SMC or beyond.

On the low energy side, we find that typical (e.g., Raymond *et al.* 1988) fully developed radiative shocks are incapable of producing the required levels of DM. As reviewed by Draine & McKee (1993), the extent of the radiative zone is solely determined by the column density, N_{rad} , of the shocked material. For typical shock speeds of $60 < v_s < 150 \text{ km s}^{-1}$ and the Alfvén Mach number¹⁸, $M_A \gg 1$, the shocked column is $N_{\text{rad}} \sim 10^{17.5} v_{s,7}^4 \text{ cm}^{-2}$ (McKee *et al.* 1987). The total column of ionized hydrogen is larger, and estimated to be on order of $N_{\text{rad}} \sim 10^{18.5} v_{s,7}^4 \text{ cm}^{-2}$ for shocks with $80 < v_s < 140 \text{ km s}^{-1}$ and $M_A \sim 10$ (Raymond *et al.* 1988; Draine & McKee 1993). This corresponds to $\text{DM} \sim 1 v_{s,7}^4 \text{ cm}^{-3} \text{ pc}$, and length scales of order $1 n_0^{-1} \text{ pc}$, again insufficient to explain the *Sparker* DM.

We may invert the question and look for the v_s required to produce $\text{DM} \sim 300$. The answer depends on the cooling function and timescales in the radiative zone, compared to the shock propagation speed. Essentially, the leading edge of the shock must move forward fast enough to accumulate the required DM before the ionized medium at the trailing edge has cooled sufficiently to recombine. Assuming a strong and steady shock, full ionization and isobaric radiative cooling, and by approximating the cooling curve of Boehringer & Hensler (1989) with $\Lambda = 10^{-23} T_7^{-1} \text{ erg cm}^3 \text{ s}^{-1}$, for $10^5 < T < 10^7 \text{ K}$, we find that $v_s \sim 840 (\text{DM}_{300})^{1/5} \text{ km s}^{-1}$. The timescale for the development of the full radiative shock is $t \sim 3 \times 10^4 n_0^{-1} \text{ yr}$; again, a lower limit. From the velocity and timescale it follows that the lower limit on the size of the radiative region is $L \sim 7.5 n_0^{-1} \text{ pc}$, excluded by existing constraints to beyond the SMC. The timescale is rather long – a typical supernova shock would have significantly slowed down by then. Increasing the ambient density, n_0 , would shorten the timescale, but would then run afoul of constraints set by SHASS, due to the increased emission measure for a smaller, denser, region.

Therefore, this possibility requires a highly elongated radiative shock with an almost edge-on viewing geometry. It is within the realm of possibilities that such a situation may take

¹⁸ M_A is the Alfvén Mach number, $M_A = v_s/v_A$ and v_A is the Alfvén velocity.

place for an RRAT located in the Galactic plane. However, the requirements of a supernova shock and edge on geometry means that we cannot routinely invoke this explanation for most FRBs.

6.2. Flash Ionized Nebula?

In the previous section we assumed that the DM causing nebula was already present when the *Sparker* event took place. We now consider the possibility that the *Sparker* was accompanied by a soft X-ray flash (*Flasher!*) and this flash resulted in the ionization of the nebula.

The soft X-ray flash has to be powerful enough to produce a nebula with electron column density of $DM = 300 \text{ cm}^{-3} \text{ pc}$ or $1.16 \times 10^{21} \text{ cm}^{-2}$ and there has to be enough circumburst gas to provide the necessary number of electrons. The number of electrons within the flash ionized nebula is

$$N_e = \frac{4\pi}{3} \left(\frac{L}{2}\right)^3 n_e = 4.6 \times 10^{53} \frac{DM}{300 \text{ cm}^{-3} \text{ pc}} \left(\frac{L_{\text{pc}}}{10^{-2} \text{ pc}}\right)^2 \quad (31)$$

The timescale for ionization at radius r is

$$\tau_{\text{ion}} = \left[\sigma_1 \left(\frac{\nu}{\nu_1} \right)^{-3} \frac{N_e / \Delta t_X}{4\pi r^2} \right]^{-1}, \quad (32)$$

where Δt_X is the duration of the soft X-ray flash, $\sigma_1(\nu/\nu_1)^{-3}$ is the photoelectric absorption at frequency ν and $\sigma_1 = 6 \times 10^{-18} \text{ cm}^2$ is the cross-section at the Lyman edge ($h\nu_1 = 13.6 \text{ eV}$). At the edge of the nebula ($r = L/2$) the ionization time is determined by the luminosity and ionization cross-section (which is dominated by the photo-ionization of Hydrogen) and is

$$\tau_{\text{ion}} = 0.001 \Delta t_X (\nu/\nu_1)^3. \quad (33)$$

Provided that $\Delta t_X \sim \Delta t$ we find τ_{ion} is much smaller than the delay between the propagation in the decimeter band (say 1.4 GHz) and that by a photon at high energies. This justifies assuming an instantaneous creation for the flash ionized nebula.

The energy of the X-ray flash is

$$E_{\text{ion}} > N_e h\nu_1 = 1 \times 10^{43} \left(\frac{DM}{300 \text{ cm}^{-3} \text{ pc}} \right) \left(\frac{L_{\text{pc}}}{10^{-2} \text{ pc}} \right)^2 \text{ erg} \quad (34)$$

The (isotropic) energy budget is quite impressive even for the smallest allowed value of L . In particular, the isotropic bolometric yield of the rare hyper-flares from soft γ -ray repeaters (SGRs) can be as high as 10^{47} erg – but with most of the release in the hard X-ray band. Furthermore, the estimate of Equation 34 does not account for radiation at energies lower or higher than $h\nu_1$. Should the nebula be a few parsecs in size, then the *Sparker* results from a cataclysmic event.

The *Sparker* took place about thirteen years ago. Given the recombination timescale of

$$\begin{aligned} \tau_R &= (n_e \alpha_B)^{-1} \\ &= 4.2 \left(\frac{DM}{300 \text{ cm}^{-3} \text{ pc}} \right)^{-1} \left(\frac{L}{10^{-2} \text{ pc}} \right) \text{ yr}, \end{aligned} \quad (35)$$

there still exists an opportunity to search for the flash ionized nebula. The flux level is the same as that estimated for the H II region model (§4.4).

We note, however, that if a comparable amount of the required energy for the “flasher” is emitted as X-rays or γ -rays,

then it would be readily detectable by the interplanetary network¹⁹ (IPN) up to the SMC distance. Lorimer *et al.* (2007) reported that the IPN, which has almost full sky coverage, did not detect any GRBs or SGR hyper flares temporally associated with the *Sparker*.

As in the previous section we can probably invoke this framework for a single source such as the *Sparker*. However, it would be difficult to do so for an entire population with a daily rate of 10^4 and not have the expected EUV/X-ray flashes remain undetected by past and existing missions.

7. STELLAR CORONAL MODEL

Taking a contrarian view Loeb, Shvartzvald & Maoz (2014) propose a scenario in which a stellar corona provides the observed DM. This means that the actual electromagnetic pulse (EMP) takes place somewhere inside the corona and the radio pulse accumulates the DM as it propagates towards the observer.

The simplest expectation for this model is that FRBs should be concentrated towards the Galactic plane. The reported events are all at high latitudes which is obviously not a good omen for the model. We eagerly await the analysis of low latitude fields from Parkes and Arecibo. Robust detection of FRBs in these data sets would certainly boost this model.

The emission mechanism is either via coherent or incoherent processes. Coherent emission within a corona (which consists of dense non-relativistic plasma) may be problematic. On the other hand, it is possible to imagine a sudden deposition of energy (e.g., magnetic reconnection) which results in ultra-relativistic shock. A radio pulse can plausibly be produced in the post-shock gas via incoherent synchrotron emission (see Blandford 1977). From Equation 5 we find $\gamma \sim 10^4$. The size of the emitting region is $2\gamma^2 c \Delta t$. For $\Delta t = 1 \text{ ms}$, the size of the emitting region is $6 \times 10^{15} \text{ cm}$ which is much larger than any plausible corona. Independent of this concern it would be useful to investigate possible modifications of the spectrum of the radio pulse as it propagates through the coronal plasma and coronal photon field.

Now let us return to some basic considerations of the model (independent of how the EMP was generated). We start with a simple model: a corona with a homogeneous electron density, n_e and radius L . We assume that the EMP is generated at radius R_* (which is not necessarily the photospheric radius). Then $DM = n_e(L_{\text{pc}} - R_{\text{pc}})$ where $R_{\text{pc}} = R_*/(1 \text{ pc})$ and $L_{\text{pc}} = L/(1 \text{ pc})$.

For high temperatures ($T > 3 \times 10^5 \text{ K}$), the free-free absorption coefficient per unit length (Lang 1974, p. 47) is

$$\alpha(\nu) = 9.79 \times 10^{-3} \frac{n_e n_i}{\nu^2 T^{3/2}} \ln \left[\frac{4.7 \times 10^{10} T}{\nu} \right] \text{ cm}^{-1}. \quad (36)$$

Normalizing $\nu = \nu_0 = 1.4 \times 10^9 \text{ Hz}$ and setting $T = 10^8 T_8$, we find

$$\tau(\nu) \approx 3.4 \times 10^{-7} \left(\frac{\nu}{\nu_0} \right)^{-2} T_8^{-3/2} \left(\frac{DM_3^2}{L_{\text{pc}}} \right), \quad (37)$$

where $DM = 10^3 DM_3 \text{ cm}^{-3} \text{ pc}$. Let us say $\tau(\nu_0) \lesssim 3$ (cf. Equation 10 and subsequent discussion). Thus, we have

$$L_{\text{pc}} - R_{\text{pc}} \gtrsim 1 \times 10^{-7} T_8^{-3/2} DM_3^2 \left(\frac{\nu}{\nu_0} \right)^{-2}. \quad (38)$$

²⁰ <http://heasarc.gsfc.nasa.gov/docs/heasarc/missions/ipn.html>

This length scale corresponds to about $4R_\odot$. Going forward we will set $v = v_0$.

The mean density, the mass and the thermal content of the corona is

$$\begin{aligned} n_e &= 1 \times 10^{10} T_8^{3/2} \text{DM}_3^{-1} \text{ cm}^{-3}, \\ M_c &= 1 \times 10^{-12} \text{DM}_3^5 T_8^{-3} M_\odot, \\ Q_c &= 5.1 \times 10^{37} \text{DM}_3^5 T_8^{-2} \text{ erg}. \end{aligned} \quad (39)$$

For the corona to be in approximate hydrostatic equilibrium we must have the thermal energy (in each of electron and proton) be less than the gravitational potential energy (per H atom) or $3k_B T < GM_H/L$; here, $m_H = m_p + m_e$. This is clearly violated and so we must assume that there is outflow. The characteristic thermal velocity that matters is

$$v = \sqrt{\frac{3k_B T}{m_H}} = 1580 T_8^{1/2} \text{ km s}^{-1}, \quad (40)$$

and the mass flux is

$$\begin{aligned} \dot{M} &= 4\pi L^2 n_e m_H \sqrt{\frac{3k_B T}{m_H}}, \\ &\approx 5 \times 10^{-8} T_8^{-2} \text{DM}_3^3 M_\odot \text{ yr}^{-1}. \end{aligned} \quad (41)$$

So even though we started with a static model for the corona we find that the corona is not dynamically stable and has a strong outflow. If so, the assumption of a homogeneous density in the corona is not correct. Therefore, we need to adopt a wind equation: $n_e \propto r^{-2}$. As noted in §C, as long as L is even modestly larger than R_* , we can approximate $\text{EM} \approx \text{DM}^2/R_{\text{pc}}$, which is similar to the homogeneous case, provided we identify R_* with L .

The free-free luminosity per unit volume is (Lang 1974, p. 46)

$$\epsilon_{\text{ff}} = 1.4 \times 10^{-27} T^{1/2} n_e^2 \text{ erg cm}^{-3} \text{ s}^{-1}, \quad (42)$$

where we have assumed a pure hydrogen plasma ($n_e = n_i$). The luminosity (assuming that the plasma is optically thin)²¹ and the bolometric flux density are, respectively,

$$\begin{aligned} L_{\text{ff}} &= \frac{4\pi}{3} L^3 \epsilon_{\text{ff}} = 1.7 \times 10^{32} T_8^{-1} \text{DM}_3^4 \text{ erg s}^{-1}, \\ f_{\text{ff}} &= 1.3 \times 10^{-12} D_{\text{kpc}}^{-2} T_8^{-1} \text{DM}_3^4 \text{ erg cm}^{-2} \text{ s}^{-1}. \end{aligned} \quad (43)$$

The cooling and the hydrodynamical timescales are

$$\begin{aligned} t_{\text{ff}} &= 3k_B T n_e / \epsilon_{\text{ff}}, \\ &= 3.43 T_8^{-1} \text{DM}_3 \text{ day}, \end{aligned} \quad (44)$$

and

$$t_h = L/v = 0.5 T_8^{-2} \text{DM}_3^2 \text{ hr}. \quad (45)$$

Since the corona is optically thin and $t_h < t_{\text{ff}}$ we expect to see a bright X-ray source with typical photon energy of $2.7k_B T = 23 T_8 \text{ keV}$ lasting for $0.5 T_8^{-2}$ hours (after the radio burst). However, we note that X-ray emission will be seen for at least a similar duration as the corona inflates to provide the necessary DM. Thus we will have X-ray emission, preceding and succeeding the EMP, with a fluence of

$$F_{\text{ff}} = 2.3 \times 10^{-9} D_{\text{kpc}}^{-2} T_8^{-3} \text{DM}_3^6 \text{ erg cm}^{-2}. \quad (46)$$

²¹ A dispersion measure of $10^3 \text{ cm}^{-3} \text{ pc}$ is Compton thin; the plasma is also thin for free-free absorption for $h\nu$ comparable to $k_B T$.

X-ray missions are more sensitive at lower energies and so better constraints on this model can be obtained by considering missions which operated primarily in the classical X-ray band or the soft X-ray band. In order to compute the X-ray light curve we would need to know the boundary conditions at the base of the corona. Since the proposed model is not sufficiently developed, any further calculation of this sort is premature. We can reasonably assume that the duration of the X-ray emission at lower energies (keV range) is longer than the $1 T_8^{-2} \text{DM}_3^2 \text{ hr}$ discussed above.

In summary, an expectation of the coronal class of models is *pre-cursor* hard X-ray emission followed by an X-ray afterglow that becomes softer with time. Given a daily FRB rate of $\mathcal{N} \approx 10^4 \text{ day}^{-1}$ the number of X-ray sources we expect to see is $\mathcal{N} \tau_X$ where τ_X is the duration over which the X-ray signal is above the detection level. For $T = 10^8 \text{ K}$ we expect about 400 sources at any given time in the sky. According to Kanner *et al.* (2013), at any given time, there are 4×10^{-4} X-ray transients per square degrees on the sky with a flux threshold greater than $3 \times 10^{-12} \text{ erg cm}^{-2} \text{ s}^{-1}$ [0.2–2 keV band], or about 16 sources over the entire sky. Most of these are identified with sources which are expected to be variable from other considerations (e.g., known flare stars primarily; see Vikhlinin 1998). Clearly, coronal models with $T = 10^8 \text{ K}$ are not favored on observational grounds.

Let us consider even hotter coronas, say $T = 3 \times 10^8 \text{ K}$. Relative to $T = 10^8 \text{ K}$ coronal model, the duration of the event is reduced by a factor of ten (from an hour to 6 minutes) and the flux decreased by a factor of three. With a mean temperature of 70 keV, this short lived object may even be mistaken for a long duration GRB! Given \mathcal{N} we would expect ten nearby (100 pc) events every day each with a fluence of $10^{-7} \text{ erg cm}^{-2}$. The Burst Alert Telescope (BAT) can detect GRBs with fluence [15–150 keV] brighter than $10^{-8} \text{ erg cm}^{-2}$ (though most of the GRBs are considerably brighter). A search through the BAT catalog (Sakamoto *et al.* 2011) would provide observational feedback to the coronal model.

8. AN EXTRAGALACTIC ORIGIN

In §4 using basic theory and archival $H\alpha$ and *GALEX* data, we attempted to constrain the size (L) and the location (distance, d) to an intervening ionized nebula that could account for the excess (over Galactic value, if the *Sparker* was located in our Galaxy or in the vicinity of the Magellanic Clouds) of the dispersion measure inferred from the frequency-dependent arrival time of the pulse from the *Sparker*. The allowed phase space for L and d is summarized in Figure 7. We concluded that the nebula cannot be located in our own Galaxy or the SMC and is not even allowed to be on the periphery of our Galaxy. After investigating possible caveats (§5–6) we concluded that the excess of dispersion measure arises in another galaxy or in the intergalactic medium (IGM) or both. Having reached this conclusion, the only issue is to apportion the dispersion measure between the inter-galactic medium (IGM) and ionized gas within the host galaxy. For the *Sparker*, in accord with Lorimer *et al.* (2007), a red-shift range $0.1 \lesssim z \lesssim 0.3$ is reasonable.²²

A similar analysis can be applied to the four FRBs reported by Thornton *et al.* (2013), but that is not educational. What is

²² As can be seen from Figure 1, there is no distinctive galaxy within the localization region. The most notable galaxy lies outside the polygon beyond the NorthWestern tip.

useful is to take the best constraints from the whole set of the Parkes events. In particular, the L_{ff} scales as DM^2 (cf. Equations 6, 7). The larger DMs of the Thornton *et al.* (2013) therefore provide the strongest constraints on compact intervening nebulae and for stellar models (§7).

We conclude that the *Sparker* and the four Parkes events have to be extra-galactic – *provided that the frequency dependent arrival time is a result of propagation through cold plasma*. In this section we investigate the consequences of the *Sparker* being located in a distant galaxy. Anticipating the later discussion to include FRBs, we set the nominal distance to 1 Gpc. We will now revisit the issue of energetics and brightness temperature (cf. §3.1-3.2).

Switching now to parameters typical of FRBs: peak flux of 1 Jy at 1.4 GHz and $\Delta t = 1$ ms, we find the isotropic energy release in the radio band is

$$\mathcal{E}_S \sim 4 \times 10^{39} D_{\text{Gpc}}^2 \text{ erg}, \quad (47)$$

assuming $\alpha = -1$ with a low frequency cutoff of $\nu_0/10$ (cf. §3.1). However, if the intrinsic spectrum is an exponential (cf. §4.1) then the isotropic energy release is larger by $\approx \exp(x_0)/(x_0 \ln(x_0))$ where $x_0 = \nu_0/\nu_c$.

The brightness temperature at ν_0 is $6 \times 10^{34} D_{\text{Gpc}}^2 \text{ K}$ and is larger by the factor $x_0^2 \exp(x_0)$ at $\nu = \nu_c$. We compare the *Sparker* to Galactic RRATs and giant pulses from pulsars. The brightest RRAT known to date has a peak flux of 3 Jy in the 21-cm band. For the RRAT sample of McLaughlin *et al.* (2006), we derive brightness temperatures as high as 10^{23} K . Next, the highest brightness temperature event to date is a 15-ns wide giant pulse from PSR 1937+214 with $T_B > 5 \times 10^{39} \text{ K}$ (in the 1.65-GHz band; after correction for interstellar scintillation & scattering; Soglasnov *et al.* 2004). Thus, apparently, pulsars can produce the high brightness temperatures that we are inferring for the *Sparker*.

We draw the readers attention to the dual-frequency (2.7 & 3.5 GHz) studies of PSR J1824–2452A (Knight *et al.* 2006). The authors report that the spectral index of ~ -5.4 was observed over the frequency range 2.7–5.4 GHz. Furthermore, it was noted that the giant pulse phenomena is not necessarily broad-band (i.e. the spectrum could be quenched at lower frequencies). Finally, many of the giant pulses are 100% elliptically polarized.

Despite the apparent agreement of brightness temperature and potential spectral similarity there is one big difference between giant pulses from pulsars and the *Sparker*: the size of the emitting region. The high brightness temperatures exhibited by pulsars is on nano-second timescales. This translates into sizes for the emitting regions from a few meters and up. In contrast, the size of the *Sparker* emitting region is $R = c\Delta t \sim 300 \text{ km}$.

Before we discuss the proposed models it is useful to discuss the most general constraint(s) that can be obtained from the observations. Clearly, the high brightness temperatures of FRBs stand out. As first discussed by Wilson & Rees (1978), the high brightness temperature inferred in the Crab pulsar requires two conditions: an extremely clean region, to prevent severe losses due to induced Compton scattering, and an ultra-relativistic flow which would then boost the inferred brightness temperature by γ^3 . Separately, matter, if present, would be accelerated by the strong electromagnetic field and rapidly dissipate energy. Propagation will also be impeded. Were the *Sparker* to be an RRAT or a pulsar, albeit at cos-

mological distances, then $\gamma \sim 10^4$ to 10^6 would be needed in order to prevent induced Compton scattering from significantly attenuating the radio emission. In this spirit we draw the reader's attention to a recent paper by Katz (2013) where he argues that $\gamma > 10^3$ and notes that a compact source or an expanding highly relativistic source are both possible.

In summary, suitable progenitor models are those which have an ultra-clean emitting region and, in addition, a low density circumstellar medium so that external absorption is not significant. This means, almost always, that the free-free optical depth should not be large (for usual parameters, the plasma frequency is usually well below the GHz band).

9. PROGENITORS

Even more remarkable than their inferred extra-galactic nature is the all-sky rate of *Sparker* and associated Parkes events. Lorimer *et al.* (2007), noting that the *Sparker* would have been detected to $z \sim 0.3$ ($D \sim 1 \text{ Gpc}$), derived a local volumetric rate of $90 \text{ Gpc}^{-3} \text{ d}^{-1}$. For the four Parkes events, Thornton *et al.* (2013) quote an all-sky-rate of $1.0^{+0.6}_{-0.5} \times 10^4 \text{ d}^{-1}$ (for fluence above a few Jy ms in the 1.4 GHz band). The co-moving distances for these events, if most of the DM is attributed to the IGM, is [2.8, 2.2, 3.2, 1.7] Gpc. From this we derive a volumetric annual rate of

$$\Phi_{\text{FRB}} = 2.4 \times 10^4 \text{ Gpc}^{-3} \text{ yr}^{-1}. \quad (48)$$

The very large volumetric rate of *Sparkers* poses great difficulty for any extra-galactic model. It is useful to compare the volumetric rate of *Sparkers* to the rates of well established cosmic explosions (Table 2). The most frequent stellar deaths are core-collapse supernovae. The FRBs would claim 10% of the core collapse rate. In this section we review and critique suggested stellar models for FRBs. We discuss the model of giant flares from soft gamma-ray repeaters as possible progenitors to FRBs in the next section. We do so because in our opinion this model stands out for having a sound physical basis.

9.1. Core Collapse Supernovae

Massive stars lose matter throughout their life. The parameter $A = \dot{M}/(4\pi v_w)$ where \dot{M} is the mass loss rate and v_w is the velocity of the mass losing wind determines the run of the circumstellar density (see §C). Even for type Ib/Ic supernovae (which have the fastest winds and the smallest mass loss rate) A_* is in the range of 0.01 to 1; here, $A_* \equiv A/5 \times 10^{11} \text{ g cm}^{-1}$. As argued in §C, this value is sufficient to cause free-free absorption (in the decimeter band) at a radius of 10^{14} cm . Thus for a successful radio burst, the radio emitting region must be located beyond this radius. For this reason we reject all ordinary core-collapse supernovae and their more exotic variants: long duration GRBs, low luminosity GRBs, as well as the model of Egorov & Postnov (2009).

9.2. The Blitzar Model

To circumvent the fundamental problem of absorption by either the ejecta or the circumstellar medium, Falcke & Rezzolla (2013) propose a novel scenario: the desired fraction of core-collapse supernovae explode and leave massive neutron stars which are rotating sufficiently rapidly that they can exceed the maximum mass of a stable but static neutron star. The neutron star spins down via the pulsar mechanism. Meanwhile the SN debris and circumstellar medium is slowly

cleared up. At some point the super-massive neutron star can no longer support itself and collapses to a black hole. During this transmutation a strong radio pulse is emitted (*Blitzar!*). We agree that the Blitzar model is a clever scenario, but below we argue that the ramifications of the model are not in accord with what we know about the demographics of pulsars and the energetics of supernovae and supernova remnants.

We consider a simple and hopefully illustrative example. Let us say that the typical period at which the super-massive neutron star is born is $P_0 = 0.75$ ms and that it transmutes (collapse) to a black hole when the spin period is, say, $P_1 = 1.5$ ms. With P_0 and P_1 fixed the only free parameter is the time, τ , it takes for the super-massive neutron star to spin down to P_1 . The magnetic field strength prior to the collapse can be computed in the vacuum dipole framework and is $B = 5.2 \times 10^{10} \tau_4^{-1/2}$ G where $\tau = 10^4 \tau_4$ yr. The spin-down luminosity of the pulsar, prior to the transmutation, is extraordinary: $\dot{E} = 2 \times 10^{40} \tau_4^{-1} \text{ erg s}^{-1}$. The spin-down luminosity at birth is $(P_1/P_0)^4$ higher.

Now we work out the ramifications of the Blitzar hypothesis. First, (i), in a typical late-type galaxy, given the putative birthrate of FRBs (1 per 10^3 yr), we should expect $10\tau_4$ such bright *young* pulsars with magnetic field strengths significantly above those of millisecond pulsars ($B \lesssim 10^9$ G). Next, (ii), given the ratio of the FRB rate to that of core-collapse supernovae, one in ten supernovae should exhibit evidence of an underlying long-lived powerful source of energy. Let us consider a specific case and set $\dot{E} = 10^{42} \text{ erg s}^{-1}$. Assuming a mean expansion speed of $5 \times 10^8 \text{ cm s}^{-1}$ (at late times), the radius of a supernova two years after the explosion is $R_S = 3 \times 10^{16} \text{ cm}$. It is safe to assume that this power input is rapidly thermalized. Equating the blackbody luminosity, $4\pi R_S^2 \sigma T_S^4$ to \dot{E} yields $T \sim 10^3$ K. A search with WISE and Spitzer missions for mid-IR emission from nearby and decade old core collapse supernovae would provide useful upper limits on the rate of Blitzars (*cf.* Helou *et al.* 2013).

Decreasing the typical time to collapse from 10^4 yr to 10^3 yr would alleviate the issue raised in (i) but exacerbate that discussed in (ii). Increasing τ to 10^6 yr would alleviate the concern raised in (ii) but lead to a large population (10^3) of millisecond young (10^6 yr) pulsars – a hypothesis that can be immediately refuted given the known demographics of Galactic pulsars. Finally, (iii), by constructions these events would release, over a timescale of τ , an energy of $\Delta E = 1/2(I_0\omega_0^2 - I_1\omega_1^2)$, – which is comparable to the typical initial rotation energy of the neutron star or 10^{52} erg; here, I is the moment of inertia, $\omega = 2\pi/P$, and the subscripts are as in the previous paragraph. There is little evidence that the inferred energy release in any Galactic supernova remnant, including those associated with magnetars, exceeds 10^{51} erg (Vink & Kuiper 2006).

9.3. Short Hard Bursts

Short hard bursts are well suited as possible progenitors. After all, these systems are clean: no supernovae ejecta, and no rich circumstellar medium. However, as has been noted earlier, the rates of the Parkes events far exceeds that of the short hard bursts (see Table 2). Additionally, we offer the following line of simple reasoning. The very large rate for the Parkes events suggests that they are not beamed. The five Parkes events have $z < 1$. In contrast, the redshift distribu-

TABLE 2
VOLUMETRIC RATES OF SELECTED COSMIC EXPLOSIONS

Class	Type	Φ Gpc $^{-3}$ yr $^{-1}$	Ref
LSB (low)	BC	100–1800	[1,2]
LSB (high)	Obs	1	[1]
	BC	100–550	[1]
SHB	Obs	> 10	[3a]
	BC	500–2000	[3b]
In-spiral	Th	3×10^3	[4]
SGR	Obs	$< 2.5 \times 10^4$	[5]
Type Ia	Obs	10^5	[6]
Core Collapse	Obs	2×10^5	[7]
FRB	Obs	$\approx 2 \times 10^4$	[8,9]

Notes: “Obs” is the annual rate inferred from observations. “BC” is the observed rate corrected for beaming. “Th” is the rate deduced from stellar models. LSB stands for GRBs of the long duration and soft spectrum variety. A gamma-ray luminosity of $10^{49} \text{ erg s}^{-1}$ divides the “low” and “high” subclasses (see Guetta & Della Valle 2007). SHB stands for GRBs of the short duration and hard spectrum class. SGR stands for Soft Gamma-ray Repeaters. Here we only include those giant flares with isotropic energy release $> 4 \times 10^{46} \text{ erg}$. Refs: [1] Guetta & Della Valle 2007; [2] Soderberg *et al.* 2006; [3a] Nakar, Gal-Yam & Fox 2006; [3b] Coward *et al.* 2012; [4] Kalogera *et al.* 2004; [5] Ofek 2007; [6] Scannapieco & Bildsten 2005; [7] Li *et al.* 2011 [8] Lorimer *et al.* 2007; [9] Thornton *et al.* 2013.

tion of short hard bursts is wider. Bearing this in mind we note that the all-sky rate of short hard bursts is $\approx 0.5 \text{ day}^{-1}$ (Nakar 2007). Thus, concordance between these two estimates would require an inverse beaming factor in excess of 2×10^4 ! There is no evidence for such a large inverse beaming factor²³ (Berger 2013). In order to preserve the connection between FRBs and coalescence events, we have to conclude that only a small fraction of coalescence events produce short hard bursts.

We now discuss specific models related to short hard bursts. Totani (2013) revives erstwhile models in which the neutron stars are reactivated as they approach coalescence. This is an attractive model from the point of view of radio pulse generation, as well as the fact that the radio emission takes place *prior* to the coalescence. However, as noted above, in this scenario Nature is bountiful with coalescence events. We should expect to see an event within 100 Mpc every 3 days once Advanced LIGO turns on. We admit that we find this scenario to be positively Panglossian.

Next, it has been noted in Zhang (2014) and Lasky *et al.* (2013), that in some short hard bursts the X-ray light curve shows a plateau. The authors interpret the cessation of this X-ray plateau as marking the transmutation of the coalescence product – a supra-massive neutron star – into a black hole. Inspired by the Blitzar model, Zhang (2014) suggest that the transmutation results in an intense radio. On general grounds one expects that the merger will be followed by the ejection of a relatively small amount ($10^{-4} M_\odot$ – $10^{-2} M_\odot$) of sub-relativistic matter (see Hotokezaka *et al.* (2013)). In §C, we construct a simple toy model with spherical ejection, constant shell thickness, and a coasting velocity and find that

²³ The beaming factor is the fraction of the celestial sphere lit up by sources with strong conical emission. If θ is the half-opening angle of each of the two jets then the beaming factor is $f_b = 1 - \cos(\theta)$. The inverse beaming factor is f_b^{-1} .

decimetric radiation will be absorbed, via the free-free process, by the expanding shell. Zhang (2014) argue that a radio pulse would be seen for those events whose axis of explosion is pointed towards us. However, if we are seeking a single explanation for FRBs, this model spectacularly fails on the grounds of demographics.

9.4. White Dwarf Magnetar

An entirely new class of models is speculated by Kashiyama, Ioka & Mészáros (2013). These authors propose that a fraction of the mergers of two white dwarfs lead to a highly magnetized white dwarf rotating rapidly and that such an object may produce a strong radio pulse. These authors make the implicit assumption that the merger takes place with no ejection of material. However, the merger is not a clean process (e.g., Marsh, Nelemans & Steeghs 2004; Raskin *et al.* 2013). The less massive white dwarf, having the lower density, is disrupted first. The disrupted material forms an accretion disk which then feeds the more massive star (primary). Accretion power heats up the primary star as well as the disk itself. As a result, one expects a strong stellar wind to accompany accretion. As noted in §8, the production of high temperature beams of radiation require a very clean environment and the few baryons that are present have to be relativistic. Leaving this general comment aside, we argue that the resulting wind cannot be any less strong than that seen for Wolf-Rayet stars and thus $A_* \sim 1$. If so, the radio pulse will be absorbed by the free-free process (§C). Calculation of A_* for merger models is beyond the scope of this paper but proponents are advised to look into this issue.

10. GIANT FLARES FROM SOFT GAMMA-RAY REPEATERS

We finally come to giant flares from soft gamma-ray repeaters which have been speculated to be the FRB progenitors by Popov & Postnov (2010) and Thornton *et al.* (2013). What makes this suggestion worthwhile is a plausible physical model (Lyubarsky 2014). In this model, following the giant flare, an electromagnetic pulse (Poynting vector) is formed and propagates outwards. The pulse eventually shocks the magnetized plasma which constitutes the plerion (inflated by steady power from the magnetar during the course of its life). Lyubarsky provides plausible arguments for strong radio emission either from both the reverse shock or the forward shock. Specifically, the model supports an efficiency of 10^{-5} to 10^{-6} in converting the energy released to bolometric radio emission. Next, the high brightness temperature is elegantly accounted for by synchrotron maser emission.

The most spectacular and energetic Galactic giant flare was observed on 2004 December 27 from SGR 1806–20 (Hurley *et al.* 2005; Palmer *et al.* 2005). We will use this event as the benchmark for giant flares from SGRs and as such its distance enters into our calculations. For simplicity, we assume a distance of 15 kpc (Svirski, Nakar & Ofek 2011) for SGR 1806–20 in all our analyses in this work. This event, at our assumed distance, had a characteristic energy release of $\mathcal{E}_* \equiv 3.6 \times 10^{46}$ erg in the X-ray band (Boggs *et al.* 2007). If we assume that the isotropic energy release in γ -rays, \mathcal{E}_γ , was approximately equal to this characteristic value, then in Lyubarsky’s model this event could explain FRBs with radio emission of $\mathcal{E}_R \sim 3.6 \times 10^{40}$ erg to ten times this value. This energy release is sufficient to account for a typical FRB at say 1 Gpc.

We now proceed to compute the volumetric rate of SGR flares. We do so in two different ways. Ofek (2007) combined the observations of Galactic SGR giant flares with the limits on giant flares in nearby galaxies. Based on these observations, Ofek finds that the rate of giant flares with energy above $\mathcal{E}_\gamma \gtrsim 3.6 \times 10^{46}$ erg is about $(0.4 - 5) \times 10^{-4} \text{ yr}^{-1}$ per SGR with an upper limit on the volumetric rate²⁴ of

$$\Phi_{\text{GF}}(\mathcal{E}_\gamma \lesssim \mathcal{E}_*) < 2.5 \times 10^4 \text{ Gpc}^{-3} \text{ yr}^{-1} \quad (49)$$

(and stated in Table 2). This upper limit is compatible with the inclusion of recent giant flares in nearby galaxies: GRB 051103 (Ofek *et al.* 2006) and GRB 070201 (Ofek *et al.* 2008). Comparison of the Galactic rate (discussed below) with the inferred extragalactic rate implies a gradual cutoff (or steepening) of the flare energy distribution at $\mathcal{E}_\gamma \lesssim \mathcal{E}_*$ (95% confidence).

Giant flares such as that of 2004 December 27 are detectable by the BAT instrument aboard the *Swift* Gamma-Ray Observatory. Hurley *et al.* (2005) quote²⁵ a detection of giant flares by BAT of $19(\tau_{\text{GF}}/30 \text{ yr})^{-1} \text{ yr}^{-1}$ where τ_{GF} is the mean time between Galactic giant flares as energetic as 2004 December 27. During the period 2005–2013 BAT discovered a total of 70 short duration events. Most of these are genuine short hard gamma-ray bursts (Berger 2013). The only short hard event in this sample which has been claimed to be an extragalactic giant flare is GRB 050906 [and associated with the star-burst galaxy IC 328 (distance of 130 Mpc; Levan *et al.* 2008)]. After discounting securely identified and strong candidate short hard bursts in the BAT sample we are led to the conclusion that τ_{GF} easily exceeds 100 years. We thus reaffirm the primary conclusion of the Ofek (2007) analysis: there is a break in the luminosity function of giant flares and the mean time between flares as bright as the 2004 December 27 event is in excess of a century.

A second approach is to use the statistics of Galactic (including satellite galaxies) giant flares including those fainter than \mathcal{E}_* . The lifetime of the field of X-ray astronomy is, say, 40 years. During this period we have observed three giant flares with energy above $\approx 10^{44}$ erg (1979 March 5, 1998 August 27 and 2004 December 27). Thus we can plausibly assume that the mean time between giant flares is $\tau_{\text{GF}} \approx 25$ years. The g-band luminosity of the Milky Way is $1.8 \times 10^{10} L_\odot$ (Licquia & Newman 2013). The local density in B-band is $1.8 \times 10^8 L_\odot \text{ Mpc}^{-3}$ (Cross *et al.* 2001). Thus the volumetric rate of giant flares is

$$\Phi_{\text{GF}}(\mathcal{E}_\gamma \gtrsim 3 \times 10^{44} \text{ erg}) \approx 4 \times 10^5 (\tau_{\text{GF}}/25 \text{ yr})^{-1} \text{ Gpc}^{-3} \text{ yr}^{-1}. \quad (50)$$

This rate applies to events which are brighter than the event of 1998 August 27 (which was approximately 100 times fainter than the event of 2004 December 27 event). This simple determination of the volumetric rate and the upper bound of Ofek discussed above (which we remind the reader applies to bursts with $\mathcal{E}_\gamma \lesssim \mathcal{E}_*$) are consistent with each other.

10.1. Dense Interstellar Medium

We draw the readers attention to an important issue. We have looked into the environments of several magnetars in our

²⁴ obtained by assuming 5 active SGRs in the Milky Way and assuming 0.01 Milky Way per Mpc^3 (Ofek 2007)

²⁵ The BAT rate is computed for events similar to the 2004 December 27 event also assumed to have a distance of 15 kpc.

Galaxy. Almost all of them, not surprisingly²⁶, are in star-forming regions (which are rich in both ionized and neutral interstellar gas) or embedded in a supernova remnant. We find DMs ranging from $100 \text{ cm}^{-3} \text{ pc}$ to nearly $10^3 \text{ cm}^{-3} \text{ pc}$. Furthermore, the X-ray flash could additionally ionize neutral matter (see §6.2). Indeed, this causal association of young SGRs with dense ISM regions provides the most reasonable explanation for scattering tails seen in one FRB and in the *Sparker* (and discussed in §11).

Consistent with this giant flare hypothesis, it follows that a significant contribution to the inferred DM arises from the vicinity (distance comparable to star-forming regions, say $\lesssim 100 \text{ pc}$) of the young magnetar. We advocate $400 \text{ cm}^{-3} \text{ pc}$ as a representative value. In this case, the effective volume of FRBs is reduced. However, the substantial Poisson error in Equation 50 shows that we can easily tolerate a reduction in the true volume by a factor of a few. In summary, it is not unreasonable to claim a good match between the true volumetric rate of FRBs and that of giant flares from SGRs.

Additionally, it may well be that for some FRBs the local ISM is dense enough that the decimetric signal is attenuated by free-free absorption.²⁷ These may further increase the volumetric rate of FRBs. Another consequence is that low frequency (meter wavelength) searches would find fewer FRBs compared to L-band searches.

10.2. Efficiency of Radio Emission

An important test for self-consistency of the giant flare model for FRBs is whether giant flares can support the required energetics. In order to correctly evaluate the isotropic bolometric energy release of the FRBs we need to know the radio spectrum of FRBs and in particular whether there is significant emission in bands outside the 1.4-GHz band. At present, we have no constraints on this and so we will assume that $\mathcal{F} = \ln(10) v S_\nu \Delta t$ is a good measure of the true fluence of the source (see Equation 2). Here S_ν is the observed peak flux density. The bolometric isotropic energy release is then $\mathcal{F}(1+z)4\pi D^2$ where D is the comoving radius. For the four FRBs we find the radio bolometric energy, \mathcal{E}_R , ranges from 10^{39} erg to 10^{41} erg . After accounting for the local DM contribution, the distances are smaller and as a result the isotropic release is smaller by a factor of a few. According to Lyubarski (*ibid*) bolometric radio emission can be produced with an efficiency of $\eta_R = \mathcal{E}_R/\mathcal{E}_\gamma = 10^{-6}$ to 10^{-5} . Thus, working backwards this model would demand energy releases for the four FRBs to range from 10^{44} erg to 10^{46} erg (where we have adopted $\eta = 10^{-5}$). This energy range is well matched to the assumptions made in computing the volumetric rate (see comments following Equation 50).

To conclude, radio emission arising from giant flares of young magnetars offer the most plausible physical model that can account for the high brightness temperature of FRBs (whilst not suffering from free-free absorption) and also account for the scattering tails seen in some FRBs. Furthermore, we find good agreement between the rates of giant flares and of FRBs.

²⁶ Active SGRs are a youthful population. For instance the true age of the prototype of the giant flare, SGR 1806–20, is only 650 yr (Tendulkar, Cameron & Kulkarni 2012).

²⁷ Those sources with a free-free optical depth of say a few would show up with strongly positive spectral index; see Equation 11 and the discussion that follows.

11. FREQUENCY DEPENDENT PULSE WIDTH

The *Sparker* as well as the brightest FRB in the Thornton *et al.* (2013) sample show a pulse width that is frequency dependent, $\Delta t(\nu) \propto \nu^m$ with $m \approx -4$. The simplest explanation (as has been noted by the discoverers) is that this broadening of the pulse is due to multi-path propagation (“Interstellar Scintillation & Scattering” or ISS). The observations of the *Sparker* with its low DM (relative to the FRBs) is the most difficult to explain – whence the focus, in this section, on the *Sparker*. Given our post-mortem of extra-galactic models we focus, in this section, only on the young magnetar model.

First, we summarize the minimum background to understand the basic physics of multi-path propagation. The spectrum of the density fluctuations is usually modeled as a power law with exponent $q^{-\beta_K}$, between spatial frequency, $q_1 = 2\pi/l_1$ and $q_0 = 2\pi/l_0$. Here, l_1 is the so-called inner scale (at which energy is dissipated) and l_0 is the outer scale (at which energy is injected). For the electrons in the diffuse ISM, it appears that the Kolmogorov spectrum ($\beta_K = 11/3$) describes the density fluctuations quite well. The normalization of the power law is described by the “Scattering Measure” (SM). For a given SM one can derive the spatial coherence scale²⁸, r_0 .

We adopt the “thin-screen” approximation (Figure 8). With reference to Figure 8, the rms angle by which a ray is bent is $\theta_s = 1/(kr_0)$; here $k = 2\pi/\lambda$. From Figure 8 we deduce that $\theta_s = \theta_1 + \theta_0$. In the small angle approximation, $\theta_1 = \theta_0 d_s/(D - d_s)$ and thus

$$\theta_0 = \theta_s \frac{D - d_s}{D}. \quad (51)$$

A burst of radiation can reach the observer via two extreme paths: a straight line or via a scattered ray. The time difference between the two rays gives rise to an exponential scattering tail whose width is given by

$$\Delta\tau \approx \frac{d_s}{2c} \theta_s^2 \left(1 - \frac{d_s}{D}\right). \quad (52)$$

Equation 52 suggests three locales: (i) $d_s \ll D$ (screen close to the observer), (ii) $d_s \sim D/2$ (screen midway to the observer and source) and (iii) $d_s \approx D$ (screen close to the source). Note that case (i) and (ii) require the same scattering properties but have very different observational manifestations.³⁰

We begin by first estimating the contribution to ISS by the Galactic ISM. To this end we apply the NE2001³¹ model (Cordes & Lazio 2002) to this line-of-sight and find that the Galactic ISM contributes a scattering measure (SM), in the usual mongrel and horrific units of $3 \times 10^{-4} \text{ m}^{-20/3} \text{ kpc}$. The associated Galactic ISS pulse broadening is $0.05 \mu\text{s}$ at 1.4 GHz. Clearly, the Galactic ISM cannot account for the 5-ms pulse width of the *Sparker*.

Luan (2014) provides good arguments why the IGM is unlikely to have the necessary level of turbulence to result in $\Delta t \approx 5 \text{ ms}$ (at 1.4 GHz). We find the explanation convincing and so now focus on the last locale. In this case, we have

$$\theta_s^2 \approx 2c\Delta t/l \quad (53)$$

²⁹ The transverse scale length over which the incident rays will accrue an rms shift of about 1 radian. This is similar to the well known Fried parameter used by aeronomers and astronomers.

³⁰ In particular, for the case of $d_s \rightarrow D$, the observed angular broadening is severely suppressed; see Equation 51.

³¹ http://rsd-www.nrl.navy.mil/7213/lazio/ne_model

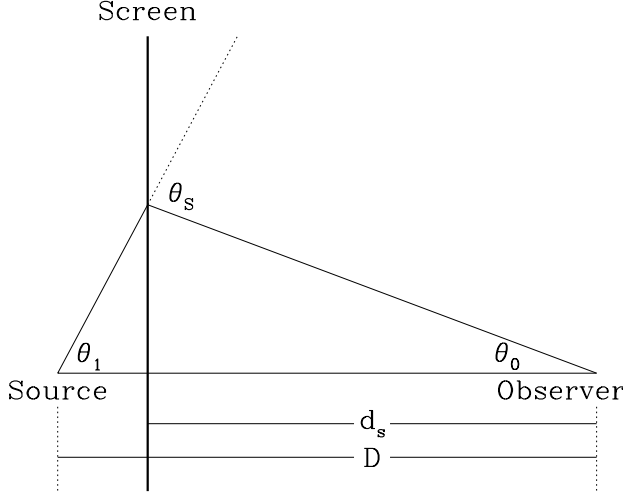


FIG. 8.— Geometry of the scattering screen. In the “thin-screen” approximation the scattering is confined to an intervening “thin” screen located at d_s . The screen scatters an incoming ray by the scattering angle, θ_s (whose value is directly related to the scattering strength of the screen). In this example, rays from the source can reach observer via a direct path and by a scattered path. The difference between the two arrival paths results in pulse broadening (amongst other effects).

where $l = D - d_s$. For $\Delta t = 5 \text{ ms}$ we find $\theta_s = 2.04 l_{\text{pc}}^{-1/2}$ arcsecond. The inferred scattering angle, θ_s , can be converted to SM using the standard formulation (Goodman 1997):

$$\theta_s(\nu) = 0.22 \text{ mas} \left(\frac{\nu}{1.4 \text{ GHz}} \right)^{-11/5} \left(\frac{SM}{10^{-3.5} \text{ m}^{-20/3} \text{ kpc}} \right)^{3/5} \quad (54)$$

where mas stands for milli-arcseconds. From this we deduce

$$\log(SM) = 3.1 - \frac{5}{6} \log(l_{\text{pc}}). \quad (55)$$

The most turbulent regions known to date are the following: the H II region NGC 6334, $\log(SM) \sim 3.3$ (Moran *et al.* 1990); the Galactic center, $\log(SM) \sim 1.2$ (Lazio *et al.* 1999); and the star-forming Cygnus region, $\log(SM) \sim 1.2$ (Molnar *et al.* 1995). These three regions are rich in gas and stars. Highly turbulent screens are usually found at the interfaces of H II regions, stellar wind bubbles and the ISM. *This is precisely the sort of locales where young magnetars are located.*

It is important to check that the scattering medium is not so dense as to absorb the decimetric pulse. Turbulence in the nebula results in variations in density of the electrons, $\langle \delta n_e^2 \rangle$. The EM from the rms variations *alone* is (Cordes *et al.* 1991)

$$\text{EM}_{\text{SM}} = 544 \text{ cm}^{-6} \text{ pc} \left(\frac{SM}{\text{kpc m}^{-20/3}} \right) \left(\frac{l_0}{1 \text{ pc}} \right)^{2/3}; \quad (56)$$

here, l_0 is the outer scale length of the turbulence spectrum. This EM should not exceed our previous constraints of $2.7 \times 10^7 < \text{EM} < 6.4 \times 10^3 \text{ cm}^{-6} \text{ pc}$ (*cf.* Table 1). It is reasonable to assume that the outer scale length will be a fraction of the size of the nebula (*cf.* NGC 6334 and the Galactic center; see Lazio *et al.* 1999). Bearing this in mind a scattering measure even as large as $\log(SM) \sim 3$ can be accommodated. However, in this extreme case the scattering screen is not only dense but also very turbulent. Parenthetically, we

wonder whether some FRBs are not detected because of free-free absorption within the host galaxy (and exacerbating the all-sky rates of FRBs).

In summary we can explain in the young magnetar model why some FRBs may exhibit frequency dependent pulses. The radio pulse is broadened by dense ISM structures that likely form the interface between the magnetar plerion (or star-forming complex) and molecular clouds illuminated by young stars. This hypothesis nicely explains why scattering tails are not seen in *all* FRBs (namely, it is seen in only those cases where the magnetar is embedded in highly turbulent structures). In contrast, in the framework where multi-path propagation takes in place in the IGM one would expect scattering tails to be seen in all FRBs.

12. NON-DISPERSED SIGNAL

The assumption that the frequency-dependent arrival time is due to propagation through an ionized medium provides the underpinnings of the discussions in §4–6. These considerations led us to reject a stellar, a Galactic, and even a Local Group origin for the *Sparker* and the four Parkes events. We were led to the conclusion that the *Sparker* and associated events must arise in other galaxies and propose in §10 that giant flares from SGRs are the most plausible progenitor. The range of models we have considered is quite comprehensive, yet we must leave no stone unturned.

Motivated thus, in this section we abandon this central assumption. We will assume that the frequency-dependent arrival time is due to a property of the source itself. We start the discussion by noting that the following three equations denote the same phenomenon³³: $t \propto \nu^{-n}$, $\dot{\nu} \propto \nu^{n+1}$ and $\nu \propto t^{-(1/n)}$.

12.1. Artificial Signals

The Ultra High Frequency (UHF) band covers the frequency range 0.3–3 GHz (aka the “decimetric” band). Starting from 1.24 GHz the frequency allocations are as follows: amateur radio, military, mobile phone (many blocks) and cordless phone. The band 1.4–1.427 MHz is exclusively allocated to radio astronomers to undertake passive observations. Perytons are seen in this band. If Perytons are artificial signals then the radio astronomy allocation is being (illegally) infringed upon.

It is important to understand that it does not take much for nearby sources to produce Jy-level signals. In appropriate units, the isotropic emitted power of the *Sparker*, $1 \times 10^6 (D/100 \text{ km})^2 \text{ erg s}^{-1}$, is easily emitted by an orbiting satellite or a terrestrial transmitter³⁵. In a similar vein the signal strength of the GPS signal at a typical location on the surface of earth³⁶ is $-138 \text{ dBW m}^{-2} \text{ MHz}^{-1}$ corresponding to $1.6 \times 10^6 \text{ Jy}$ at the primary carrier frequency (L1) of GPS (1575 MHz; 2 MHz wide). Next, the leisurely drift (half a second to traverse 300 MHz of bandwidth) and the quadratic chirp of the Perytons bear no similarity to artificial signals. Incidentally this discussion also shows it will take some effort to post-facto detect (from musty archives at various radio observatories and monitoring facilities) radio bursts expected from the past giant flares of SGR 1900+14 and SGR 1806–20.

³⁴ In communications a frequency-dependent arrival time is referred to as a “chirp”. Propagation through a cold plasma has a specific chirp signature, $t \propto \nu^{-2}$.

³⁵ For comparison, the power emitted by an active typical cell (mobile) phone is 0.5 watts or $\sim 3 \times 10^6 \text{ erg s}^{-1}$

³⁶ <http://gpsinformation.net/main/gpspower.htm>

12.2. Solar Flares

A search of the literature revealed Type III solar radio-bursts (Bastian, Benz & Gary 1998) as examples of drifting signals. Of specific interest are decimetric Type III bursts (“Type III_{dm}”): short pulses of radiation in the 1–3 GHz range. The characteristics of typical Type III burst are: i) a duration of $(\nu/(220\text{MHz}))^{-1}\text{s}$, ii) a frequency drift of $\dot{\nu}_{\text{GHz/s}} \sim \nu_{\text{GHz}}^{1.84}$, iii) a strength of 10 – 100 sfu³⁷, and iv) a brightness temperature in excess of 10^{12}K indicating that the emission is due to a coherent process. Type III_{dm} bursts usually appear in a series of hundreds to thousands of bursts, but single bursts have been observed as well (see Figure 7 of Isliker & Benz 1994).

While their physics is poorly understood, Type III_{dm} bursts are thought to be caused by downward (or upward) directed beams of non-thermal electrons in the solar corona. The frequency drift is believed to be caused by the change in the plasma frequency, $\omega_p^2 = 4\pi n_e(r)e^2/m_e$, a result of the gradient of the ambient electron density $n_e(r)$ felt by the moving beam.

Except for the weak energetics, the characteristics of the *Sparker* event fit to an order of magnitude the description of a Type III_{dm} burst. However – at the time of observation (Aug 24 2001, 19:50:01 UT, or 05:50 local time) – the Sun was $\sim 7^\circ$ below the horizon at the Parkes radio-telescope site and the angular distance from the Sun (with respect to the pointing of the telescope) was $\sim 111^\circ$. This excludes the Sun as the direct origin of the event. The hypothesis could still be saved by assuming that emission from a solar burst was reflected off an orbiting reflector (e.g., a satellite, or a piece of debris) or the moon³⁸. This would explain the relative weakness of the event, since, depending on the characteristics of the reflector and the flare, the signal may be attenuated at will. However, it would require a series of very fortunate events to have a very fine-tuned Sun-reflector-Earth configuration occurring at precisely the right time to reflect a ν^{-2} Type III_{dm} burst³⁹ towards the telescope antenna. All of the above makes this hypothesis highly implausible. Additionally, a search of the Virtual Solar Observatory⁴⁰ revealed no flares around the time of the *Sparker* event.

Other than the Sun, the planet Jupiter is the only significant source of bursty radio-emission in the Solar system. Jupiter’s emission is dominated by strong ($10^5 - 10^6\text{Jy}$) bursts, but primarily in the decameter band. Furthermore, at the time of observation Jupiter was at $\alpha = 6^{\text{h}}37'$, $\delta = 22^\circ 56'$, more than 120° away from the location of the event.

12.3. Stellar Flares

A promising source of drifting signals similar to the *Sparker* are the stellar analogs of Type III_{dm} bursts. Flaring at GHz radio wavelengths has been observed in late-type main sequence stars (Bastian *et al.* 1990) and, as discussed in the previous Section, Type III_{dm} flares are particularly good candidates for a *Sparker*-like signal. For example, a Type III-like burst has recently been observed in AD Leonis (Osten & Bastian 2006), a young, nearby ($D = 4.9\text{pc}$) dM4e star. It’s

quiescent 1.5 GHz radio luminosity is $5.5 \times 10^{13}\text{erg s}^{-1}\text{Hz}^{-1}$ (Jackson, Kundu & White 1989), equivalent to flux density levels of $\sim 2\text{mJy}$, with transient flux density enhancements of up to 1 Jy.

Despite the superficial similarities, the details of stellar flares and the *Sparker* event are in qualitative disagreement. First, decimetric bursts observed in flare stars show evidence for substructures (a series of smaller sub-bursts) not observed in the *Sparker* event [e.g., compare the dynamic spectra in Figures 1 and 5 of Osten & Bastian (2006) to Figure 2 in Lorimer *et al.* 2007]. Second, the drifts of coronal radio-bursts are typically well fit with a simple linear dependence or a $t \propto \nu^{-0.84}$ power law in case of the Sun, significantly different from the observed $t \propto \nu^{-2}$ drift. A stellar radio burst compatible with the *Sparker* would need to be one of a kind and unusually fine tuned, in addition to coming from a yet unknown nearby flare star.⁴¹ We therefore consider this explanation unlikely.

We next consider neutron-star analogs of solar Type III_{dm} bursts, recently proposed to exist in magnetar magnetospheres (Lyutikov 2002). Observationally seen as SGRs and anomalous X-ray pulsars (AXPs), magnetars are young, strongly magnetized ($B \gtrsim 10^{14}\text{G}$), and slowly spinning ($P \sim 1 - 10\text{s}$) neutron stars. By extrapolating the scales known for solar flares and magnetically active T-Tauri stars, Lyutikov (2002) proposed that magnetars should exhibit short ($< 1\text{s}$), coherent, strong ($\sim 0.1 - 100 \times D_{10\text{kpc}}^{-2}\text{Jy}$), drifting ($\nu_{\text{max}} \propto t^{\pm 2}$) decimetric radio-bursts. The expected signal drift of $t \propto \nu^{-1/2}$ is in disagreement with the strongly constrained observation of $t \propto \nu^{-2}$, but this may or may not be a serious problem given the heuristic derivation of the burst properties that Lyutikov (2002) employs.

However, the known magnetars are all in the Galactic plane whereas the *Sparker* and the FRBs are found at high latitude regions and so we do not consider the Galactic magnetar model to be reasonable. Parenthetically, as can be gleaned from this discussion, it would be useful to search for chirped bursts with different chirp signals ($t \propto \nu^n$ with values other than $n = -2$) in archival pulsar data, especially at low Galactic latitudes.

13. UNIFYING PERYTONS & FRBS

In this section we attempt to unify Perytons and FRBs. We are motivated by the fact that Perytons which are a ν^{-2} chirped signal are somehow produced either in our atmosphere or by an artificial source or sources. Perytons must be nearby because they are seen in almost all beams. FRBs are also chirped signals but since they appear almost always in single beams they must be located in the far-field. Naturally, it is tempting to unify the two classes of chirped signals by putting Perytons nearby and FRBs further away. It is the exploration of this simple idea that constitutes the primary focus of this section.

We submit that examining the detailed properties of radio telescope optics is helpful in our quest for unification. Since Perytons are generally considered to be “nearby” it is possible that the events are not sufficiently far away to assume that they are in the Fraunhofer regime, as would normally be the case for celestial events. In addition to helping unify these

³⁷ “sfu” is the solar flux unit, 1 sfu = 10^4Jy .

³⁸ Such an event may have been detected during night time at the Bleien Observatory; see Saint-Hilaire, Benz & Monstein (2014).

³⁹ This in itself would be unusual given the $t \propto \nu^{-0.84}$ dependence for typical solar Type III_{dm} bursts.

⁴⁰ <http://virtualsolar.org>

⁴² A Simbad search reveals no known flare stars in the vicinity of the *Sparker*.

phenomena, these details inform us that some care is needed in interpreting Peryton rates.

This section is organized as follows. In (§13.1) we summarize what we know about Perytons. The necessary background of the Fresnel-Fraunhofer regimes in optical theory is given in §13.2. We then summarize searches for Perytons at other Observatories (§13.3–13.6). We end the section by constructing a unified model for Perytons and FRBs (§13.7).

13.1. A Primer on Perytons

To date Perytons have been reported from two observatories: Parkes (§13.5) and the Blein Observatory (§13.3). Kocz *et al.* (2012) provide a succinct description: “Perytons are signals with swept-frequency characteristics that mimic the dispersion of a pulsar, are detected in multiple receiver beams with approximately the same signal-to-noise ratio (*sic*), and cannot be traced to an astronomical source.” It is worth noting that some of the Perytons show a ν^{-2} arrival time delay to within experimental errors (e.g., Peryton 12 and 13 listed in Table 1 of Burke-Spolaor *et al.* 2011) and that others show an approximate quadratic sweep. The DMs inferred from the frequency sweeps lie in the range 200–400 $\text{cm}^{-3} \text{ pc}$ with a mode at about 380 $\text{cm}^{-3} \text{ pc}$ (Figure 9).

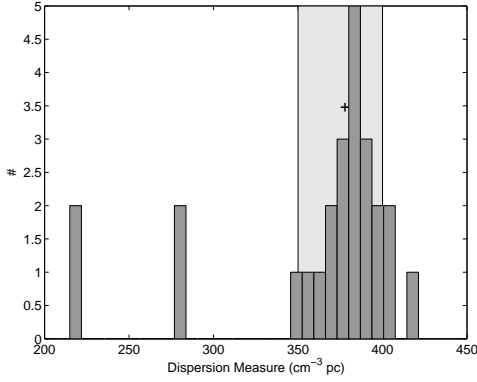


FIG. 9.— Histogram of the Perytons observed at Parkes. The *Sparker* with a $\text{DM}=375 \text{ cm}^{-3} \text{ pc}$ is shown by a ‘+’ sign. The four daytime Perytons found at the Blein Observatory (§13.3) span the range 350–400 $\text{cm}^{-3} \text{ pc}$ (this range is shown by light shading).

Perytons show symmetric pulses with pulse widths which are tens of milliseconds. The widths remain the same across the 1.28–1.52 MHz band of the Parkes pulsar spectrometer. In contrast, the pulse widths of FRBs are less than ten milliseconds with many being unresolved at the millisecond scale. The brightest FRB exhibits an exponential decay which is also frequency dependent. The *Sparker* shows a frequency dependent width but not an exponential tail.

Perytons show a strong propensity to occur during daytime and many occur during clear days (Bagchi, Nieves & McLaughlin 2012). Furthermore, some Perytons occur closely spaced in time: five Perytons within a two-minute interval (Kocz *et al.* 2012) and two Perytons within a minute of each other (Bagchi, Nieves & McLaughlin 2012). In contrast FRBs are not seen to recur despite several hour-long stares at the same position (Lorimer *et al.* 2007; Thornton *et al.* 2013). We defer the discussion of the rates of Perytons to later subsections.

13.2. Fresnel & Fraunhofer Regimes

There are two considerations that matter when observing nearby objects with large aperture telescopes. First, the beam response of a large aperture (diameter, \mathcal{D}) telescope depends strongly on whether the source is “near-field” (Fresnel regime) or “far-field” (Fraunhofer regime; Fourier optics). Next, the angular resolution of a telescope is $\theta_D = \lambda / \mathcal{D}$ where λ is the wavelength of the radio signal. We have no knowledge of the angular sizes of Perytons and it may well be that Perytons will be resolved by sufficiently large telescopes (and this may account for their presence in several beams).

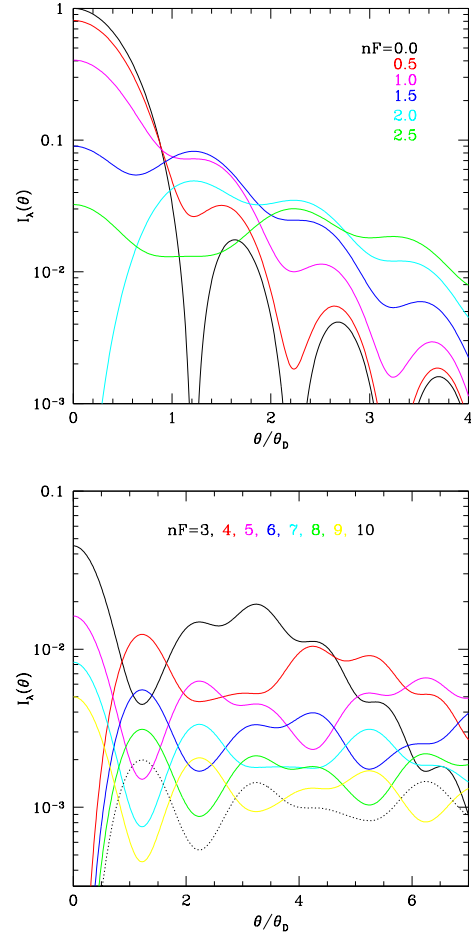


FIG. 10.— The response of a circular aperture (diameter, \mathcal{D}) to a point source located at a distance $r = a_F / n_F$ where $a_F = \mathcal{D}^2 / \lambda$ is the Fresnel scale. The horizontal axis is in units of $\theta_D = \lambda / \mathcal{D}$ with λ being the wavelength. The normalization is such that the beam response for a point source at infinity and on axis is unity.

The Fresnel scale and Fresnel zone number are, respectively,

$$a_F = \frac{\mathcal{D}^2}{\lambda} \quad \text{and} \quad n_F = \frac{a_F}{r}, \quad (57)$$

where r is the distance to the source. The Fraunhofer approximation is applicable when $n_F \rightarrow 0$. The Fresnel formulation is applicable when n_F is in the vicinity of unity (with ray optics applicable when $n_F \rightarrow \infty$). As a matter of reference, at $\lambda = 21 \text{ cm}$, the Fresnel scales for a 6-m (ATA), 25-m (VLA or VLBA antennas), 64-m (Parkes) and 305-m telescope (Arecibo) are 0.18 km, 3 km, 20 km and 440 m, re-

spectively. This wide variation in a_F means that care must be taken when comparing Peryton detections and statistics at the various facilities.

The response, at wavelength λ , of a telescope with a circular aperture (diameter, \mathcal{D}), to a point source located at distance r is given by

$$I_\lambda(\theta|n_F, \theta_D) = \text{abs} \left(\int_0^1 J_0[\pi \rho(\theta/\theta_D)] \exp(in_F \pi \rho^2) 2\rho d\rho \right)^2. \quad (58)$$

Here, θ is the angular offset of the receiving beam with respect to the bore-sight. This response is graphically summarized in Figure 10 for a range of n_F . As can be seen from this figure, even with a modest Fresnel number a point source will appear as extended for a telescope which is focused for observing sources at infinity.

In the Fraunhofer regime the only way a distant compact source can be seen in multiple beams is by side-lobe “pick up”. For an unobscured circular aperture the beam response, in the Fraunhofer regime, is give by

$$I_\lambda(\theta) = \left[\frac{2J_1(\pi\theta/\theta_D)}{\pi\theta/\theta_D} \right]^2, \\ \approx \frac{2}{\pi^4} \left(\frac{\theta}{\theta_D} \right)^{-3} \text{ for } \theta/\theta_D \gg 1. \quad (59)$$

As before, here $I(\theta)$ is normalized to unity for a point source at infinity and located on axis.

However, structures which obscure the aperture cause additional side-lobes (and in some cases result in side-lobes with responses greater than expected from Equation 58). Let η_m be the beam response obtained by integrating from say $\theta = 0$ to a few θ_D (“main beam response”). Then $1 - \eta_m$ must account for the integrated response of the these wayward side lobes. The smallest response by these side-lobes is obtained by spreading $1 - \eta_m$ uniformly over a solid angle Ω_{SL} which can reasonably account for most of the side-lobes. With these two simplifying assumptions the side-lobe response is

$$I_{SL} = (1 - \eta_m) \frac{\theta_D^2}{\Omega_{SL}}. \quad (60)$$

For the Parkes telescope we find $I_{SL} = 2 \times 10^{-6} \Omega_{SL}^{-1}$ where we assume $\eta_m = 0.8$ and Ω_{SL} has the units of steradian.

13.3. Perytons from Bleien Observatory

An important very recent development is the detection of Peryton-like events at the Bleien Observatory located 50 km west of Zurich, Switzerland (Saint-Hilaire, Benz & Monstein 2014). These authors recorded the radio spectrum of the sky with a log-periodic antenna in the band 1.15–1.74 GHz. The spectrometer channel width and dump time was 1 MHz and 10 ms, respectively. The beam of the antenna was 110° in the North-South direction and 70° in the East-West direction. Over 288 days (from 3 June 2009 to 18 March 2010) the authors found four *day-time* pulsed events with pulse widths of about 20 ms and peak fluxes ranging from 250 to 840 kJy, exhibiting a trajectory in the frequency-time plane consistent with a ν^{-2} sweep.

The inferred DMs are in the range 350–400 cm^{-3} pc even though the search covered the range 50–2000 cm^{-3} pc. The DM determinations are necessarily crude, being limited by coarse time binning and low SNR (8 to 16). Apart from their

apparent brilliance, these events appear to share all the properties of Perytons including the strong clustering of the inferred DMs around 300 cm^{-3} pc. It is not unreasonable to conclude that these events are also Perytons. With this independent detection at an Observatory far away from Parkes we can reasonably conclude that Perytons are truly a world-wide phenomenon.⁴³

The mean time between the bright Perytons detected at the Bleien Observatory is 72 days. Next, the beam of the log-period antenna is 1.75 steradians. Thus the daily *all-sky* rate of the bright Bleien Perytons is 0.1 per day or 36 per year.

13.4. Search for Perytons at ATA

A search for FRBs was undertaken at the Allen Telescope Array (ATA, Siemion *et al.* 2012). This array consists of 42 dishes each of 6-m diameter and operates in the 1.4-GHz band. We note the Fresnel radius for the ATA antennas is 0.18 km. This length scale is small enough that we can assume that the intensity response of each antenna to Perytons, $I_\lambda(\theta)$, is securely in the Fraunhofer regime.

In the Fly’s Eye experiment each antenna was pointed to a different region of sky and search was undertaken for dispersed pulses (Siemion *et al.* 2012). The resulting instantaneous field-of-view was an impressive 150 square degrees and the experiment lasted 450 hours. The authors state “This wide-field search yielded no detections, allowing us to place a limiting rate of less than $2 \text{ sky}^{-1} \text{ hr}^{-1}$ for 10 ms duration pulses having mean apparent flux densities greater than 44 Jy.” Apparently, despite a gain of nearly 10^4 in peak flux sensitivity the ATA experiment could not detect Perytons.

Adopting a mean peak flux of 440 kJy for the Bleien sample we deduce that the all-sky daily rate of Perytons as a function of peak flux (S), $\mathcal{N}_P(S) \propto S^q$ would require that $q \gtrsim -0.67$. We appreciate that this inference is subject to Poisson errors but nonetheless are intrigued by the fact that the value of q hints at a disk or even a curved atmosphere geometry for the distribution of Perytons (§D).

We now estimate whether a typical bright Bleien Peryton could have been detected by the ATA dishes via side-lobes (Equation 59). Thus a 440 kJy compact source would be detectable to a single ATA antenna via off-axis response provided that $\theta/\theta_D < 6$. In this case, the effective field-of-view of the Fly’s Eye can be as large as 5400 square degrees. The product of the solid angle (where all sky is set to unity) and the exposure time of the Fly’s Eye experiment is 2.53 day-sky. The mean Poisson expectation is 0.25. Thus the lack of detection of a single bright Peryton ($S \gtrsim 440$ kJy) via a side-lobe does not violently violate the Bleien rate.

13.5. Perytons from Parkes

Burke-Spolaor *et al.* (2011) and Kocz *et al.* (2012) report Perytons found in the analysis of the high-latitude data while Bagchi, Nieves & McLaughlin (2012) report events found in Galactic Plane survey. In both cases, the same (analog-filter bank) backend that was used to detect the *Sparker* was used with the Multi-Beam receiver. Perytons have been found with the new digital filter bank⁴⁴ (S. Burke Spolaor & M. Bailes, pers. comm).

⁴³ The Parkes data certainly required Perytons to be of local origin (the Shire of Parkes). The observations of Saint-Hilaire, Benz & Monstein (2014) elevate Perytons to world-wide or terrestrial status.

⁴⁴ from which FRBs were found and reported by Thornton *et al.* (2013)

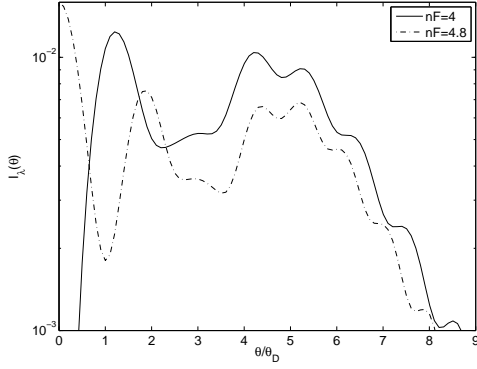


FIG. 11.— The response of the Parkes 64-m telescope to a point source located at $r = 4.4$ km. The corresponding Fresnel zone number at the lower edge (1.28 GHz) of the frequency band (1.28 GHz–1.52 GHz) is 4 and that at the higher edge is 4.8.

The observed rate of Perytons appears to be dependent on which survey the search (and analysis) was based upon. Burke-Spolaor *et al.* (2011) spent 45 days of observing and found 16 Perytons (or 6 if those which occurred in a short period counts as only one Peryton). Thus their observed rate is 0.36 (0.13) per day where the quantity in brackets refers to “independent” Perytons. The typical peak flux density for this sample is 0.1 Jy. Bagchi, Nieves & McLaughlin (2012) analyzed the Galactic Plane data and found four Perytons over 75 days. The typical flux density is higher, 0.5 Jy. The daily observed rate is thus 0.05 (0.04) per day⁴⁵. At low Galactic latitudes the system temperature (T_{sys}) is higher than at high latitudes. So one expects a higher limiting flux and thus fewer Perytons but the large difference between the rates of the two surveys (admittedly subject to severe Poisson errors) needs careful investigation.

The above rates are *observed* rates. Translation of these rates to *all-sky* rates depends upon the location of Perytons (near-field or far field). Burke-Spolaor *et al.* (2011) assume that Perytons are via pickup of bright source by side-lobe which are severely off-axis: $\theta \gg 5^\circ$ from the principal pointing axis. Burke-Spolaor *et al.* (2011) go further and assume that the instantaneous field-of-view for the Perytons is the visible sky ($\Omega = 2\pi$ steradians). This would, via Equation 60, require a pickup level of about 10^{-7} and thus in this framework Perytons are Mega Jansky sources. The apparent coincidence of the Bleien rate and the Peryton rate of Burke-Spolaor *et al.* (2011) could be seen as supporting the implicit assumption of Burke-Spolaor *et al.* (2011). However, if we accept this conclusion then it would mean that there are very few Perytons which are fainter than those found at Bleien Observatory – which, while convenient, we find to be discomfiting.

We take the following two views. (1) It is by no means clear that Perytons are distant sources, or that one can securely assume that the Perytons are in the far-field. (2) We assume that there is a range of luminosities for the Perytons and the apparent coincidence between the Bleien and the Parkes rate is a victim of small number statistics. Consistent with this view we have to consider the possibility that some Perytons will be nearby and some far away. With these views we now re-interpret the Parkes Peryton data.

⁴⁵ Bagchi, Nieves & McLaughlin (2012) quote a rate that is smaller than those quoted here because they treat each beam as an independent stream. Perytons are found in all beams and thus the beams should not be counted as being independent.

The Parkes Multi-Beam field-of-view is circumscribed by a circle of radius⁴⁶ $\theta_{\text{MB}} = 1.3^\circ$. A source located at $a_F/4$ will easily illuminate all the thirteen beams. Thus the Parkes Peryton all-sky rate can be as high as $\dot{\mathcal{N}}_P \times 4\pi/\Delta\Omega$ per day where $\dot{\mathcal{N}}_P$ is the daily observed Parkes Peryton rate and $\Delta\Omega$ is the average angular “size” of Perytons (as seen by the Parkes telescope). Since all the Parkes Perytons reported to date are found in all thirteen beams we can safely conclude that $\Delta\Omega > \pi\theta_{\text{MB}}^2$. The typical flux density of the Parkes Peryton (in each beam) is a few tenths of Jansky. The integrated flux density is larger by at least $\pi\theta_{\text{MB}}^2/\theta_D^2 \approx 150$. Thus the Parkes Perytons have a peak flux of 15 Jy or larger.

Since most of what we know about Perytons has come from Parkes it is worth our time to study the Parkes beam response in some detail. The beam response function across the Parkes bandwidth is shown in Figure 11. We draw the reader’s attention to three points. First, in the Fresnel approximation, the source is picked up at a level of 10^{-2} as opposed to the much smaller pickup hypothesized by Burke-Spolaor *et al.* (2011). Next, for most of the solid angle (angular offset, $\theta \gtrsim 2\theta_D$), the spectrum can be approximated by a power law with a small value of α .⁴⁷ Third, as can be seen from Figure 10, it is difficult (in the absence high SNR), to distinguish a Peryton with $n_F = 1/2$ from that located at infinity ($n_F = 0$).

13.6. Searches for Perytons at Other Observatories

Currently, a search for FRBs is being carried out at the Expanded Very Large Array (EVLA)⁴⁸. The array has 27 antennas with $\mathcal{D} = 25$ m. The Fresnel scale for a single antenna, at a wavelength of 21 cm, is 3 km. Likely most Perytons will be in the far-field regime. A search for Perytons in the signal streams from each antenna would be useful. Perytons as nearby objects, given the spatial width of the B-array, will have substantial parallax. For instance, the sky angular position of a Peryton hypothetically located at 5 km will vary by $\pm 45^\circ$ as we go from one end of the array to the other. Thus, curiously enough, for the study of Perytons, the instant field of view of the VLA is 27 times that of a single 25-m telescope. This total field-of-view exceeds that of the Parkes Multi-Beam system. Furthermore, given a smaller a_F Perytons are likely to be in “focus” (relative to the situation at Parkes) and thus the Perytons will be brighter. Going forward it appears to us that it would be quite promising to undertake commensal or archival analysis of L-band data. A single detection of a Peryton will immediately inform us of its parallax.

The same comments apply to the search for FRBs with the Very Long Baseline Array (VLBA) system – the V-FASTR experiment (Wayth *et al.* 2012). An additional advantage of the V-FASTR experiment is that it can simultaneously search for Perytons in ten different weather regions.

The Arecibo 305-m radio telescope is also equipped with a Multi-Beam pulsar receiver and signal processing system⁴⁹. For the Arecibo telescope $a_F = 443$ km at $\lambda = 21$ cm. Thus, relative to Parkes, the Perytons will be considerably out of focus (see Figure 12) and it may be well be that Arecibo, despite its larger collecting area, will not detect any Perytons.

⁴⁶ We give the radius in units of degrees but when computing solid angles we switch to radians.

⁴⁷ Conversely, we note that strong spectral indices, positive or negative and with large magnitudes can also be obtained.

⁴⁸ Principal Investigator: Casey Law.

⁴⁹ <http://www.naic.edu/alfa/pulsar/>

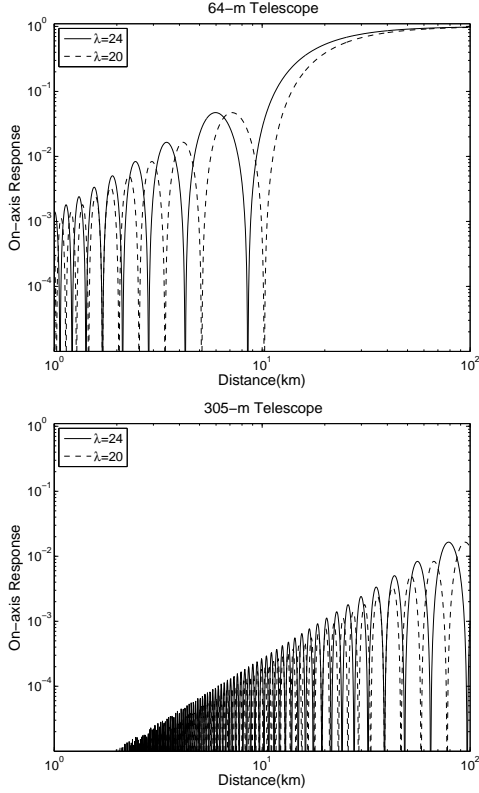


FIG. 12.— The on-axis response for a point source by the Parkes 64-m telescope (top) and the Arecibo 305-m telescope (bottom) operating in 1.4-GHz band for point sources located between 1 km and 100 km. For *each* telescope, the response is normalized to be unity for a source at a very large distance ($n_F \rightarrow 0$).

13.7. A Working Hypothesis

We propose a *working hypothesis* aimed at unifying Perytons, the *Sparker* and FRBs. The underpinnings are the following:

1. Perytons are atmospheric phenomena which are detected essentially on axis (and not via side lobes located a radian or two away from the bore-sight).
2. Perytons are seen in many beams for the Parkes multi-beam receiver. Ergo we deduce that they be located in the near-field (“out of focus”). Thus we infer that Perytons are located at distances not beyond the first Fresnel zone for the Parkes telescope at 21-cm wavelength.
3. The *Sparker* is a Peryton that probably occurred close to the Fresnel radius of the telescope, a_F (Equation 57). The higher distance ensures that the *Sparker* will appear more or less in good focus. Our primary motivation for claiming that the *Sparker* is a Peryton is that the DM of the *Sparker* coincides with the peak of the DM distribution for Perytons (see also Bagchi, Nieves & McLaughlin 2012).
4. The FRBs appear to be in good focus and therefore in this hypothesis have to occur beyond the Fresnel radius of the Parkes telescope at $\lambda = 21$ cm. As can be seen from Figure 10 the beam response for a source with $n_F \lesssim 1$ is not different from that of cosmic sources ($n_F \rightarrow 0$).

In this framework, for Perytons, the effective field-of-view is the larger of the circumscribed circle discussed above (5.3 square degrees) and the solid angle covered by the Fresnel point-spread function. The all-sky Peryton rate is then $(4\pi/\Delta\Omega)\mathcal{N}_P$ where $\Delta\Omega$ is the larger of 5.3 square degrees and the apparent angular size of Perytons (as seen by the Parkes telescope in the 20-cm band). The bulk of the Perytons in this hypothesis would be intrinsically weak signals, perhaps 100 Jy to a few kJy.

We are acutely aware that our working hypothesis glosses over many key issues. To start with, we have provided no strong reasons for a natural, or atmospheric origin for Perytons as opposed to a man made origin. Next, we have not provided any physical model for the Perytons, nor have we even suggested why Peryton-like phenomenon (the *Sparker* and FRBs), occurring at supposedly larger heights⁵⁰ in the atmosphere, should exhibit narrower pulses, show a ν^{-2} sweep of arrival time, nor why the *Sparker* and one of the FRBs exhibit a frequency-dependent pulse width. In our defense, we note that Perytons are accepted to be local events and some of them show a ν^{-2} sweep of arrival time (within experimental errors; see above). So our suggestion has some basis in reality.

We end this section with two observations. In the proposed framework, for the Arecibo telescope, the Perytons, the *Sparker*, and the FRBs will be deeply into the Fresnel region. Assigning nominal heights⁵¹ of 5 km, 20 km and 40 km for Perytons, the *Sparker*, and FRBs, we find Fresnel zone numbers of 86, 21 and 11. As can be seen from Figure 12, the pick up of Perytons by the giant Arecibo reflector, relative to the Parkes telescope, is diminished severely. Next, we note that a source even at a height of 100 km has $n_F \approx 4$ and the Fresnel beam would be quite out of focus (see Figure 11). Our proposed working hypothesis would have great difficulty (perhaps even to a fatal level) in explaining a single beam detection of an FRB by the Arecibo multi beam system. We do note that, to date, no Peryton and for that matter no robust FRB has been reported from archival analyses of the Arecibo data (Deneva *et al.* 2009).

We conclude this section by noting that the Fresnel scale for the VLBA is 3×10^3 AU and that for the VLA is approximately the distance to the moon. In that sense, a *single* detection of an FRB by the VLA will immediately establish an extra-lunar origin and that by the VLBA an extra-solar-system origin.

14. CONCLUSIONS

From analysis of archival pulsar data obtained at the Parkes Observatory astronomers have reported radio pulses with millisecond duration and with a frequency dependent arrival time which if interpreted as due to propagation would require dispersion measures considerably exceeding that expected from the Galactic interstellar medium (Lorimer *et al.* 2007; Thornton *et al.* 2013). The short durations of these events require a high brightness temperature, even if their origin is Galactic, let alone extragalactic. The all-sky rate of FRBs is an astounding 10^4 per day. In this paper we have explored a wide range of scenarios capable of explaining the properties

⁵⁰ We caution that what matters is the distance to the Peryton as opposed to the height. A Peryton at an altitude of say 3 km can be beyond the first Fresnel zone if viewed at low elevation angles.

⁵¹ Arecibo is a transit instrument and so the sources are observed overhead.

and suggested progenitors of the *Sparker* (which has the lowest inferred DM; Lorimer *et al.* 2007) and Fast Radio Bursts (FRBs; Thornton *et al.* 2013). Complicating this discussion is the presence of “Perytons” which share the properties of FRBs but are conclusively identified as arising locally (terrestrial origin). The inferred DMs of the Perytons are strongly clustered in the range $300\text{--}400\text{ cm}^{-3}\text{ pc}$.

We started our investigation of these sources by accepting that the large inferred DM for the *Sparker* is indeed a result of a signal propagating through a cold plasma. We arrived at the following conclusions.

1. Based on available archival imaging, the nebula that produces the large DM for the *Sparker* can be no closer than 300 kpc. The minimum distance for the four FRBs (with their larger inferred DMs) would be higher. This conclusion led us to investigate extra-galactic models for the sources.
2. We consider a host of plausible extra-galactic progenitors including supernovae, blitzars, short hard bursts, white dwarf mergers and soft gamma-ray repeaters. The models either are physically inconsistent (lack a suitable clean and relativistic environment to produce high brightness temperature bursts or suffer from free-free absorption in the general vicinity of the progenitor) or are unable to account for the high all-sky FRB rate (10^4 day^{-1}).
3. Of all the possible progenitors, giant flares from young magnetars present the most attractive physical model. This model has the advantage of naturally explaining why some FRBs show frequency-dependent pulse widths. The model can also account for the rates provided that an efficiency of 10^{-5} can be achieved in converting the energy release in giant flares into radio emission.

We believe that we have explored all reasonable *stellar* models for FRBs. Thus, should it turn out that FRBs are not of stellar origin then non-stellar models (e.g., quasars - E. S. Phinney, pers. comm.; cosmic superconducting strings - Vachaspati 2008) have to be considered.

Consistent with our agnostic exploration of the FRB phenomenon we drop the requirement that the *Sparker*’s large DM was produced by propagation through a cold plasma. In this framework the source produce a “chirped” signal (frequency dependent arrival time). Chirped signals are used by the military (radar), communications (spread spectrum) and also arise from natural phenomenon (e.g., bursts from the Sun, atmospheric events). We propose an empirical model unifying Perytons with FRBs with the Perytons being in the near-field of the Parkes telescope (where the Fresnel approximation holds) and FRBs being in the far-field (where the traditional Fourier optics assumed by radio astronomers holds).

The inferred DM for the *Sparker* is similar to the mode of the Peryton distribution (Figure 9). Next, it is not obvious to us (from the signal level in different beams) that the *Sparker* has to be a source at a very large distance (§A). Economy of hypotheses lead us to suggest that the *Sparker* itself is a Peryton that occurred at a height of about 20 km (the Fresnel scale for the Parkes 64-m telescope at a wavelength of 21 cm). In order to explain FRBs as Perytons we require that the chirp rate of Perytons must scale proportionally with their distance (height). We offer no explanation for this requirement.

Perytons form a formidable foreground for FRBs. As such further progress will require astronomers to understand the distribution of and distances to Perytons. Perytons show clearly that Nature can produce chirped signals in the 21-cm band and so a thorough understanding of the Perytons will only help astronomers distinguish local sources from cosmic sources. Since Perytons are local sources with as yet unknown distances some care is needed prior to comparing the rates of Perytons from different telescopes (with differing Fresnel scales).

In summary, there is no compelling evidence to support an extra-terrestrial origin for FRBs. A plausible argument can be made to relate giant flares from SGRs to FRBs. In this picture the typical redshift of an FRB is $z \approx 0.5$. An interferometric localization of FRBs will immediately rule out a local origin. The same data will either show a host galaxy (which would then revive stellar models or quasar models) or no host galaxy (which will favor truly exotic origins). A modest investment in several clusters of simple dipoles tuned to the 1–2 GHz band and separated moderately (tens to hundreds of kilometers) would be a worthwhile investment (if only to explore strong decimetric pulses not only from Galactic giant flares but from the gamut of Galactic sources).

Despite the current murky situation it is tempting to think of bountiful diagnostics that can be provided by millisecond bursts of extra-galactic origin. In §E we review a couple of these diagnostics. In particular we draw the reader’s attention to a unique way by which astronomers can search for solar-mass intergalactic MACHOs through FRBs.

We conclude by noting that in the title of the paper: “Giant Sparks at Cosmological Distances?”, the adjective giant refers to the nominal length scale of the emitting region (300 km; §8), and the word spark has the same meaning as in pulsar phenomenology. We point out that the traditional outcome of papers that pose a question in their title is generally in the negative. Nonetheless, one could take some comfort from the history of gamma-ray bursts (GRBs). This was an exotic phenomenon even for astronomers. The history of GRBs started with searches for possible terrestrial (artificial) signals. Since their discovery in 1967, the diversity of observed phenomena has grown tremendously. Bursts of gamma-rays are now seen from atmospheric events (Fishman *et al.* 1994), from the Sun (Third Orbiting Solar Observatory, Kraushaar *et al.* 1972), from compact stellar sources in our Galaxy (Mazets *et al.* 1979; Cline *et al.* 1980; Kasliwal *et al.* 2008), and from cosmological distances (Metzger *et al.* 1997) and that too from at least two distinct populations (Kouveliotou *et al.* 1993). So, at early times, what one could have considered to be a single phenomenon literally spans terrestrial to cosmological scales. It may well be that astronomers are on a similar adventure in the radio band.

SRK would like to thank the hospitality of the Institute for Advanced Study (IAS). The sylvan surroundings and verdant intellectual ambiance of IAS resulted in a fecund mini-sabbatical stay (Fall 2007). We are grateful to M. Bailes, S. Burke-Spolaor and D. Lorimer for sharing with us the details of the Parkes Multi-Beam Survey. We thank M. Putman and S. Stanimirovic for help with the H I data on the SMC and S. B. Cenko, D. B. Fox and J. Kanner discussions about X-ray transients. We gratefully acknowledge C. Hirata for careful reading, feedback and instructions of basic physics; and P. Kumar and J-P Macquart for discussions about rel-

ativistic flows. We thank J. Cordes for sharing his ideas about detection strategies. We acknowledge useful discussions with D. Bhattacharya, G. Bower, Y-H Chu, J. Condon, D. A. Frail, P. M. Goldreich, A. Gruzinov, G. Hallinan, C. Heiles, E. S. Phinney, S. Thorsett, D. Q. Wang and E. Witten. We especially thank Y. Cao, S. Tendulkar and M. H. van Kerkwijk for a careful reading of the paper. Finally, we acknowledge robust discussions with authors of several recent papers attempting to explain the origin of FRBs: H. Falcke, J. I. Katz, A. Loeb, P. Mészáros, T. Totani and B. Zhang.

EOO is incumbent of the Arye Dissentshik career develop-

ment chair and is grateful to support by grants from the Willner Family Leadership Institute Ilan Gluzman (Secaucus NJ), Israeli Ministry of Science, Israel Science Foundation, Minerva and the I-CORE Program of the Planning and Budgeting Committee and The Israel Science Foundation.

This work is supported in part by grants from NSF and NASA. We gratefully acknowledge the use of the following archives: Southern H α Sky Survey, UK Schmidt Surveys, the Digital Sky Survey, *GALEX* and the ATNF Pulsar catalog. As usual, the authors are indebted to the librarians who maintain ADS and *Simbad*.

APPENDIX

A. A BETTER LOCALIZATION OF THE SPARKER

With a single detection of a pulse by a single beam, the localization is necessarily poor – no better than the area of sky illuminated by the main beam. However, the *Sparker* was detected in 3 out of the 13 beams, with SNRs of > 100 , ~ 21 and ~ 14 ; a summary can be found in Table 3. This pattern of detections, in principle, should allow us to improve the position of the *Sparker*. To this end we need the location of the beams and the response of the beams. We tried several assumptions which we briefly summerize. First, as a zero order approximation, we assume that the beam shapes are Gaussian with the widths and gains specified In Table 3, and that the ratio in intensities in the different beams are provided by the square of the SNR. We also assumed that the relative intensities are known to precision of about 5% and that the real S/N ratio of the saturated beam is smaller than about 1000. Given these assumptions we find that the Sparker localization is within the error region specified in Table 4. However, it is well known that the beam shapes of radio instruments are non-Gaussian. Therefore, next we attempt to use an electromagnetic model of the beam response supplied to us by L. Staveley-Smith (updated from Staveley-Smith *et al.* 1996, see Figure 13). The response function is valid for point sources located well beyond the first Fresnel zone.

TABLE 3
SNR OF THE *Sparker* IN THE BEAMS

Beam	RA (J2000)	Dec (J2000)	SNR	FWHM	Gain
			arcmin		
1	01 : 21 : 18.0	-74 : 46 : 01	< 5	14.0	0.74
2	01 : 17 : 09.8	-74 : 22 : 04	< 5	14.1	0.69
3	01 : 24 : 19.5	-74 : 19 : 33	< 5	14.1	0.69
4	01 : 28 : 37.7	-74 : 43 : 00	< 5	14.1	0.69
5	01 : 25 : 39.1	-75 : 09 : 40	< 5	14.1	0.69
6	01 : 18 : 06.0	-75 : 12 : 19	> 100	14.1	0.69
7	01 : 13 : 55.8	-74 : 48 : 09	14	14.1	0.69
8	01 : 09 : 53.4	-74 : 23 : 32	< 5	14.5	0.58
9	01 : 20 : 13.1	-73 : 55 : 27	< 5	14.5	0.58
10	01 : 31 : 30.8	-74 : 15 : 57	< 5	14.5	0.58
11	01 : 33 : 14.5	-75 : 06 : 15	< 5	14.5	0.58
12	01 : 22 : 30.3	-75 : 36 : 34	< 5	14.5	0.58
13	01 : 10 : 25.8	-75 : 14 : 14	21	14.5	0.58

Notes: The entry in bold-face is the beam in which the *Sparker* signal is saturated (SNR >100). FWHM stands for Full Width at Half Maximum of the beam. The adopted FWHM values are 14, 14.1 and 14.5 arc minute, for the central beam, inner-ring beams and outer-ring beams, respectively (see Manchester *et al.* 2001). The gain is the mean aperture efficiency of each beam (*ibid*). The positions of the beams were provided to us by M. Bailes and D. Lorimer.

TABLE 4
Sparker ERROR REGION

RA (J2000)	Dec (J2000)
18.85619	-75.12665
19.34551	-75.18275
19.37912	-75.19694
19.34551	-75.20249
18.83199	-75.14258
18.83064	-75.13011

We adopted the SNRs given above for beams 6, 7, and 13, and < 5 in the rest of the beams (Table 3). Since the SNR values are subject to Poisson errors, we allow for 3σ uncertainties in the SNR values that we used. However, we were not able to find

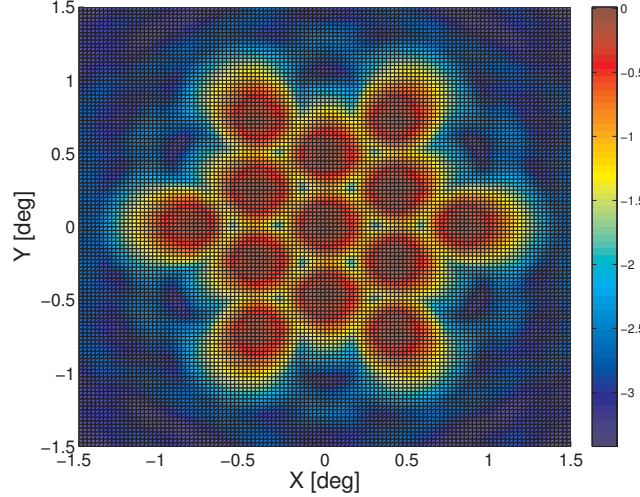


FIG. 13.— The Parkes Multi-Beam relative response pattern, based on electromagnetic modeling, as a function of position in degrees relative to the center of the field-of-view (L. Staveley-Smith, pers. comm; updated from Staveley-Smith *et al.* 1996). The response function is valid for point sources located well beyond the first Fresnel zone.

RA (J2000)	Dec (J2000)
deg	deg
19.5250	−75.2053
18.4825	−74.8025
17.6075	−75.2372
18.5900	−75.3647

TABLE 5
THE VERTICES OF THE POLYGON WHICH ENCLOSES ALL POSSIBLE POSITIONS OF THE *Sparker*.

any position within the Parkes multi beam field-of-view which can reproduce the observed detections. This failure could be due to (i) the electromagnetic model is not adequate to model responses at large angles ($2\theta_D$ to $3\theta_D$) or (ii) the *Sparker* is not located at a great distance (in which case our use of the Multi-Beam pattern is incorrect).

Burke-Spolaor *et al.* (2011) used an empirical beam response (by scanning the multi-beam receiver across a bright pulsar) and found a best-fit position: RA= $19.44^\circ \pm 0.08^\circ$ and Declination= $-75.17^\circ \pm 0.08^\circ$ (J2000). This position almost coincides with beam 6 (see Figure 1 and also Table 3). The *Sparker* is detected in beam 7 (due North West) and beam 13 (due West). However, given the claimed location we would have expected the *Sparker* to be detected by the beams due South East, due East and due North East. The lack of detection in these three beams is troubling.

In order to deduce the most conservative localization of the *Sparker* we adopted an approach based primarily on symmetry. We assumed that the beam pattern has circular symmetry. Since the *Sparker* was detected in three beams, but not in all the other beams, we conclude that the *Sparker* should be in the region between the three beams. Beam 7, 6 and 12 are on a straight line, therefore the lower part of the localization region is perpendicular to the line connecting these beams. We assumed that the region is symmetric, mostly because beam 6 had the strongest detection. These considerations led us to a polygon (aka “kite”). The vertices of this polygon are listed in Table 5. The North-East side of the polygon is defined by the centers of beams 6 and 7 (see Table 3), while the North-West side is defined by the centers of beams 7 and 13. The South-East side is perpendicular to the line joining beams 6 and 7, and the South-West side is the intersection of the line joining beams 13 and 12 and the South-East side.

B. MONO-ENERGETIC PARTICLE SYNCHROTRON SPECTRUM

The simplest model for producing an arbitrarily steep spectrum radio emission is to have mono-energetic electrons gyrating in a magnetic field. Starting at lower frequencies the spectrum rises as $x^{1/3}$, peaking at $x = 0.29$ and declining as

$$S(x) = A\sqrt{x}\exp(-x), \quad x \gg 1. \quad (\text{B1})$$

Here, A is a normalization factor, $x = v/v_c$ and

$$v_c = \frac{3}{4\pi} \gamma^3 \omega_B \sin(\alpha) \quad (\text{B2})$$

is the so-called “gyro-synchrotron” frequency. Here, $\omega_B = eB/(\gamma m_e c)$ is the gyro-frequency of an electron with Lorentz factor γ and gyrating in a magnetic field of strength B and moving in the mean at an angle α with respect to the field lines (Rybicki & Lightman 1979, Chapter 6).

For $x \gg 1$ the power law slope is given by

$$\alpha \equiv \frac{d \ln S_\nu}{d \ln \nu} = \frac{1}{2} - \frac{\nu}{\nu_c}. \quad (\text{B3})$$

At high frequencies, an arbitrarily large spectral index can be obtained by invoking a smaller value of ν_c .

C. STARS & SUPERNOVAE: DM & EM

Consider a star with a mass loss rate of \dot{M} and radius R_* . In a steady state this leads to a wind with a density radial distribution, $\rho(r)$, given by

$$\dot{M} = 4\pi r^2 v_w \rho(r). \quad (\text{C1})$$

Here, v_w is the radial velocity of the wind many stellar radii away from the star. The dispersion measure, DM, emission measure, EM, and plasma frequency, ν_p , are then given by

$$\text{DM} = \int_{R_*}^{\infty} \frac{\rho(r)}{\mu m_H} dr = \frac{\dot{M}}{4\pi v_w \mu m_H} R_*^{-1}, \quad (\text{C2})$$

$$\text{EM} = \int_{R_*}^{\infty} \left(\frac{\rho(r)}{\mu m_H} \right)^2 dr = \left(\frac{\dot{M}}{4\pi v_w \mu m_H} \right)^2 \frac{R_*^{-3}}{3}, \quad (\text{C3})$$

$$\nu_p = \frac{1}{2\pi} \sqrt{\frac{4\pi n_e e^2}{m_e}} \text{ Hz}, \quad (\text{C4})$$

where μ is mean molecular weight of electrons.

The stellar wind velocity is clearly greater than the escape velocity. For stars on the lower main sequence, the escape velocity is constant since $R \propto M$. We set $v_w = 10^3 \text{ km s}^{-1}$ and for simplicity let $\mu = 1$. Then we find

$$\begin{aligned} \text{DM} &= 17B \left(\frac{R_*}{R_\odot} \right)^{-1} \text{ cm}^{-3} \text{ pc}, \\ \text{EM} &= 4 \times 10^9 B^2 \left(\frac{R_*}{R_\odot} \right)^{-3} \text{ cm}^{-6} \text{ pc}, \\ \nu_p &= 223 B^{1/2} \left(\frac{R_*}{R_\odot} \right)^{-1} \text{ MHz}, \end{aligned} \quad (\text{C5})$$

where $B = \dot{M}_{-10}/(v_w/10^3 \text{ km s}^{-1})$ and $\dot{M}_{-10} = \dot{M}/10^{-10} M_\odot \text{ yr}^{-1}$. These equations show why stellar models cannot produce sufficient dispersion measure without producing a very large emission measure leading to free-free absorption in the decimetric band.

In the model of Loeb, Shvartzvald & Maoz (2014), the radio pulse is produced at some radius within an extended corona and the DM results from the pulse propagating to the surface. Such an extended corona cannot be stably bound to the star and it is reasonable to assume a wind solution as above. However, we will not assume a steady state. Let the radio pulse be emitted at radius R_* and the edge of the corona be at L . In this case and the DM and EM are

$$\begin{aligned} \text{DM} &= n_* R_* \left[1 - (R_*/L) \right], \\ \text{EM} &= \frac{n_*^2 R_*}{3} \left[1 - (R_*/L) \right]^3, \\ &= \frac{\text{DM}^2}{3R_{\text{pc}}} \left[1 - (R_*/L) \right]^3, \end{aligned} \quad (\text{C6})$$

where $n_* = n_e(R_*)$ and $R_{\text{pc}} = R_*/(1 \text{ pc})$. Even if L is greater than R_* , by as little as a factor of 1.3, we have $\text{EM} \approx \text{DM}^2/R_{\text{pc}}$.

One of the models suggested for the Parkes events is the merger of two white dwarfs that eventually forms a magnetar. Our current understanding of the merger is as follows: the lower mass white dwarf is tidally disrupted and accretes onto the other (“primary”) white dwarf. During the mass buildup of the primary white dwarf, a fraction of the accretion energy drives a very strong stellar wind. The relevant outflow velocity is the escape velocity of the primary star and so $v_w \approx 5 \times 10^8 \text{ cm s}^{-1}$. Using the convention from supernovae, we have $A_* \equiv \dot{M}/(4\pi v_w)/5 \times 10^{11} \text{ gm cm}^{-1}$ (Chevalier & Fransson 2006). $A_* = 1$ for $v_w = 5 \times 10^3 \text{ km s}^{-1}$ and $\dot{M} = 5 \times 10^{-5} M_\odot \text{ yr}^{-1}$. Rescaling from Equation C5 and using Equation 7 we obtain the free-free optical depth at $\nu_0 = 1.4 \text{ GHz}$ to be

$$\tau_{\text{ff}}(\nu_0) = 1.9 A_*^2 r_{15}^{-3}. \quad (\text{C7})$$

Here, the radial distance $r = 10^{15} r_{15} \text{ cm}$. The run of plasma frequency with density is

$$\nu_p = 5 A_*^{1/2} r_{15}^{-1} \text{ MHz}. \quad (\text{C8})$$

These two equations inform us that only radio emission emitted after the blast wave has crossed the radius at which the free-free optical depth is sufficiently small will reach the observer. For instance, even if the stellar wind lasts for a day the circumstellar medium will be optically thick to decimetric radiation (provided A_* is comparable to unity).

Next, we consider the case of a merger product transmuting to the next level of compactness: merged white dwarfs to magnetar, or merged neutron stars to a rapidly spinning black hole. We will assume a mass ΔM is ejected at sub-relativistic velocities v in a spherical geometry. Numerical simulations suggest $10^{-4} \lesssim \Delta M \lesssim 10^{-2} M_\odot$ (Hotokezaka *et al.* 2013).

Let us assume that the debris is a shell of radius, $R = vt$ and has a width, $\Delta R = fR$ with f being assumed to be a constant (with time). Then

$$n_e = 9.5 \times 10^9 f_{-1}^{-1} \Delta M_{-2} v_{10}^{-3} t_5^{-3} \text{ cm}^{-3}, \quad v_p = 878 (f_{-1}^{-1} \Delta M_{-2} v_{10}^{-3} t_5^{-3})^{1/2} \text{ MHz}, \quad (\text{C9})$$

$$\text{DM} = 3.1 \times 10^5 \Delta M_{-2} v_{10}^{-2} t_5^{-2} \text{ cm}^{-3} \text{ pc}, \quad \text{EM} = 3 \times 10^{15} f_{-1}^{-1} \Delta M_{-2} v_{10}^{-5} t_5^{-5} \text{ cm}^{-6} \text{ pc}, \quad (\text{C10})$$

where $\Delta M = 10^{-2} \Delta M_{-2} M_\odot$, $v = 10^{10} v_{10} \text{ cm s}^{-1}$, $f = 0.1 f_{-1}$ and $t = 10^5 t_5 \text{ s}$. Thus, for these nominal parameters one would have to wait many months before any radio emission from the central source can successfully propagate to the outside world.

D. SOURCE COUNTS

Here we review the source count for several geometries (in particular curved atmosphere). This section may be useful in inferring the geometry of Perytons (from observations).

Spherical Geometry. Consider the following case: a homogeneous population of sources, density s per unit volume, with identical luminosity, L in Euclidean geometry. Then the volume within distance r is $V(< r) = \frac{4}{3} \pi r^3$. to Zheng *L*. The flux density at Earth is $S = L/(4\pi r^2)$. Thus number of sources with flux density less than S is

$$N(< S) = s \frac{4\pi}{3} r^3 \propto S^{-p} \quad (\text{D1})$$

with $p = 3/2$.

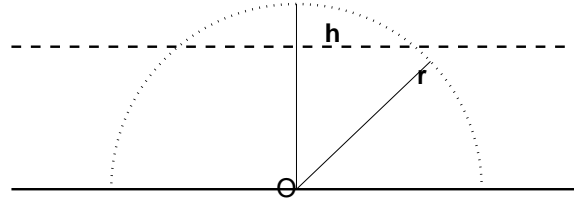


FIG. 14.— Geometry of plane-parallel atmosphere. The scale height is h . The solid line indicates the horizontal plane on which the telescope (marked at ‘O’) is located. The dotted line shows the hemisphere of radius r .

Plane Parallel Geometry. Now consider, a slab of height h and extending indefinitely along its length as shown in Figure 14. For $r < h$ we have the same scaling as in the spherical case. For $r > h$ the volume of the atmosphere is the difference between the volume of the hemisphere of radius r and the volume of the polar cap whose height is $r - h$. This volume is

$$V(< r) = \pi h^3 \left[\frac{r^2}{h^2} - \frac{1}{3} \right]. \quad (\text{D2})$$

Thus in this case $V(< r)$ asymptotically approaches r^2 (as $r \gg h$) and $N(S) \propto S^{-p}$ with $p \rightarrow 1$.

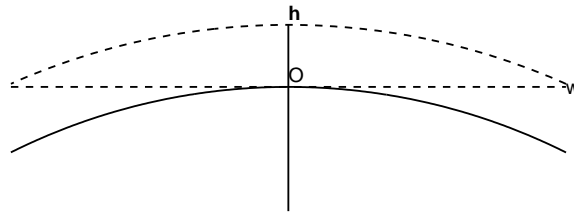


FIG. 15.— The scale height of the atmosphere is h and the radius of Earth is R (not shown). Only sources are above the local horizontal plane are visible to the radio telescope (located at ‘O’). The maximum horizontal distance is $w = \sqrt{2hR + h^2}$.

Curved Atmosphere Geometry. Now consider an atmosphere enclosing a sphere (as in the case of our atmosphere). In this case as can be seen from Figure 15 $V(r)$ has a maximum value. For $r \lesssim h$ a sphere of radius r will be within the atmosphere and thus

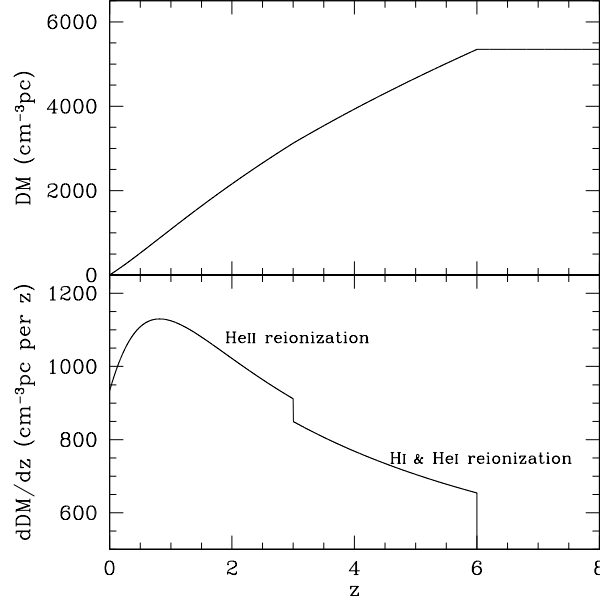


FIG. 16.— Illustration of using Dispersion Measure to probe the epoch of re-ionization of Helium II. Top and bottom panels show DM and its derivative as a function of redshift, respectively. A sharp H I and He I re-ionization at $z \sim 6$ and a sharp He II re-ionization at $z \sim 3$ are assumed.

$p \approx 3/2$. Next, the maximum value for r is $w = \sqrt{2Rh + h^2}$. Clearly, we run out of volume, $V(< r)$, when $r > w$. Thus $p = 0$, asymptotically. Thus a flat power law index (especially $p \lesssim 1/2$) would indicate a population within a curved atmosphere.

An elegant derivation of the differential and the integral was obtained by E. S. Phinney and is given below

$$\begin{aligned} \frac{dV}{dr} &= 2\pi r^2 \left[\frac{(R+h)^2 - R^2 - r^2}{2Rr} \right] = \frac{\pi r}{R} [2Rh + h^2 - r^2] \\ V(< r) &= \frac{2\pi}{3} h^3 + \frac{\pi(r^2 - h^2)}{2R} [2Rh + h^2] + \frac{\pi}{4R} (h^4 - r^4) \end{aligned} \quad (\text{D3})$$

and valid for $h < r < w$. In the limit of $h \ll R$ the formula for plane parallel distribution is recovered (Equation D2). The differential formula is well suited for computing the population distribution with a specified vertical dependence for the density of the sources.

E. FAST RADIO BURSTS AS PROBES

In this section, we explore potential applications of a *Sparker*-like population. Specifically, we develop a recipe to calculate the DM induced by the IGM (§E.1). We then comment about the potential use of FRBs for detecting a cosmological population of MACHOs (§E.2).

E.1. The Inter-Galactic Medium

Haddock & Sciama (1965) proposed to detect IGM dispersion measurements by making use of the variability of the radio signal from quasars. Their goal was to use the inferred DM to distinguish different cosmological models. Weinberg (1972) and Ginzburg (1973) suggested the use of radio flares to measure dispersion measure and thus probe the IGM density. Later, radio emission from GRBs and afterglows were proposed as means to determine distances to GRBs and probe the IGM (Palmer 1993), to study the prehistory of GRBs (Lipunova, Panchenko & Lipunov 1997), and to constrain the hydrogen re-ionization history of the universe (Ioka 2003; Inoue 2004).

However, radio quasars and GRBs, despite the aspirations of the authors, simply lack sharp features that allow their signals to be used to probe the intervening electrons. On the other hand *Sparker*-like signals are well suited for such uses, making them very useful probes of the IGM. Furthermore, DM measurements have been proposed to probe missing baryons around halos of galaxies (McQuinn 2014), baryons in the IGM (Deng & Zhang 2014) and constrain the equation of state of dark energy (Zhou *et al.* 2014).

In this subsection, we specifically focus on the potential use of *Sparkers* to probe the era of Helium re-ionization. Stars are not hot enough to ionize He II with an ionization potential of 54.4 eV. However, there is some evidence that He II re-ionization occurred at $z \sim 3$ from the transmission of the He II Ly α forest and the temperature change of the IGM [see Furlaneto & Oh (2007a, b) and references therein]. The ionization is attributed to soft X-ray emission from activate galactic nuclei (AGNs). Thus, observations of He II re-ionization provide a new diagnostic of the build-up of the AGN population. The same observations also provide important clues to the structure and thermal evolution of the IGM. Clearly there is great value in using *Sparker*-like objects in our study of cosmology and AGNs.

For the purpose of computing the DM, there are three effects on the propagation time, t_p , of a photon traveling through the

IGM to reach the observer from a cosmological distance: the continuous change of the photon's frequency, ω , due to the redshift of light, the change of the plasma frequency, $\omega_p^2 = 4\pi n_e(z)e^2/m_e$, due to the change in the IGM electron density, $n_e(z)$, with redshift, and the time dilation effect. The first two effects lead to a change in the group velocity, $v_g = c(1 - \omega_p^2/\omega^2)^{1/2}$, with redshift. The propagation time of a photon emitted at redshift z seen by an observer at redshift 0 is then

$$\begin{aligned} t_p &= \int_0^z dz \frac{dl}{dz} \frac{1}{v_g} (1+z), \\ &= \int_0^z \frac{cdz}{(1+z)H(z)} \frac{1}{c} \left(1 + \frac{1}{2} \frac{\omega_p^2}{\omega^2}\right) (1+z), \end{aligned} \quad (\text{E1})$$

where $H(z) = H_0[\Omega_m(1+z)^3 + \Omega_\Lambda]^{1/2}$ (here we assume a flat Universe) is the Hubble constant at z and the last $(1+z)$ factor accounts for time dilation. The frequency, ω , is related to the observed frequency, ω_{obs} , through $\omega = (1+z)\omega_{\text{obs}}$.

The IGM electron density $n_e(z)$ can be expressed as

$$\begin{aligned} n_e(z) &= n_0(1+z)^3 \left[(1-Y)f_{\text{HII}} + \frac{1}{4}Y(f_{\text{HeII}} + 2f_{\text{HeIII}}) \right], \\ &= n_0(1+z)^3 f_e(z), \end{aligned} \quad (\text{E2})$$

where

$$n_0 = \frac{\Omega_b \rho_c}{m_H} = 2.475 \times 10^{-7} \left(\frac{\Omega_b h^2}{0.022} \right) \text{cm}^{-3} \quad (\text{E3})$$

is the mean number density of nucleons at $z = 0$. Since we assume to observe a large number of FRBs at each redshift, it is appropriate to use the mean density of the IGM in the calculation without worrying about the density fluctuations. In the expression, $Y \simeq 0.25$ is the mass fraction of helium, f_{HII} is the ionization fraction of hydrogen, and f_{HeII} and f_{HeIII} are the ionization fractions of singly and double ionized helium. After helium re-ionization ($z \sim 2-3$), we essentially have $f_{\text{HII}} = 1$, $f_{\text{HeII}} = 0$, and $f_{\text{HeIII}} = 1$, which gives $f_e \simeq 0.88$ at low redshifts.

The observed dispersion measure (DM) is defined as

$$\frac{dt_p}{d\omega_{\text{obs}}} = - \frac{4\pi e^2}{cm_e \omega_{\text{obs}}^3} \text{DM}. \quad (\text{E4})$$

In combination with equation (E1), we have

$$\begin{aligned} \text{DM} &= n_0 \frac{c}{H_0} \int_0^z \frac{dz(1+z)f_e(z)}{\sqrt{\Omega_m(1+z)^3 + \Omega_\Lambda}}, \\ &= 1060 \text{cm}^{-3} \text{pc} \left(\frac{\Omega_b h^2}{0.022} \right) \left(\frac{h}{0.7} \right)^{-1}, \\ &\quad \times \int_0^z \frac{dz(1+z)f_e(z)}{\sqrt{\Omega_m(1+z)^3 + \Omega_\Lambda}}. \end{aligned} \quad (\text{E5})$$

For a constant f_e , the above integral can be approximated as

$$\begin{aligned} \text{DM} &= 933 \text{cm}^{-3} \text{pc} \left(\frac{f_e}{0.88} \right) \left(\frac{\Omega_b h^2}{0.022} \right) \left(\frac{h}{0.7} \right)^{-1} \left[\left(\frac{\Omega_m}{0.25} \right)^{0.1} a_1(x-1) + \right. \\ &\quad \left. \left(\frac{\Omega_m}{0.25} \right) a_2(x^{2.5}-1) + \left(\frac{\Omega_m}{0.25} \right)^{1.5} a_3(x^4-1) \right], \end{aligned} \quad (\text{E6})$$

with $x = 1+z$, $a_1 = 0.5372$, $a_2 = -0.0189$, and $a_3 = 0.00052$. The accuracy of this approximation is better than $\sim 2\%$ for $z < 5$. At low redshifts, one can use the following approximation,

$$\text{DM} = 933 \text{cm}^{-3} \text{pc} \left[z + (0.5 - 0.75\Omega_m)z^2 \right] \left(\frac{f_e}{0.88} \right) \left(\frac{\Omega_b h^2}{0.022} \right) \left(\frac{h}{0.7} \right)^{-1}, \quad (\text{E7})$$

which has a 5% accuracy up to $z = 0.6$. Given the currently accepted value of $\Omega_m = 0.27$ we present the following convenient formula for future observers of *Sparker*-like events:

$$\text{DM} = 933 \text{cm}^{-3} \text{pc} (z + 0.3z^2) \left(\frac{f_e}{0.88} \right) \left(\frac{\Omega_b h^2}{0.022} \right) \left(\frac{h}{0.7} \right)^{-1}. \quad (\text{E8})$$

The DM as a function of z is displayed in Figure 16. This is an idealized plot since we assume a sharp He II re-ionization at $z \sim 3$. The re-ionization is better seen in the slope or derivative of the DM curve. The jump is about 8%. Whether this jump will

be seen or not will depend very strongly on the contribution to the DM of the *Sparker*-like events by the electrons in the host galaxies and whether *Sparker*-like events can be found to redshifts as high as $z \sim 3$.

Similarly, we can obtain the rotation measure (RM). The Faraday rotation is

$$\Delta\theta = \frac{2\pi e^3}{m_e^2 c^2 \omega_{\text{obs}}^2} n_0 B_0 \frac{c}{H_0} \int_0^z \frac{f_e(z) b_{\parallel}(z) dz}{\sqrt{\Omega_m(1+z)^3 + \Omega_\Lambda}}, \quad (\text{E9})$$

where $b_{\parallel}(z) \equiv B_{\parallel}(z)/B_0$ is the line-of-sight magnetic field, $B_{\parallel}(z)$, in units of the local IGM magnetic field, B_0 . We then have

$$\text{RM} = 8.61 \text{ rad m}^{-2} \left(\frac{\Omega_b h^2}{0.022} \right) \left(\frac{h}{0.7} \right)^{-1} \left(\frac{B_0}{10 \text{ nG}} \right) \int_0^z \frac{f_e(z) b_{\parallel}(z) dz}{\sqrt{\Omega_m(1+z)^3 + \Omega_\Lambda}}. \quad (\text{E10})$$

At low redshifts, where we approximate $f_e = 0.88$ and $b_{\parallel} = 1$, RM can be written as

$$\text{RM} = 7.57(z - 0.75\Omega_m z^2) \text{ rad m}^{-2} \left(\frac{f_e}{0.88} \right) \left(\frac{\Omega_b h^2}{0.022} \right) \left(\frac{h}{0.7} \right)^{-1} \left(\frac{B_0}{10 \text{ nG}} \right). \quad (\text{E11})$$

So far, there are no accurate measurements for the magnetic field in the IGM with densities of the order of the mean density (see Kronberg *et al.* 2008). We note that the local IGM magnetic field would have a strength of $4(T_{\text{IGM}}/10^4 K) \text{ nG}$ if energy equipartition is assumed. Radio-synchrotron radiation has been detected in the Coma super-cluster (Kim *et al.* 1989), implying a field strength of 0.3 to 0.6 μG .

Measurement of RM will provide a strong clue to the location of the scattering (and thus dispersion) screen. If the scattering arises in the IGM then the RM from the IGM is less than 30 rad m^{-2} for $z \lesssim 0.3$ (Kronberg *et al.* 2008). A much larger RM can be produced if the screen is located in the host galaxy.

E.2. Intergalactic Machos

Another potential use of *Sparker*-like events is to constrain the existence of floating MACHO-like objects in the IGM via gravitational lensing (e.g., Gould 1992; Stanek, Paczynski & Goodman 1993; Marani *et al.* 1999). A fortunate alignment of an intervening point mass object of mass M with a *Sparker* will result in two images. The time delay for each image, with respect to a ray that arrives by the shortest path, is the sum of a geometric term and a gravitational delay term and is given by (Narayan & Bartelmann 1996) as

$$t(\theta) = \frac{1+z_l}{c} \frac{4GM}{c^2} \left(\frac{1}{2} \frac{\theta^2}{\theta_E^2} - \ln|\theta| \right), \quad (\text{E12})$$

where z_l is the redshift of the lens, θ is the angular distance between the lens and the image, and θ_E is the annular radius of the Einstein ring,

$$\theta_E = \sqrt{\frac{4GM}{c^2} \frac{D_{\text{ls}}}{D_l D_s}}. \quad (\text{E13})$$

Here, D_l , D_s , and D_{ls} , are the observer-lens, observer-source and lens-source angular diameter distances, respectively. The positions of the two images are

$$\theta_{\pm} = \frac{1}{2} \left(b \pm \sqrt{b^2 + 4\theta_E^2} \right), \quad (\text{E14})$$

where b is the impact parameter (i.e., source-lens angular distance).

From equations (E12) and (E14), the lensing time delay between the two images is

$$\begin{aligned} \Delta t_l &\equiv t(\theta_-) - t(\theta_+) \\ &= \frac{1+z_l}{c} \frac{4GM}{c^2} \left[\frac{1}{2} u \sqrt{u^2 + 4} + \ln \left(\frac{\sqrt{u^2 + 4} + u}{\sqrt{u^2 + 4} - u} \right) \right], \end{aligned} \quad (\text{E15})$$

where $u \equiv b/\theta_E$ is the impact parameter in units of the Einstein ring radius. For a typical value of $u = 1$:

$$\Delta t_l = 41(1+z_l)(M/1M_\odot) \mu\text{s}. \quad (\text{E16})$$

The two images have different amplifications, $A_{\pm} = 1/2 \pm (u^2 + 2)/(2u\sqrt{u^2 + 4})$ and the time delay ensures they also have different phases. Therefore, the two images undergo constructive and destructive interference. The total amplification is

$$A(\omega) = \frac{u^2 + 2}{u\sqrt{u^2 + 4}} + \frac{2}{u\sqrt{u^2 + 4}} \cos(\omega \Delta t_l), \quad (\text{E17})$$

where $\nu = \omega/(2\pi)$ is the frequency in the observer's frame. The spectrum will thus consist of maxima and minima with the separation of two maxima (or minima) being $\Delta\nu = \Delta t_l^{-1}$, which is tens of kHz for $M \sim 1M_\odot$ and $u \sim 1$ – well within the reach of current technology. Note that $\Delta\nu$ is independent of the observing frequency, if the time delay is purely caused by lensing.

However, in general Δt_l in equation (E17) should be replaced by the sum of all possible time delays. There could be dispersive delay due to the rays suffering different DM or delay to due multi-path propagation. For the *Sparker*, this latter effect destroys the coherence⁵² of the rays. For this reason, observing at higher frequencies (i.e., $\gtrsim 5$ GHz) is highly desirable. Furthermore, a matched-filter approach⁵⁴ can additionally improve the detection.

Finally, we can estimate the optical depth for lensing (e.g., Narayan & Bartelmann 1996). Assuming a homogeneous distribution of lenses, the optical depth for lensing is

$$\tau = \frac{2\pi}{3} \frac{G\rho_l}{c^2} D_s^2 \simeq 0.014 \Omega_l (D_s/1\text{Gpc})^2, \quad (\text{E18})$$

where ρ_l is the mass density of lenses and Ω_l is this mass density in units of the critical density of the universe.

REFERENCES

- Backer, D. C., Kulkarni, S. R., Heiles, C., Davis, M. M., and Goss, W. M. 1982, *Nature*, 300, 615.
- Bagchi, M., Nieves, A. C., and McLaughlin, M. 2012, *MNRAS*, 425, 2501.
- Bannister, K. W. and Madsen, G. J. 2014, *ArXiv e-prints*.
- Bastian, T. S., Benz, A. O., and Gary, D. E. 1998, *ARA&A*, 131.
- Bastian, T. S., Bookbinder, J., Dulk, G. A., and Davis, M. 1990, *ApJ*, 353, 265.
- Berger, E. 2013, *ArXiv e-prints*.
- Bhat, N. D. R. *et al.* 2007, *ApJ*, 665, 618.
- Bianchi, L. *et al.* 2007, *ApJS*, 173, 659.
- Blandford, R. D. 1977, *MNRAS*, 181, 489.
- Bloom, J. S. *et al.* 2011, *Science*, 333, 203.
- Boehringer, H. and Hensler, G. 1989, *A&A*, 215, 147.
- Boggs, S. E., Zoglauer, A., Bellm, E., Hurley, K., Lin, R. P., Smith, D. M., Wigger, C., and Hajdas, W. 2007, *ApJ*, 661, 458.
- Bregman, J. N. 2007, *ARA&A*, 45, 221.
- Burke-Spolaor, S., Bailes, M., Ekers, R., Macquart, J.-P., and Crawford, III, F. 2011, *ApJ*, 727, 18.
- Burrows, D. N. *et al.* 2011, *Nature*, 476, 421.
- Cardelli, J. A., Clayton, G. C., and Mathis, J. S. 1989, *ApJ*, 345, 245.
- Chevalier, R. A. and Fransson, C. 2006, *ApJ*, 651, 381.
- Cline, T. L. *et al.* 1980, *ApJ*, 237, L1.
- Cordes, J. M. 2013, in *IAU Symposium*, volume 291 of *IAU Symposium*, 211.
- Cordes, J. M. and Lazio, T. J. W. 2002, *ArXiv Astrophysics e-prints*.
- Cordes, J. M., Weisberg, J. M., Frail, D. A., Spangler, S. R., and Ryan, M. 1991, *Nature*, 354, 121.
- Coward, D. M. *et al.* 2012, *MNRAS*, 425, 2668.
- Cox, A. N. 2000, *Allen's astrophysical quantities*, (New York: Springer).
- Crawford, F., Kaspi, V. M., Manchester, R. N., Lyne, A. G., Camilo, F., and D'Amico, N. 2001, *ApJ*, 553, 367.
- Cross, N. *et al.* 2001, *MNRAS*, 324, 825.
- Deneva, J. S. *et al.* 2009, *ApJ*, 703, 2259.
- Deng, W. and Zhang, B. 2014, *ArXiv e-prints*.
- Draine, B. T. and McKee, C. F. 1993, *ARA&A*, 31, 373.
- Egorov, A. E. and Postnov, K. A. 2009, *Astronomy Letters*, 35, 241.
- Erickson, W. C. 1983, *ApJ*, 264, L13.
- Falcke, H. and Rezzolla, L. 2013, *ArXiv e-prints*.
- Falcke, H. D. *et al.* 2007, *Highlights of Astronomy*, 14, 386.
- Fishman, G. J. *et al.* 1994, *Science*, 264, 1313.
- Frail, D. A., Kulkarni, S. R., and Bloom, J. S. 1999, *Nature*, 398, 127.
- Frail, D. A., Kulkarni, S. R., Ofek, E. O., Bower, G. C., and Nakar, E. 2012, *ApJ*, 747, 70.
- Fruchter, A. S. *et al.* 1990, *ApJ*, 351, 642.
- Furlanetto, S. R. and Oh, S. P. 2008a, *ApJ*, 682, 14.
- Furlanetto, S. R. and Oh, S. P. 2008b, *ApJ*, 681, 1.
- Gaustad, J. E., McCullough, P. R., Rosing, W., and Van Buren, D. 2001, *PASP*, 113, 1326.
- Giménez de Castro, C. G., Costa, J. E. R., Silva, A. V. R., Simões, P. J. A., Correia, E., and Magun, A. 2006, *A&A*, 457, 693.
- Ginzburg, V. L. 1973, *Nature*, 246, 415.
- Goodman, J. 1997, *New Astronomy*, 2, 449.
- Gould, A. 1992, *ApJ*, 386, L5.
- Guetta, D. and Della Valle, M. 2007, *ApJ*, 657, L73.
- Haddock, F. T. and Sciama, D. W. 1965, *Physical Review Letters*, 14, 1007.
- Helou, G., Kasliwal, M. M., Ofek, E. O., Arcavi, I., Surace, J., and Gal-Yam, A. 2013, *ApJ*, 778, L19.
- Heng, K. and McCray, R. 2007, *ApJ*, 654, 923.
- Hotokezaka, K., Kiuchi, K., Kyutoku, K., Okawa, H., Sekiguchi, Y.-i., Shibata, M., and Taniguchi, K. 2013, *Phys. Rev. D*, 87(2), 024001.
- Hurley, K. *et al.* 2005, *Nature*, 434, 1098.
- Hyman, S. D., Lazio, T. J. W., Kassim, N. E., Ray, P. S., Markwardt, C. B., and Yusef-Zadeh, F. 2005, *Nature*, 434, 50.
- Hyman, S. D., Roy, S., Pal, S., Lazio, T. J. W., Ray, P. S., Kassim, N. E., and Bhatnagar, S. 2007, *ApJ*, 660, L121.
- Inoue, S. 2004, *MNRAS*, 348, 999.
- Ioka, K. 2003, *ApJ*, 598, L79.
- Isliker, H. and Benz, A. O. 1994, *A&AS*, 104, 145.
- Jackson, P. D., Kundu, M. R., and White, S. M. 1989, *A&A*, 210, 284.
- Johnston, S. *et al.* 2008, *Experimental Astronomy*, 22, 151.
- Kalogera, V. *et al.* 2004, *ApJ*, 601, L179.
- Kanner, J., Baker, J., Blackburn, L., Camp, J., Mooley, K., Mushotzky, R., and Ptak, A. 2013, *ApJ*, 774, 63.
- Kashiyama, K., Ioka, K., and Mészáros, P. 2013, *ApJ*, 776, L39.
- Kasliwal, M. M. *et al.* 2008, *ApJ*, 678, 1127.
- Katz, J. I. 2013, *ArXiv e-prints*.
- Keane, E. F., Stappers, B. W., Kramer, M., and Lyne, A. G. 2012, *MNRAS*, 425, L71.
- Keith, M. J. *et al.* 2010, *MNRAS*, 409, 619.
- Kellermann, K. I. and Pauliny-Toth, I. I. K. 1969, *ApJ*, 155, L71.
- Kim, K.-T., Kronberg, P. P., Giovannini, G., and Venturi, T. 1989, *Nature*, 341, 720.
- Knight, H. S., Bailes, M., Manchester, R. N., and Ord, S. M. 2006, *ApJ*, 653, 580.
- Kocz, J., Bailes, M., Barnes, D., Burke-Spolaor, S., and Levin, L. 2012, *MNRAS*, 420, 271.
- Kouveliotou, C., Meegan, C. A., Fishman, G. J., Bhat, N. P., Briggs, M. S., Koshut, T. M., Paciesas, W. S., and Pendleton, G. N. 1993, *ApJ*, 413, L101.
- Kraushaar, W. L., Clark, G. W., Garmire, G. P., Borken, R., Higbie, P., Leong, V., and Thorsos, T. 1972, *ApJ*, 177, 341.
- Kronberg, P. P., Bernet, M. L., Miniati, F., Lilly, S. J., Short, M. B., and Higdon, D. M. 2008, *ApJ*, 676, 70.
- Lang, K. R. 1974, *Astrophysical formulae: A compendium for the physicist and astrophysicist*, (New York, Heidelberg, Berlin: New York, Springer-Verlag New York, Inc., 1974. 760 p.).
- Lasky, P. D., Haskell, B., Ravi, V., Howell, E. J., and Coward, D. M. 2013, *ArXiv e-prints*.
- Lazio, T. J. W., Cordes, J. M., Anantharamaiah, K. R., Goss, W. M., and Kassim, N. E. 1999, in *The Central Parsecs of the Galaxy*, ed. H. Falcke, A. Cotera, W. J. Duschl, F. Melia, and M. J. Rieke, volume 186 of *Astronomical Society of the Pacific Conference Series*, 441.
- Le Petit, F., Roueff, E., and Herbst, E. 2004, *A&A*, 417, 993.
- Levan, A. J. *et al.* 2011, *Science*, 333, 199.
- Levan, A. J. *et al.* 2008, *MNRAS*, 384, 541.
- Li, W., Chornock, R., Leaman, J., Filippenko, A. V., Poznanski, D., Wang, X., Ganeshalingam, M., and Mannucci, F. 2011, *MNRAS*, 412, 1473.
- Licquia, T. and Newman, J. 2013, in *American Astronomical Society Meeting Abstracts*, volume 221 of *American Astronomical Society Meeting Abstracts*, 254.11.
- Lipunova, G. V., Panchenko, I. E., and Lipunov, V. M. 1997, *New Astronomy*, 2, 555.
- Loeb, A., Shvartzvald, Y., and Maoz, D. 2014, *MNRAS*.
- Lorimer, D. R., Bailes, M., McLaughlin, M. A., Narkevic, D. J., and Crawford, F. 2007, *Science*, 318, 777.
- Luan, J. 2014, *ArXiv e-prints*.
- Lyubarsky, Y. 2014, *ArXiv e-prints*.
- Lytikov, M. 2002, *ApJ*, 580, L65.
- Macquart, J.-P. and Koay, J. Y. 2013, *ApJ*, 776, 125.
- Manchester, R. N., Fan, G., Lyne, A. G., Kaspi, V. M., and Crawford, F. 2006, *ApJ*, 649, 235.
- Manchester, R. N., Hobbs, G. B., Teoh, A., and Hobbs, M. 2005, *AJ*, 129, 1993.
- Manchester, R. N. *et al.* 2001, *MNRAS*, 328, 17.
- Marani, G. F., Nemiroff, R. J., Norris, J. P., Hurley, K., and Bonnell, J. T. 1999, *ApJ*, 512, L13.
- Marsh, T. R., Nelemans, G., and Steeghs, D. 2004, *MNRAS*, 350, 113.
- Martin, D. C. *et al.* 2005, *ApJ*, 619, L1.
- Mazets, E. P. *et al.* 1979, *Pisma v Astronomicheskii Zhurnal*, 5, 307.
- McConnell, D., McCulloch, P. M., Hamilton, P. A., Ables, J. G., Hall, P. J., Jacka, C. E., and Hunt, A. J. 1991, *MNRAS*, 249, 654.
- McGarry, M. B., Gaensler, B. M., Ransom, S. M., Kaspi, V. M., and Veljkovic, S. 2005, *ApJ*, 627, L137.

⁵³ Equivalently, the de-coherence is the size of the scattered disk exceeding the image separation with the attendant loss of visibility function.

⁵⁴ naturally obtained via the cross-correlation function in a XF-type interferometer.

- McKee, C. F., Hollenbach, D. J., Seab, G. C., and Tielens, A. G. G. M. 1987, *ApJ*, 318, 674.
- McLaughlin, M. A. *et al.* 2006, *Nature*, 439, 817.
- McQuinn, M. 2014, *ApJ*, 780, L33.
- Metzger, M. R., Djorgovski, S. G., Kulkarni, S. R., Steidel, C. C., Adelberger, K. L., Frail, D. A., Costa, E., and Frontera, F. 1997, *Nature*, 387, 878.
- Molnar, L. A., Mutel, R. L., Reid, M. J., and Johnston, K. J. 1995, *ApJ*, 438, 708.
- Moran, J. M., Greene, B., Rodriguez, L. F., and Backer, D. C. 1990, *ApJ*, 348, 147.
- Nakar, E. 2007, *Phys. Rep.*, 442, 166.
- Nakar, E., Gal-Yam, A., and Fox, D. B. 2006, *ApJ*, 650, 281.
- Narayan, R. and Bartelmann, M. 1996, *ArXiv Astrophysics e-prints*.
- Ofek, E. O. 2007, *ApJ*, 659, 339.
- Ofek, E. O. *et al.* 2006, *ApJ*, 652, 507.
- Ofek, E. O. *et al.* 2008, *ApJ*, 681, 1464.
- Oke, J. B. 1974, *ApJS*, 27, 21.
- Osten, R. A. and Bastian, T. S. 2006, *ApJ*, 637, 1016.
- Osterbrock, D. E. and Ferland, G. J. 2006, *Astrophysics of gaseous nebulae and active galactic nuclei*, (Sausalito, California: University Science Books).
- Padmanabhan, T. 2002, *Theoretical Astrophysics - Volume 3, Galaxies and Cosmology*, (Cambridge, United Kingdom: Cambridge University Press).
- Palmer, D. M. 1993, *ApJ*, 417, L25+.
- Palmer, D. M. *et al.* 2005, *Nature*, 434, 1107.
- Popov, S. B. and Postnov, K. A. 2010, in *Evolution of Cosmic Objects through their Physical Activity*, ed. H. A. Harutyunian, A. M. Mickaelian, and Y. Terzian, 129.
- Raskin, C., Kasen, D., Moll, R., Schwab, J., and Woosley, S. 2013, *ArXiv e-prints*.
- Raymond, J. C., Hester, J. J., Cox, D., Blair, W. P., Fesen, R. A., and Gull, T. R. 1988, *ApJ*, 324, 869.
- Reynolds, R. J. 1984, *ApJ*, 282, 191.
- Rybicki, G. B. and Lightman, A. P. 1979, *Radiative processes in astrophysics*, (New York, Chichester, Brisbane, Toronto: New York, Wiley-Interscience, 1979. 393 p.).
- Saint-Hilaire, P., Benz, A. O., and Monstein, C. 2014, *ArXiv e-prints*.
- Sakamoto, T. *et al.* 2011, *ApJS*, 195, 2.
- Scannapieco, E. and Bildsten, L. 2005, *ApJ*, 629, L85.
- Schaerer, D. and de Koter, A. 1997, *A&A*, 322, 598.
- Schlegel, D. J., Finkbeiner, D. P., and Davis, M. 1998, *ApJ*, 500, 525.
- Siemion, A. P. V. *et al.* 2012, *ApJ*, 744, 109.
- Soderberg, A. M. *et al.* 2006, *Nature*, 442, 1014.
- Soglasnov, V. A., Popov, M. V., Bartel, N., Cannon, W., Novikov, A. Y., Kondratiev, V. I., and Altunin, V. I. 2004, *ApJ*, 616, 439.
- Spitzer, L. 1978, *Physical processes in the interstellar medium*, (Yew York: Wiley-Interscience, 1978. 333 p.).
- Stanek, K. Z., Paczynski, B., and Goodman, J. 1993, *ApJ*, 413, L7.
- Stanimirovic, S., Staveley-Smith, L., Dickey, J. M., Sault, R. J., and Snowden, S. L. 1999, *MNRAS*, 302, 417.
- Staveley-Smith, L. *et al.* 1996, *Publications of the Astronomical Society of Australia*, 13, 243.
- Storm, J., Carney, B. W., Gieren, W. P., Fouqué, P., Latham, D. W., and Fry, A. M. 2004, *A&A*, 415, 531.
- Svirski, G., Nakar, E., and Ofek, E. O. 2011, *MNRAS*, 415, 2485.
- Tendulkar, S. P., Cameron, P. B., and Kulkarni, S. R. 2012, *ApJ*, 761, 76.
- Thornton, D. *et al.* 2013, *Science*, 341, 53.
- Totani, T. 2013, *PASJ*, 65, L12.
- Vachaspati, T. 2008, *Physical Review Letters*, 101(14), 141301.
- Valls-Gabaud, D. 1998, *Publications of the Astronomical Society of Australia*, 15, 111.
- Vikhlinin, A. 1998, *ApJ*, 505, L123.
- Vink, J. and Kuiper, L. 2006, *MNRAS*, 370, L14.
- Wang, Q. D. 2007, in *EAS Publications Series*, ed. E. Emsellem, H. Wozniak, G. Massacrier, J.-F. Gonzalez, J. Devriendt, and N. Champavert, volume 24 of *EAS Publications Series*, 59.
- Wayth, R. B., Tingay, S. J., Deller, A. T., Briske, W. F., Thompson, D. R., Wagstaff, K. L., and Majid, W. A. 2012, *ApJ*, 753, L36.
- Webber, W. R. 1998, *ApJ*, 506, 329.
- Weinberg, S. 1972, *Gravitation and Cosmology: Principles and Applications of the General Theory of Relativity*, (New York: Wiley-VCH).
- Wilson, D. B. and Rees, M. J. 1978, *MNRAS*, 185, 297.
- Wolfire, M. G., McKee, C. F., Hollenbach, D., and Tielens, A. G. G. M. 2003, *ApJ*, 587, 278.
- Wyder, T. K. *et al.* 2007, *ApJS*, 173, 293.
- Zauderer, B. A. *et al.* 2011, *Nature*, 476, 425.
- Zhang, B. 2014, *ApJ*, 780, L21.
- Zhou, B., Li, X., Wang, T., Fan, Y.-Z., and Wei, D.-M. 2014, *ArXiv e-prints*.